THE EFFECT OF ENGINEERED TOPOGRAPHIES ON MARINE ADHESIVE

By

FRANCISCO CASTRO CARA

A THESIS PRESENTED TO THE GRADUATE SCHOOL OF THE UNIVERSITY OF FLORIDA IN PARTIAL FULFILLMENT OF THE REQUIREMENTS FOR THE MASTER OF SCIENCE

UNIVERSITY OF FLORIDA

2014

To my beloved parents and my amazing wife

ACKNOWLEDGMENTS

I can say with certainty that I could not have achieved half of what I have done without the encouragement and help of a select group of individuals.

First and foremost, I must thank my advisor and committee chairman Dr. Anthony Brennan for his encouragement and support during my studies at University of Florida. I also want to mention the other two members of my committee, Dr. Josephine Allen and Dr. Christopher Batich, who have offered her knowledge and expertise when I have needed.

I want to make a special mention to all my fellow group members, who provided me with a priceless experience, personal and professional, and who shortly after I joined the group became friends. This thesis would have never been written if I did not count with all their help and patience with me. My deepest gratitude and appreciation go to the group members who have seen me through this entire process: Dr. Canan Kizilkaya, Cary Kuliasha, Clayton Argenbright, Danessa Jerome, Joe Decker, Laura Villada and Shanna Smith.

It is very important for me the assistance provided in my investigation by Dr. Shane Stafslien (University of North Dakota), who helped me to improve my procedure and Dr. Daniel Rittschof (Duke University) who took part of his time to collect and deliver the mussels used in this research project.

My biggest appreciation to my family and friends, who have offered emotional support and love during this entire process. Especially my parents, Francisco and Encarnacion who did not doubt to trust completely in my skills to provide me with this opportunity, and my wife, Andrea, the one that has always been strong at my side especially in those moments I was more vulnerable.

TABLE OF CONTENTS

page

ACKNOWLEDGMENTS 4

LIST OF TABLES 7

LIST OF FIGURES 8

LIST OF ABBREVIATIONS 11

ABSTRACT 12

CHAPTER

1 INTRODUCTION 13

2 BACKGROUND 16

Marine biofouling and marine adhesives 16
Mussel adhesion 18
Byssus: water-adhesive interaction and mechanism of attachment 19
Byssus: chemistry 21
Polydimethylsiloxane elastomer (PDMSe) 23
Mechanical and chemical properties 24
Surface energy 25
Wettability, surface energy and topography 26
Contact angle: Young equation 27
Wettability: Wenzel and Cassie-Baxter models 28
Engineered Roughness Index (ERI) 29

3 MATERIALS 36

Setting up the tank: cultivating mussels 36
Testing kits 36
DT's Premium Reef Blend Phytoplankton 37
Silicone elastomer: SILASTIC T-2 37
Allyltrimethoxysilane (ATS): silane coupling agent 38
Hexamethyldisiloxane (HMDS) 38

4 METHODS 41

Cultivating mussels 41
Setting up the aquarium. Safety and previous considerations 41
Conditions in the tank 43
Mussel aquarium maintenance protocol 43
PDMSe patterned samples preparation 45

PDMSe patterned samples characterization 47
Mussel plaque production 48
Extraction procedure 50
Measuring number of plaques 50
Measuring surface area and Nuclear Form Factor (NFF) 51
Degree of penetration (Scanning Electron Microscope) 52
Tensile test (texture analyzer) 52

5 RESULTS AND DISCUSSION 63

Number of plaques 63
Plaque surface area 64
Nuclear Form Factor (NFF): Morphology of the plaques 66
Degree of penetration 67
Texture analyzer 68
Tensile force 72
Tensile force versus plaque surface area 73
Tensile stress 74

6 CONCLUSIONS AND FUTURE WORK 107

Conclusions 107
Future work 109
Comparison with commercial adhesives 109
Test other engineered topographies 109
Measure the penetration degree 110
Measure the exact volume of adhesive secreted by the mussel 110
Analyze the surface where adhesive failure happens. 110

LIST OF REFERENCES 113

BIOGRAPHICAL SKETCH 118

LIST OF TABLES

Table		page
2-1	DOPA-containing proteins of the byssus of Mytilus species.	32
3-1	Typical properties of Silastic® T2 (Dow Corning), from Dow Corning product information sheets	39
4-1	Water tank maintenance monthly schedule	55
5-1	Different sizes of the features in the different patterns	77
5-2	Table with the more significant statistical values of number of plaques for the different samples (data collected from the texture analyzer tests)	79
5-3	Plaque surface area statistically most important parameters	81
5-4	ANOVA variance study for the plaque surface area values on the different topographies	82
5-5	Tukey post-hoc analysis of plaque surface area values (being 1=smooth, 2=5x5, 3=20x20, 4=50x50, 5=100x100, 6=200x200)	83
5-6	Nuclear Form Factor statistically most important parameters	85
5-7	ANOVA variance study for the Nuclear Form Factor (NFF) values on each topography	86
5-8	Tukey post-hoc analysis of nuclear form factor values (being 1=smooth, 2=5x5, 3=20x20, 4=50x50, 5=100x100, 6=200x200)	87
5-9	Values of tensile force (mN) and Tensile stress (mN/mm^2) including basic statistical analysis for every sample tested in the texture analyzer	101
5-10	ANOVA variance study for tensile force values for each topography	102
5-11	Tukey post-hoc analysis of tensile force values (being 1=smooth, 2=5x5, 3=20x20, 4=50x50, 5=100x100, 6=200x200)	103
5-12	Comparison with ANOVA statistical analysis (Minitab) between plaque surface area values of the 48 h and 72 h experiments	105

LIST OF FIGURES

Figure page

2-1 Progress of movements during mussel plaque deposition. 31

2-2 Scheme of the distribution of the different mussel foot protein along the byssus structure. 32

2-3 Chemical structure of L-3,4-Dihydroxyphenilalanine 33

2-4 Adhesive and cohesive interactions of mussel protein through DOPA 33

2-5 Basic structure of a PDMS chain segment 34

2-6 Diagram of forces on molecules in a liquid.. 34

2-7 Schematic diagram of liquid droplet on solid surface..... 35

2-8 Schematics representation of Wenzel model (left) and Cassie Baxter (right).. ... 35

3-1 Curing reaction between the base resin and the curing agent of SILASTIC silicone 39

3-2 ATS coupling agent reaction with silica glass 40

3-3 HMDS reaction onto silica glass slide..... 40

4-1 Mold setup for preparation of patterned PDMSe on glass slides (sectional view) 56

4-2 SEM captures the different topographies used in this study (3.67 kV) 57

4-3 General plaque production experiment set and the direction corresponding to the position of the mussel 58

4-4 SEM micrograph of the edge of a plaque onto 10 CH 20x20. 59

4-5 Optical microscope picture of mussel plaques onto 20 CH20x20 at x10 magnification 60

4-6 Optical microscope image of two mussel plaques onto 10 CH 20x20. On the left without image processing. 60

4-7 Schematic of the measurements taken by ImageJ® to calculate NFF 61

4-8 Tensile analyzer (XT plus Texture analyzer from Texture Technologies Corp.) used in tensile force measurements 61

4-9 Texture analyzer set-up. Mussel is attached to the sample by different byssus structures..... 62

4-10 Example of force versus distance plot produced from data collected by texture analyzer for an individual mussel in a plaque strength test..... 62

5-1 Pictures that illustrate the mussel plaque production extends beyond the patterned area. 78

5-2 Number of plaques in different patterns (texture analyzer test) compared with control sample (smooth PDMSe).. 80

5-3 Plaque surface area values (mm2) of the different patterns tested. 82

5-4 Plaque surface area values (mm^2) vs. size of the features (μm^2).. 84

5-5 NFF values of the different patterns tested. 86

5-6 NFF values vs. size of the features. 88

5-7 SEM pictures of detached mussel plaques on 20x20 microns channels feature 89

5-8 SEM pictures of attached mussel plaques on 20x20 microns channels feature (A) and 50x50 microns feature (B) 90

5-9 SEM pictures of attached mussel plaques on 50x50 microns channels feature (A) and 20x20 microns feature (B) 91

5-10 SEM pictures of attached mussel plaques on 50x50 microns feature 92

5-11 Tensile test performed in texture analyzer. A number of threads can be observed going from the shell of the mussel to the substrate..... 93

5-12 Results for the texture analyzer tensile test on smooth PDMSe.. 93

5-13 Results for the texture analyzer tensile test on channels 5x5 microns features.. 94

5-14 Results for the texture analyzer tensile test on channels 20x20 microns features.. 94

5-15 Results for the texture analyzer tensile test on channels 20x20 microns features.. 95

5-16 Results for the texture analyzer tensile test on channels 100x100 microns features.. 95

5-17 Results for the texture analyzer tensile test on channels 200x200 microns features.. 96

5-18 Histogram for the tensile force (mN) values of the different plaques for those tests on smooth PDMSe 96

5-19 Histogram for the tensile force (mN) values of the different plaques for those tests on 5x5 microns channels samples 97

5-20 Histogram for the tensile force (mN) values of the different plaques for those tests on 20x20 microns channels samples 97

5-21 Histogram for the tensile force (mN) values of the different plaques for those tests on 50x50 microns channels samples 98

5-22 Histogram for the tensile force (mN) values of the different plaques for those tests on 100x100 microns channels samples 98

5-23 Histogram for the tensile force (mN) values of the different plaques for those tests on 200x200 microns channels samples 99

5-24 Adhesive failures of mussel plaques in the different topographies. 100

5-25 Tensile force (mN) for every sample (5x5, 20x20, 50x50, 100x100, 200x200, width x spacing in microns) and blank.. 102

5-26 Comparison between data collected for tensile force (left axis) and plaque surface area (right axis).. 104

5-27 Tensile stress (x10-3 Pa) for every sample (5x5, 20x20, 50x50, 100x100, 200x200, width x spacing in microns) and blank applying roughness index..... 106

5-28 Comparison between data collected for tensile force (right axis) and tensile stress (left axis).. 106

6-1 Scheme of the effect of the topography size on mussel plaque adhesion (adhesive attachment) 112

LIST OF ABBREVIATIONS

5x5	Channel pattern sample 5 micron by 5 micron (width by spacing)
CH	Channel pattern
Mfps	Mussel foot protein(s)
NFF	Nuclear Form Factor
PDMSe	Polydimethylsiloxane elastomer is a rubber (viscoelastic behavior), with a highly cross-linked structure based on polydimethylsiloxane chains.
SEM	Scanning Electron Microscope
SK	Sharklet ® pattern

Abstract of Thesis Presented to the Graduate School
of the University of Florida in Partial Fulfillment of the
Requirements for the Master of Science

THE EFFECT OF ENGINEERED TOPOGRAPHIES ON MARINE ADHESIVE

By

Francisco Castro Cara

May 2014

Chair: Anthony Brennan
Major: Materials Science and Engineering (MTL)

Mussels have the ability to attach to a wide variety of materials by the production of a structure known as byssus. This byssus is formed by a number of adhesive plaques each connected to the inside of the animal through a collagen thread. The byssal plaque is a highly cross-linked protein adhesive that is segregated by the foot, a specialized appendix organ capable to identify chemical and physical features on the surface in order to identify a suitable attachment spot. This experiment is intended to investigate the effect of the micro-engineered pattern size in mussel attachment process.

CHAPTER 1
INTRODUCTION

Biofouling is the formation of an undesired film, generally on man-made structures, produced by organic products and organisms present in the environment. The film may vary in thickness and it exists a wide range of organisms (Schumacher et al. 2007) that take part in the fouling process from algal zoospores (Ulva linza) to macroscopic species (adult cyprids), that differ from each other in size, type and mechanism of action.

Biofouling has a major economic and environmental effect. It increases the fuel consumption rate of ships about 10% plus all the expenses of maintenance (paint, hull cleaning) and other extra cost associated with these treatments (Schultz et al. 2010). Power plants and other industry facilities where water intake from natural sources are used have remarkable losses too. Macrofouling affects the plant operation and safety as it may produce shutdowns (Wells et al. 2009). At the same time, biofouling has a critical impact in the environment. Adult and juvenile mussels specifically, attached to the hull of ships or inside the ballast water of boats, may manage to travel from far areas and invade different wetlands and coast waters, such as zebra mussel in the Great Lakes region.

Mussels attach successfully to a variety of substrates in an aqueous environment by using a strong protein-based adhesive, including PVC, PMMA, Aluminum, Stainless Steel, wood and concrete (Ackerman et al. 1996; Ackerman et al. 1992). Mussels use a specialized organ known as “foot” to taste chemically and physically the surface and select an appropriate site to produce the byssus, an anchor-like structure that fix the organism to the surface and make it possible for the animal to survive in the intertidal

zone where they live (Silverman and Roberto 2007). The byssus consist of an organ inside the shell, called stem, a collagen thread that may vary on length and a plaque, that is directly in contact with the surface.

Mussels present two different stages in their life cycle in which they settle on the surface, known as primary settlement and secondary settlement (Bayne 1964). The first settlement process take place in an early stage in the development of the mussel, also called as pediveliger (170-300 μm), and the second settlement occurs when the mussel is transforming into the adult form, also called as plantigrades/juvenile (Ackerman et al. 1994). The animal preferences about attachment sites in each stage vary with complexity being a key factor. Mussels prefer more complex structures in early stages of development for protection and less complex later to promote growth and more availability of food source (Carl et al. 2012c).

Different coatings to prevent from the adhesion of mussels have been tested. Considerations about toxicity, resistance and long-term use have come to be critical. Legal levels of copper and zinc leaking into the environment are lower and lower each year, and toxicity becomes a very important issue. Fouling release materials may not be appropriate for a high flow conditions like those in intake pipes for big facilities, because they may be peeled off the treated surface, and secondary toxic effects have been reported. Most of the coatings require substitution after an average of 5-7 years (Wells et al. 2009).

Surface patterning of polymer systems has shown a very good performance in antifouling. Polymer surface properties such as surface energy can be altered by modifying the size, shape and type of material used (Carman et al. 2006).

Microchannels and Sharklet®, have already been tested and proved valid for different organisms such as shellfish (Scardino et al. 2008) and algae (Hoipkemeier-Wilson et al. 2004), mussel pediveligers (Carl et al. 2012a) and barnacle cyprids (Aldred et al. 2009). It has also been shown that the performance of a specific topography is highly specie-specific, due to the different properties, sizes and mechanism of adhesion of the wide range of organisms that are part of biofouling (Schumacher et al. 2007).

Some research has been done about the effect of surface roughness and engineered topographies on the settlement and attachment of mussels and other macrofoulers such as barnacles, but all of them have used organisms in an early stage of development, like mussel pediveliger (Carl et al. 2012a) and barnacle cyprids (Aldred et al. 2010). More studies have been done in adult mussels attachment mechanism and strength, but not taking into account topography, for example enhancing the efficacy of fouling-release coatings using nanofillers (Carl et al. 2012b) or measuring the attachment strength onto different surfaces (Burkett et al. 2009).

The purpose of this study was to test the effect of different engineered topographies on the process of attachment of adult mussels (specifically Geukensia demissa). Surface topography size was introduced as a key factor for mechanical adhesion strength of the byssus, spreading behavior of the plaque adhesive onto the surface, and size and shape of the plaque. The substrate selected was silicone elastomer for its well-known foul-release properties and the good results in previous experimentations.

CHAPTER 2
BACKGROUND

Marine biofouling and marine adhesives

Controlling biofouling in a marine environment represents a very difficult challenge. Water provides an ideal living medium for a wide range of species, some of them needing of a substrate to attach in order to grow and develop (i.e. algae, barnacles or tubeworms). Each of these organisms possess different mechanisms of attachment, as well as they use different adhesives, what makes biofouling phenomena very complex. A good review of current commercially available products used nowadays can be found in Wells and Sytsma (2009).

Chemical and physical properties of water have played a very important role on fouling organism's adhesives development since water limits the chemistry of the compounds that can bind to a surface. In adhesive bonding industry, water presence leads to a bad performance of the adhesive through some mechanism such as moisture-induced plasticization, swelling, erosion, and hydrolysis of polymers and interfacial wicking and crazing (Wake and Kinloch 1977). Water decrease largely the electrostatic interaction between opposite charges as a consequence of the high dielectric constant, and it was also further decreased as an effect for the strong solvation of ions (i.e. Mg^{2+} or Li^{+}). When talking of surfaces interaction, the term adhesion energy and adhesion work must be taken into account, since the dispersion and polar interactions (as surface energy terms) in water produce the value of the adhesion work to be a lot less than it is expected in non-wet conditions. This means that the strength of the interaction between the surface and the adhesive is much lower in water if it exists (Lee et al. 2006).

An adhesive in underwater conditions, in order to be effective needs to work quickly. First, the adhesive needs to be fluid to spread onto the surface and second, at the same time, it needs to have a surface tension to prevent from being dissolved by the water. These two conditions seem to be a bit of a contradiction, so a balance between spreading properties and surface tension is an important requirement. Adhesive must be able to displace water molecules that are already bonded (electrostatically) to the surface, so the attachment process competes directly with water molecules. Finally, the adhesive has to undergo a crosslinking process, in order to acquire the stiffness and cohesion enough to endure (Smith and Callow 2006).

The zoospore of the Ulva algae, has been extensively used as a model fouling agent in a lot of research projects. An important stage in the reproduction and spreading of this alga is the production of motile zoospores that need to attach to a surface to get to the next stage of development. The zoospore has the ability to actively identify a suitable site on the surface and the attachment is performed by the secretion of an adhesive which anchors the spore to the surface. This adhesive is stored inside vesicles within the membrane and the composition has not been completely characterized yet (Callow and Callow 2006).

Diatoms are a group of unicellular microalgae whose common feature is the production of a silicified cell wall after settlement. Diatoms do not actively search to attach to surfaces but they are moved by the water currents. The adhesive used by this organism has been described as mucilaginous material, as well known as extracellular polymeric substances, which are completely non-soluble compounds (Chiovitti et al 2006).

Barnacles are a well-known fouling agent. Barnacles are a type of macrofouler that can be described as a shellfish that attach to surfaces for protection, increase the access to resources and improve reproduction rates, since they usually are found in colonies. During barnacle reproduction process they produce larva, as well known as cyprids. These cyprids possess antennules that are used to get information from the substrate and identify a convenient site for attachment. The binding process happens by the secretion of a cement, which composition varies from earlier stages in the life of the barnacle to the adult and last stage, but can be described as a multi-protein complex (over 90% of content in protein). The chemical analysis of the barnacle cement in any case has revealed DOPA, as a big difference with mussel adhesive. (Kamino 2006).

A big effort in marine bio-fouling prevention has been done in the direction of mimicking natural surfaces that are not fouled in natural conditions, so some biomimetic models and bioinspired surfaces have shown encouraging results (Scardino and de Nys 2011). Some of them worth to be mention are gorgonian corals (Vrolijk et al. 1990), pilot whale skin (Baum et al. 2001), shark skin (Brennan et al. 2010) and molluscs (Scardino et al. 2009).

Mussel adhesion

Mussels life-cycle go through different stages, 1) pelagic larval forms, 2) primary settlement and metamorphosis, 3) post metamorphic settlement (secondary settlement), where the animal differ not only in size but in preferences for attachment (Ackerman et al 1994). During the primary settlement, the larvae actively search for those sites that provide increased surface area and protection, being normally sites with a higher complexity. However the preferences change when the animal develops into a more mature form, when space availability and a more abundant food source become more

important. For this reason, during maturation the second settlement takes place on different sites, producing the mussel to move to a more open area (Carl et al. 2012c; Bayne 1964).

Settlement always takes place through the same process at all stages of development. This process starts with the mussel foot, a retractile tongue-like organ that the mussel uses to “taste” the surface previous to the attachment. The mussel foot is able to detect differences in chemistry and morphology onto the surface, what permits the animal to detect the more favorable sites. Different studies have shown attachment preferences over different material, being those materials with a higher surface energy more likely to be used by the animal (Ackerman et al. 1996; Ackerman et al. 1992; Aldred et al. 2006). It has been proved that surface topography play an important role in the process of site selection by the mussel, being preferred those topographies that protect the larvae in early stages (Carl et al. 2012c).

Once the site is located, the mussel foot proceeds to secrete the byssus structure, a protein complex that anchors the mussel to the surface. This structure is connected by the stem inside the shell, and is bonded through the plaque on the surface. The process is shown with pictures of the most relevant moments during plaque production in Figure 2-1. Plaque and stem are connected by a high-collagen content thread. This structure provides the mussel with the ability to survive the wave-breaking and intertidal zone where they inhabit.

Byssus: water-adhesive interaction and mechanism of attachment

Water and adhesives are in conflict. This is a major challenge when designing a good adhesive to perform in underwater conditions or in moist areas. The water effects adhesion in 4 different ways: 1) forming a strongly/weakly bonded layer at interfaces, 2)

wicking or crazing into interfaces, 3) hydrolysis and erosion, 4) swelling or plasticization of adhesive by water absorption, or a combination of two or more of these effects (Wake and Kinloch 1977).

Mussels need to overcome all the issues addressed above, 1) removing weak boundary layers, 2) efficient spreading of the adhesive onto the surface, 3) developing an appropriate chemistry to produce high energy and durable contacts and 4) crosslinking the protein structure to increase the tenacity of the byssus (Waite 1987).

Water is squeezed out of the foot-surface interface by physical pushing. Once the water layer has been removed, the foot is able to produce a depression of vacuum by cavitation, where the adhesive precursor is injected in the absence of water, for spreading and later, crosslink (Waite 1987).

There is a continuous and direct contact at the plaque-substrate interface that presents a uniform, electron-dense layer (around 10-20 nm thick), which is completely created by the mussel (no biofilm deposited previously). This layer has been identified with the adhesive component of the plaque (Farsad and Sone 2012).

It is controversial the correlation between plaque surface area and surface energy. Waite 1987 stated that in non-polar surfaces (low surface energy), larger (surface area) plaques are produced with lower attachment strength. Smaller surfaces and stronger attachment have been observed in polar (high surface energy) substrates. On non-polar surfaces water interacts more weakly. Since the polyphenolic proteins are much larger, they offer a more dispersive interaction to the surface such that the water molecules are displaced and a high degree of spreading occurs. On polar substrates, water molecules are more strongly attached to the surface so the spreading does not

happen spontaneously, causing the mussel-adhesive to create a front where high energy interactions take place (Waite 1987). On the other hand, a more recent study (Aldred et al. 2005) with Self-Assembled Monolayers (SAM) has been proved the opposite effect, that is, mussels produce larger plaques in high surface energy substrates. Other different study establish no relation at all between these two parameters (Burcket et al. 2009).

When the process of attachment is finished, a byssus structure anchors the mussel onto the surface. Experiments with Mytilus Edulis demonstrate that an average of 10-20 plaques was produced after 72 hours (Burkett et al. 2009). The values of the maximum load were highly dependent on the substrate (Ackerman et al. 1996 and Burkett et al. 2009). Generally when the byssus structure undergoes loading, the failure appears at the interface adhesive-substrate, rather than in the collagen thread or in the plaque-thread connection (Burkett et al. 2009). A different approach to measure adhesion of the mussel foot proteins (Mfps) of the mussel has been developed with a surface force apparatus (SFA) (Lu et al. 2013).

Byssus: chemistry

The byssus structure has been characterized as a multi-protein complex, the thread being mainly formed by collagen and the plaque formed by 6 different proteins, known generally as mussel foot proteins (Mfp). The composition of the byssus may vary between species of mussels, while certain species have a byssus chemistry characterization that is a more challenging issue than others, as is the case of the Dreissena Polymorpha. This is because immediately after (even during) the mussel secretes the adhesive it undergoes a curing process, in other words, the proteins crosslink with each other to create a crosslinking network. This fact makes it very

difficult to isolate the different proteins and its characterization (Gantayet et al. 2013; Gilbert and Sone 2010).

Nevertheless, the whole sequence of amino acids has been obtained for the proteins that form the byssus structure in the mussel genre Mytilus. In

Table 2-1 the different composition and sequences for each protein are shown (Lin et al. 2007). Something that makes the mussel adhesive so special is the content in the protein code of a rare component called L-3, 4-dihydroxyphenylalanine, which is well known as DOPA (Figure 2-3.). DOPA is not only suggested to mediate adhesion to the surface, but is a cross-linking agent contributing to the cohesive strength of the adhesive plaque (Wiegemann 2005). This component is found in different molar percentages in each of the Mfps, being an important characterizing factor. DOPA plays an important role in surface attachment.

Table 2-1 shows how the highest content of DOPA is present in Mfp-3 and Mfp-5, so these two proteins need to be in a higher degree forming the plaque-substratum interface (Figure 2-2). The DOPA content of each protein and the degree of crosslinking can vary according to several factors, including the chemistry of the substrate. The DOPA can be modified to readjust different substrate chemistries. The time of the year is also an important factor (Matos-Perez et al. 2012).

Important factors when defining the adhesion strength of the plaque are the pH and the redox condition. It has been shown that lower values of pH improve adhesion, mainly because the oxidation of DOPA is less likely to happen (Nicklisch and Waite 2012). It is also worth mentioning the importance of the Mfp-6 in modulating the redox process. Mfp-6 presents low DOPA content and high cysteine content. Most of the thiol

groups in cysteine are not coupled leaving a great number of them reduced as cysteine decomposes. Experiments have proved that modification of the pH is not enough to prevent oxidation of DOPA, so the antioxidant effect of Mfp-6 is an important factor (thiol groups produce the reduction of dopaquinone form from Mfp-3 and Mfp-5 in a stoichiometric fashion) (Yu et al. 2011).

The spatial distribution of the proteins along the byssus structure is not well known due to the extensive crosslinking that prevents from an exact characterization. Threads and plaques present very similar amino acid contents but the composition is different. The composition of the bulk plaque as well as the plaque-substrate interface also differs in composition. Variation between fresh and aged mussel interfacial composition prove that the maturation and crosslinking process of the byssus does not stop directly following the initial curing process, but some of these proteins keep curing through a secondary period of time (Gilbert and Sone, 2010).

The polyphenolic-content of the mussel proteins interact with the substrate through 4 different energetic interactions, 1) hydrogen bonds, 2) metal-ligand complexes, 3) covalent cross-links which are initiated by a free radical mechanism between two quinones and 4) Michael-type addition compounds derived from a o-quinones (Wiegemann, 2005). Hydrogen bonds and metal-ligands are shown in Figure 2-4. It is also notable that a very unique iron-induced mechanism may play a major role during crosslinking in the curing process (Wilker, 2010).

Polydimethylsiloxane elastomer (PDMSe)

Over the past decade silicon has become a very popular material in developing devices for biological adhesion testing, microfluidic devices and a variety of experiment

set-ups related to organic and biological systems interaction (Gibson 2002, Holm et al. 2006).

Polydimethylsiloxane (PDMS) is a semicrystalline polymer, with a glass transition temperature of -120ºC and a melting point of -40ºC. The basic structure is formed by silica, oxygen and hydrogen atoms. Silica atoms are bond through oxygen within the backbone. The low electronegativity of silica (1.8) means a very polarized Si-O bond forming a polymer chain with strong bonding energy (Si-O 443 kJ/mol). This polarization however does not lead to strong intermolecular forces between the chains, since the interactions between methyl groups are very weak and shield the interaction between polar groups within the molecules. PDMS also exhibits a low bond rotation energy (3.3 kJ/mol, nearly free rotation) being the nominal bond angle 145 degrees (tetrahedral), but variable from 100 to 170 degrees without an important energy penalty. This effect makes the PDMS polymer chains very flexible and able to adapt many different configurations (Lötters et al. 1997). The basic structure of a PDMS chain segment is represented in Figure 2-5. .

PDMS elastomer (PDMSe) is a rubber (viscoelastic behavior), with a highly cross-linked structure based on polydimethylsiloxane chains and approximately 10% fumed silica filler. It is commercially available in different forms
(oil, grease, rubber, resin, or caulk).

Mechanical and chemical properties

The strong bond energy within the chain (Si-O and Si-C) makes silicones chemically stable. Silicones also present a good thermal stability and electrical insulation properties. Degradation starts only at around 400ºC and properties such as heat capacity are constant in a wide range of temperature (from -120 ºC to 240 ºC).

Optical clarity is another highly appreciated property of silicones, mostly when forming films in biological system testing because it permits for easy observation under the optical microscope.

High chain flexibility produces the presence of a high free volume giving the polymer good gas permeability to oxygen, nitrogen and even water vapor, being an important factor when using PDMSe for biological assays. (Lötters et al. 1997).

PDMSe has a very low toxicity. An initial abiotic reaction may start depolymerization followed by biological degradation (fungi or bacteria), which can produce dimethylsilanediol as a byproduct (Stevens 1998). Nevertheless this degradation does not state a hazard to the environment. Some experiments have taken place in the lab to prove possible leaching of PDMSe into salt water, but no appreciative quantities were observed (data not shown).

Surface energy

Silicones present a very low surface tension. The weak interaction between methyl group and the high flexibility of the chain allow the polymer to acquire a configuration that exposes the maximum number of methyl groups to the outside, forming a very hydrophobic surface, good for applications such as biomaterials and foul releasing technologies. Critical surface tension of wetting for silicones is higher than their own surface tension, so silicones can wet themselves making it easier to produce films and form molded pieces.

The number of low molecular weight siloxane species increases as the silicone age by the effect of prolonged radiation in field exposure tests, which produce a detriment in the mechanical behavior of the rubber that becomes more brittle and less elastic (Homma et al. 2000). When silicones are exposed to plasma treatment or partial

electrical discharge, the hydrophobic surface of the rubber can also be turned into hydrophilic by the production of radicals. Different mechanisms have been studied to explain hydrophobic recovery of PDMSe. When a PDMS surface is plasma treated, a mechanism associated with burial of polar groups in the bulk and the condensation of silanol groups occurs. This was an early attempt to explain the process of hydrophobic recovery (Morra et al. 1990). A different study theorized that polar groups are created on the surface after plasma treatment, and those new polar groups created, reorient themselves attempting to decrease the surface energy of the system (Tóth et al. 1994). However, the role of these polar groups in the hydrophobic recovery is much less important than the diffusion of LMW from the bulk to the surface. Later in time, a different study proposed that a wettable silica-like brittle layer is produced on the surface of PDMSe as an effect of exposure to partial electrical discharge. Analysis of the surface composition with XPS at different depths of this layer shows that cracks are produced in the process and a diffusion of PDMS chains must occur through those cracks (Smith et al. 1992). In another experiment, where thermally induced or mechanically deformed PDMS films were studied, confirmed that a cracked surface presents a faster rate of hydrophobic recovery than those untouched samples, so the silica-like layer inhibits diffusion of LMW chains (Hillborg and Gedde 1998).

Wettability, surface energy and topography

Some concepts need to be explained to understand the subject of this thesis. Wettability is the ability of a liquid to interact through different intermolecular forces with a solid surface when brought together. It is said that a liquid will wet well a surface when enough strong interactions between the molecules in the liquid and those in the surface exist, so the liquid spreads. What happens during this process is that a new interface

(liquid-surface) is created and a new balance between cohesive and adhesive forces appears. Cohesive forces are attractive forces (intermolecular forces) that exist between molecules of the *same* substance which cause a tendency in liquids to resist separation. Adhesive forces are attractive forces between two different substances (in this case, liquid and solid surface). In order to achieve a good wetting ability in a specific system formed by a liquid and a solid surface of different composition, the formation of the interface must be favorable, in other words, the system must lower its overall energy by spreading and forming new intermolecular interactions within the interface.

Surface energy is a measure of the energy associated with the disruption of the chemical bonds that occurs when a new surface is created. Molecules in the surface of a material have a higher energy state than those same molecules in the bulk; since the forces acting on a molecule at the surface are pulling the molecule inward (Figure 2-6.). The difference in energy between the surface molecules and the bulk molecules is the surface energy.

Contact angle: Young equation

Consider a droplet in equilibrium with its own vapor and a flat, solid surface at constant temperature. The balance of cohesive and adhesive forces occurring in the system is going to determine the shape of the droplet, which can be geometrically defined by measuring the contact angle.

γ_L and γ_S are defined as the liquid-vapor and the solid-vapor interfacial surface energies, and γ_{LS} as the liquid-solid interfacial surface energy (Figure 2-7). The angle θ is called the contact angle, and gives an idea of whether the interaction between the liquid and the solid (wettability) is good. Contact angle over 90º represents a

hydrophobic surface. If we are considering that the liquid is water and less than 90º would mean good interaction (hydrophilic). The Young equation is an application of Laplace derivation to the case of a single droplet on top of a flat surface. In this case, a simple force balance equation can be written as follow:

$$\gamma_S = \gamma_{SL} + \gamma_L \cos\theta \quad (2\text{-}1)$$

Wettability: Wenzel and Cassie-Baxter models

The wettability of a liquid over a solid surface is mostly determined by two different factors: the surface chemistry and the topography. It is important to recall that good chemical interaction (i.e. hydrogen bond, Van der Wall's forces…) between the molecules of the liquid and those on the surface of the solid will improve the contact and as a result the wettability increases. Wenzel model describes a homogenous wetting behavior (Figure 2-8). On the other hand, Cassie and Baxter model represents better the wetting behavior in heterogeneous surfaces (Figure 2-8). It is common to associate non-wettability with the latter model.

Contact angle (CA) is frequently used as a technique to characterize the wettability of a surface. CA greater than 150º are usually related to superhydrophobic surfaces. The larger the angle the better the hydrophobic character of the material. Roughness of the sample also has a great effect on wettability since it can positively contribute to the destabilization of the liquid on top of the material enhancing the hydrophobic character. Research has been done about the metastable state of liquid drops on top of a surface that has proved how the roughness geometry needs to follow

a mathematical distribution in order to enable stable or unstable Cassie-Baxter state (Marmur 2013).

Engineered Roughness Index (ERI)

Different methods of surface modification have been researched in order to prevent marine biofouling through a non-chemical approach. Hierarchically wrinkled topographies has been produced on PDMS through ultraviolet/ozone treatment, with reproducible results that go from tens of nanometers to a fraction of a millimeter in the same sample, decreasing barnacle settlement with no necessity of chemical modification (Efimenko et al. 2009).

In order to evaluate the effect of feature size, shape and roughness on the settlement of different microorganisms, an empirical factor known as Engineered Roughness Index (ERI) was proved to be valid through several tests. An indirect relationship exists between ERI and organisms settlement. A first attempt was made by taking into account Wenzel's roughness factor (r), depressed surface fraction (f_D) and freedom for movement (df) (Schumacher et al. 2007b).

$$ERI_I = \frac{r * df}{f_D} \quad (2\text{-}2)$$

Wenzel's roughness factor (r) is the ratio between the actual surface area, which takes into account the side area of the ridges as well as the top of the features and depressions, to the projected surface area. This factor is always more than 1 when roughness of any kind exists. Depressed surface fraction (f_D) is the ratio between the surface area between protruded features and the projected surface area. Freedom of movement (df) refers to the complexity of the features and how the organism is allowed to move between them. The new ERI offers the possibility to analyze more accurately

the effect of surface roughness with respect to the Wenzel model and antifouling behavior (Schumacher et al. 2007b). Other related experiments showed how the aspect ratio is an important factor when designing an effective engineered topography for antifouling (Schumacher et al. 2007a).

In the same line of study, Long et al. (2010) refined ERI by the substitution of the term “df” (degree of freedom) by “n”, number of different features on the surface. The term $1-\varphi_S$ is equivalent to depressed surface fraction (f_D). (See equation 2-3).

$$ERI_{II} = \frac{r*n}{1-\varphi_S} \quad (2\text{-}3)$$

Experiment regression is done by a natural logarithmic transformation that yields a linear correlation. The equation states as follows:

$$ln\left(\frac{S}{S_{SM}}\right) = m * ERI_{II} + b \quad (2\text{-}4)$$

S represents the number of organisms settled in the modified surface, $\mathbf{S_{SM}}$ the number of organisms attached to the smooth surface (control), **m** is the value of the slope in the regression and **b** the Y-axis interception when x=0. Typically linear correlations values over 85% were reached.

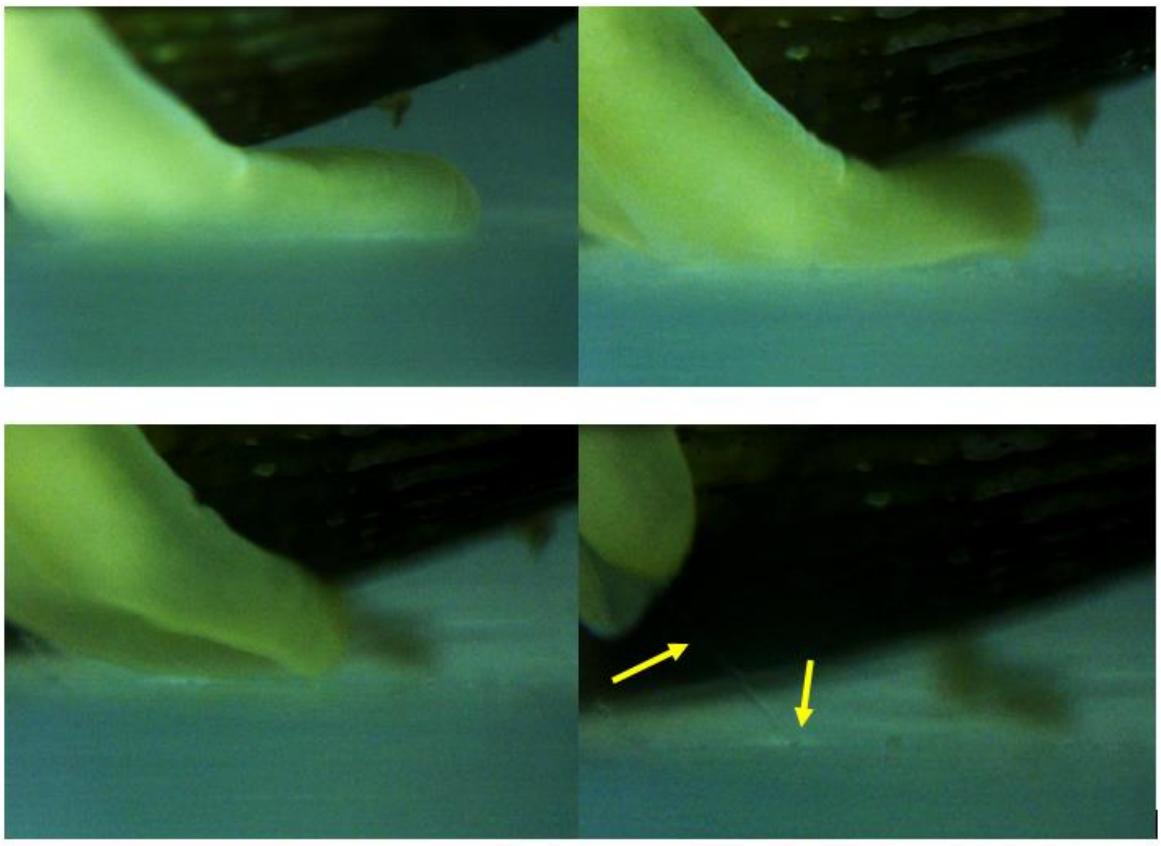

Figure 2-1. Progress of movements during mussel plaque deposition. Fresh deposited byssus can be observed (arrows point the location). The process takes around 3 minutes (Data not shown) (Photo taken by author).

Table 2-1. DOPA-containing proteins of the byssus of Mytilus species. Reused from Lin, Q., Gourdon, D., Sun, C., Holten-Andersen, N., Anderson, T. H., Waite, J. H., et al. (2007). Adhesion mechanisms of the mussel foot proteins mfp-1 and mfp-3. Proceedings of the National Academy of Sciences, 104(10), 3782-3786. Copyright 2007 by PNAS. Reused with permission.

Protein	Mass, kDa	pI	DOPA, mol%	Location	Ref.
mfp-1	108	10	10–15	Cuticle	5, 6
mfp-2	45	9	5	Plaque	7, 8
mfp-3	5–7	8–10	10–20	Plaque	9
mfp-4	90	10.5	2	Plaque	10
mfp-5	9	9–10	30	Plaque	11
mfp-6	11	10	2	Plaque	12
preColD	240	9	<1	Thread, plaque	13
preColNG	240	9	<1	Thread, plaque	2

Results for mfp-6 are for *M. californianus*; all others are for *M. edulis*.

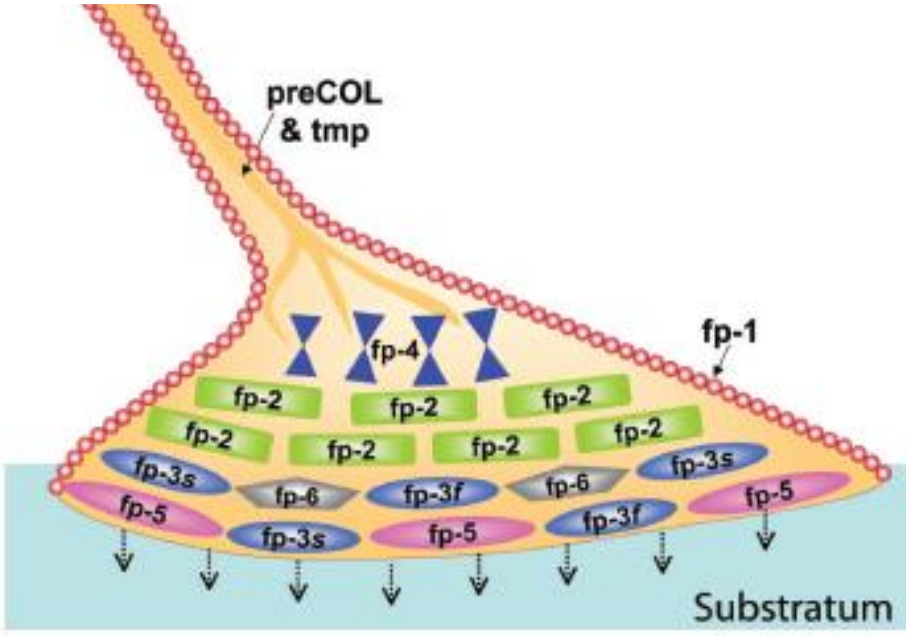

Figure 2-2. Scheme of the distribution of the different mussel foot protein along the byssus structure Reused from. Nicklisch, S. C., & Waite, J. H. (2012). Mini-review: The role of redox in Dopa-mediated marine adhesion. Biofouling, 28(8), 865-877. Copyright 2012 by Taylor & Francis. Reused with permission.

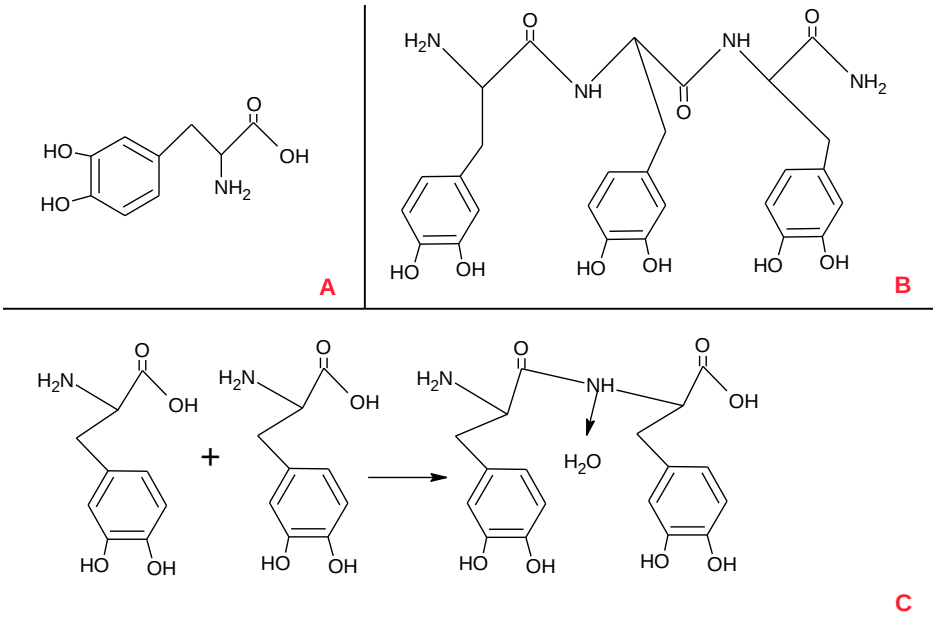

Figure 2-3. Chemical structure of L-3,4-Dihydroxyphenilalanine A) Basic structure of (S)-2-amino-3-(3,4-dihydroxyphenyl) propanoic acid, as well known as L-DOPA B) Chain of DOPA molecules C) Reaction of two molecules of L-DOPA

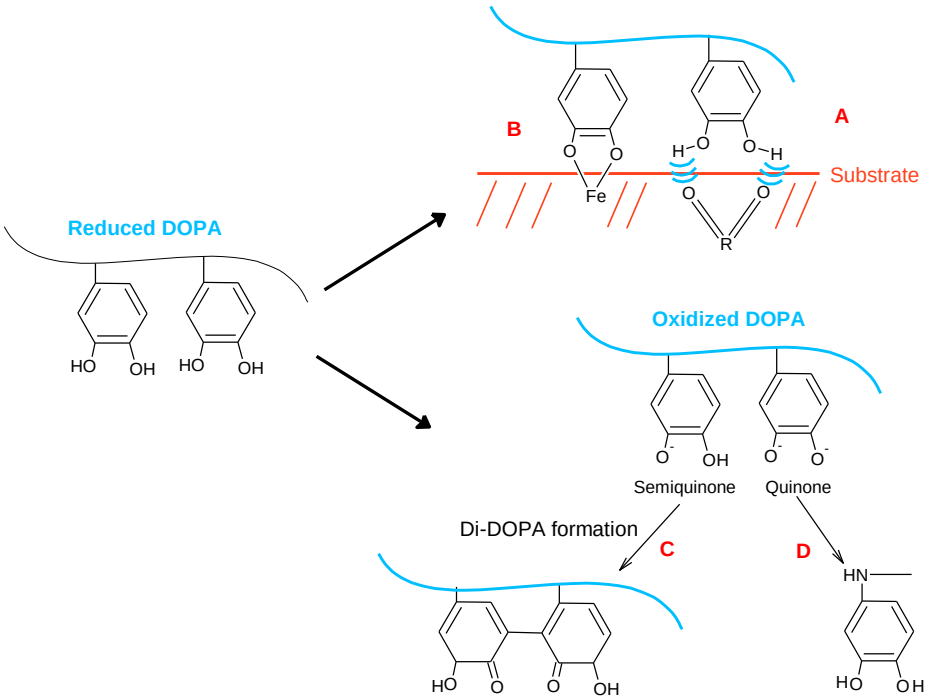

Figure 2-4. Adhesive and cohesive interactions of mussel protein through DOPA, A) Hydrogen bond, B) Metal complex formation, C) Di-DOPA formation and D) Michael addition.

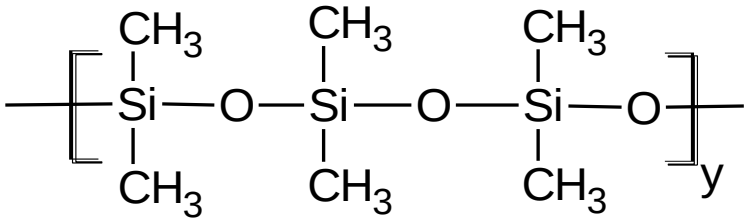

Figure 2-5. Basic structure of a PDMS chain segment

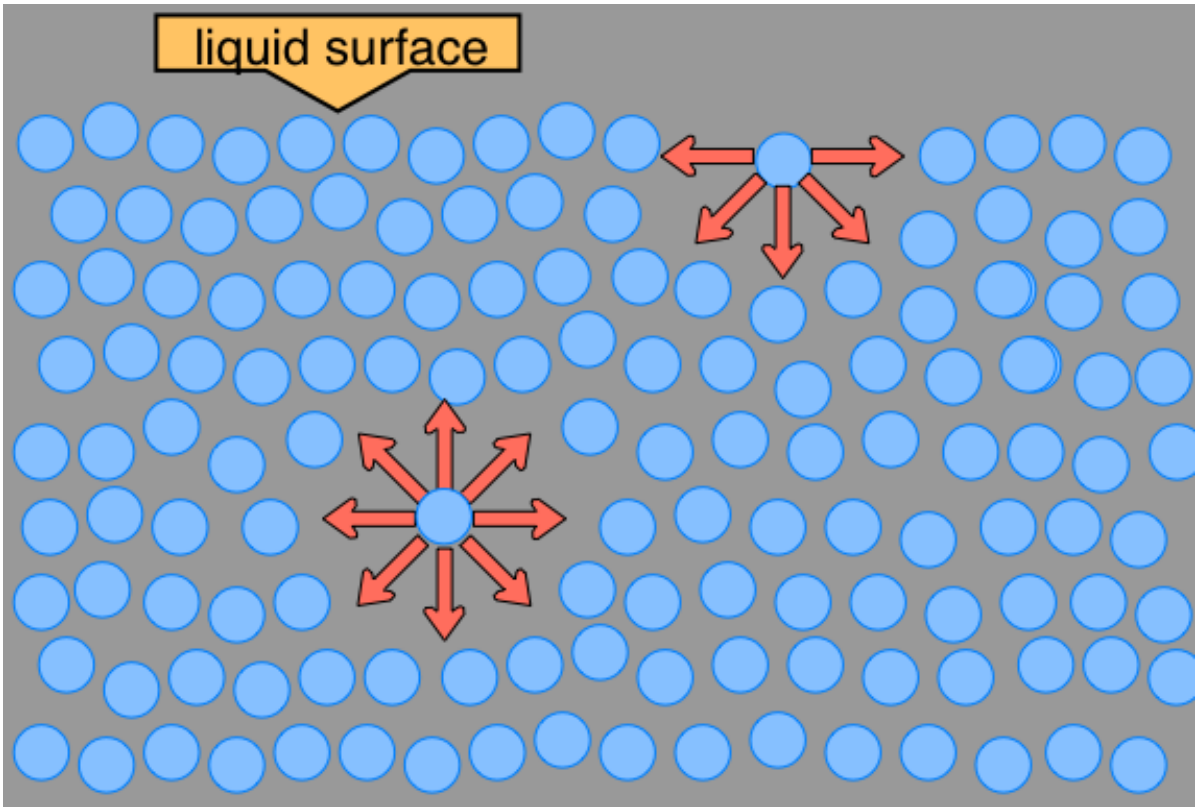

Figure 2-6. Diagram of forces on molecules in a liquid. Above a molecule in the surface, being pulled inwards. Below a molecule in the bulk, being pulled in all directions. Blue dots represent water molecules and arrows are forces.

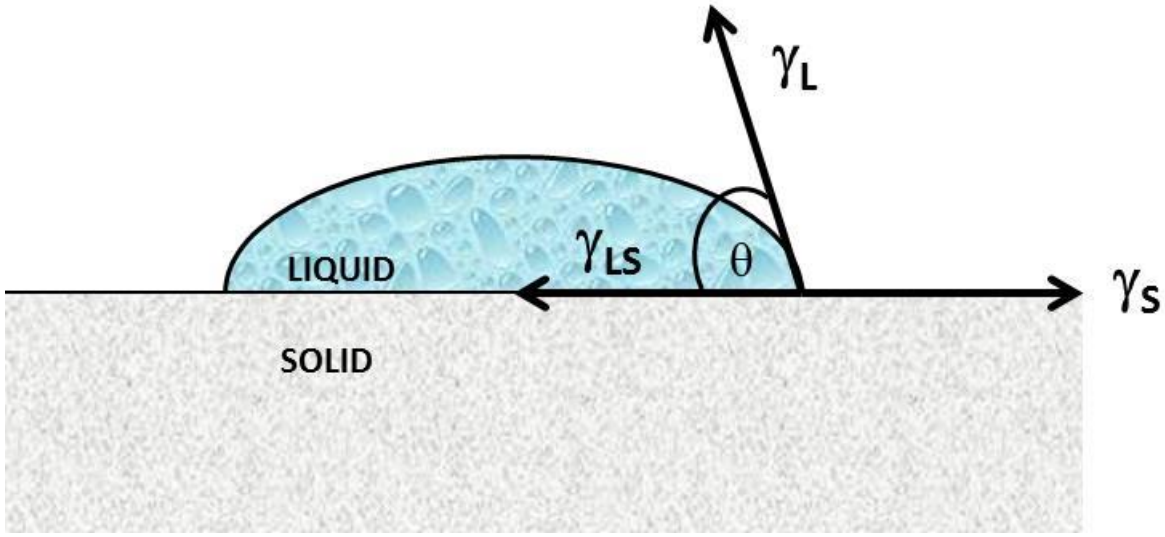

Figure 2-7. Schematic diagram of liquid droplet on solid surface.

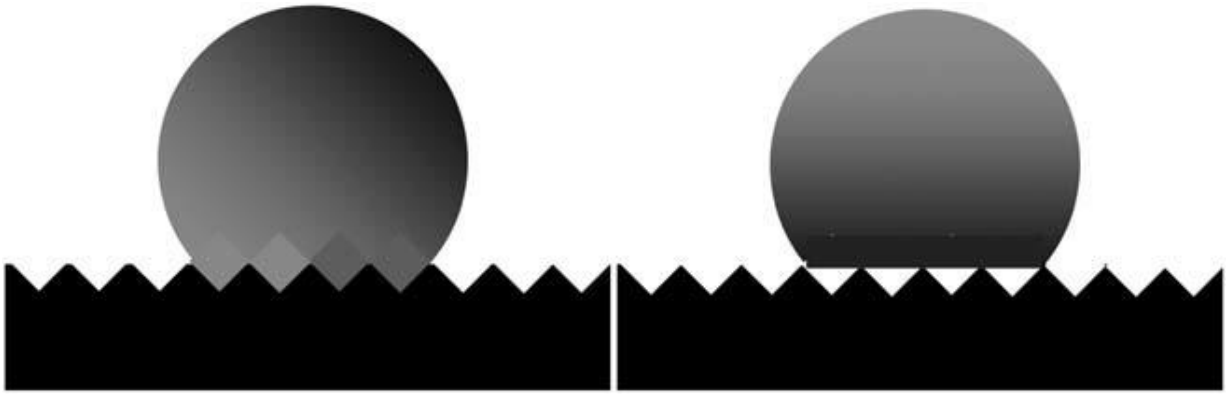

Figure 2-8. Schematics representation of Wenzel model (left) and Cassie Baxter (right). Reused from Marmur, A. (2013). Superhydrophobic and superhygrophobic surfaces: From understanding non-wettability to design considerations. Soft Matter. Copyright 2013 by Royal Society of Chemistry. Reused with permission.

CHAPTER 3
MATERIALS

Setting up the tank: cultivating mussels

Mussels are cultivated in a tank in the lab, where simulated conditions similar to the natural environment of the animals are kept at all times, in order to minimize negative effects in the experiment. The response of the mussels in the tests must be the closest to the response expected in natural conditions. For this experiment the next list of supplies has been required:

- Two glass tanks, 10 and 40 gallons respectively.
- Clear airline tubing (Top Fin® Airline tubing-25'' long).
- Bubbling air stones (Top Fin® Airstones with nozzles)
- Air pump (Top Fin® Air pump AIR 3000)
- Gravel (Top Fin® Premium quality aquarium gravel-50lb)
- Salt (Instant Ocean® Sea Salt)
- Hydrometer (Instant Ocean® hydrometer)
- Dechlorinator (Kordon® NovAqua® Plus water conditioner and Dechlorinator)
- Water filter (Marineland® Penguin® Bio-wheel aquarium power filter mod. 100B and 200B)
- Thermometer (Top Fin® floating glass aquarium thermometer)
- Valves (Top Fin® Metal T-valve)

Testing kits

As recommended in the literature (Burkett et al. 2009), to ensure appropriate conditions in the tank when raising mussels in the lab, different properties must be analyzed and controlled at all times. The water was tested for pH (8.5), salinity (specific gravity=1.025), temperature (22-25 ºC), ammonia (0.1 ppm max), nitrite (0.2 ppm max),

nitrate (10 ppm max), carbonate (7-11 ºdKH) and phosphate (0.03 ppm) once a week using test kits. For salinity, simple measures with a hydrometer were used. Ammonia, nitrite, nitrate, carbonate and phosphate were tested with API (American Pharmaceuticals) test kits.

DT's Premium Reef Blend Phytoplankton

Feeding animals when being raising in a lab is a critical element of the process. In this case, following advice from literature (Burkett et al. 2009), DT's Premium Reef Blend Phytoplankton was utilized.

Silicone elastomer: SILASTIC T-2

A silicone based elastomer polymer was used in order to modify the topography. The product was Silastic ® T-2, shipped from Dow Corning. This product is a silicone moldmaking rubber, translucent and with high strength. It is based on two component materials consisting of SILASTIC T-2 base (referred as the "base") and SILASTIC T-2 high durometer curing agent (referred as the "curing agent"). There are trimethylated silica particles also present in Dow Corning's formulation in order to increase the material's mechanical stability. The curing reaction is shown in Figure 3-1. .

SILASTIC T-2 has been extensively used in Dr. Brennan's research group and the material has shown to be suitable due to its transparency, low shrinkage and its ability to reproduce topography (even those in the range of a few micrometers) in a high quality standard. The typical properties of this material after cured according to specifications and provided by the manufacturer (Table 3-1.)

The ratio of base to curing agent in weight used was 10:1, even though it has been shown experimentally in previous work in the lab (data not shown) that ratios 9:1 and 11:1 did not modify significantly some important properties of the elastomer such as

crystallization temperature, melting temperature or glass temperature, by mechanical properties measured with Dynamic Mechanical Thermal Analysis (DMTA).

Allyltrimethoxysilane (ATS): silane coupling agent

Silane coupling agents such as ATS are silicon-based components containing both organic and inorganic reactivity in the same molecule. These chemicals work as a bond between an inorganic substrate and an organic component. By using ATS a connecting interface can be created between PDMSe and the glass even though the dissimilarities.

ATS is used in this study in order to achieve a higher degree of interaction between the silica glass slide and the PDMSe that was cast onto its surface, without which the PDMSe film would just peel off the glass surface. Methoxy groups from ATS react with the hydroxyl radical produced onto the surface from the silica structure through a condensation reaction producing methanol as a byproduct (Figure 3-2). ATS is applied onto the slide as a solution with ethanol in a controlled pH environment (pH=4.5), so more hydroxyl groups are produced from the silica structure.

Hexamethyldisiloxane (HMDS)

HMDS was used in our experiments to prevent strong bonding between the wafer and the PDMSe film cast on top of it. On water-free surfaces, HMDS chemically bonds its Si atom to the oxygen of hydroxyl groups from the silica glass, releasing ammonia in this reaction. The methyl groups of the HMDS fragment, thereby forming a hydrophobic surface and thus resisting wetting and adhesion (Figure 3-3.).

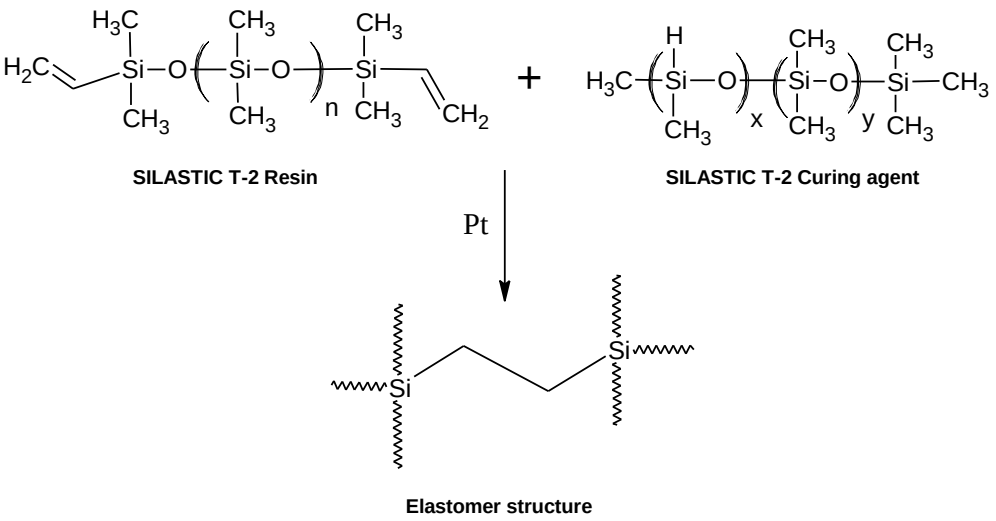

Figure 3-1. Curing reaction between the base resin and the curing agent of SILASTIC silicone

Table 3-1. Typical properties of Silastic® T2 (Dow Corning), from Dow Corning product information sheets

Characterization test	Value
Color appreciation	Translucent/transparent
Viscosity (Base)	50,000 cp
Viscosity (Curing agent)	550 cp
Mixed (10:1 weight) specific gravity	1.12
After 24 hours of curing	
Tensile strength	0.55 Mpa
Elongation	290%
Tear strength	120 ppi (Die B)
Linear shrinkage	<0.1%

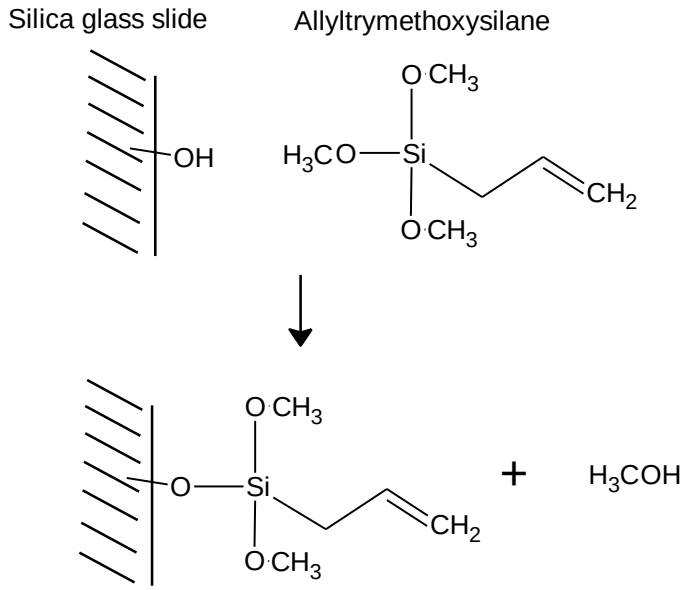

Figure 3-2. ATS coupling agent reaction with silica glass

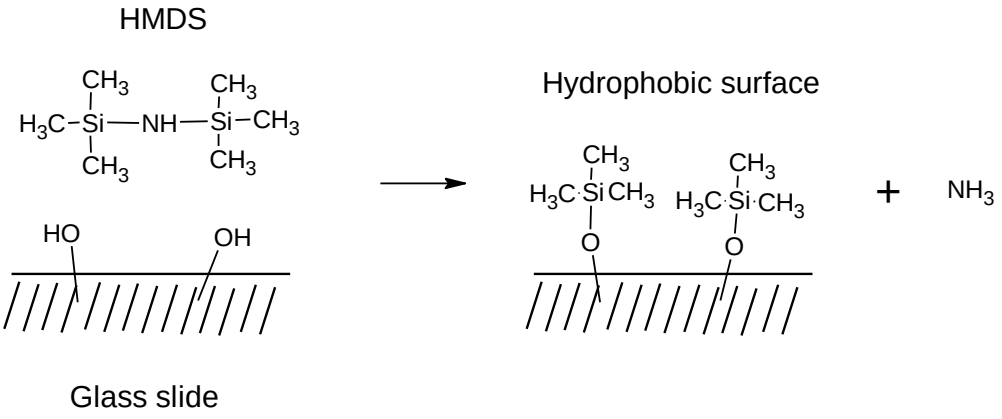

Figure 3-3. HMDS reaction onto silica glass slide.

CHAPTER 4
METHODS

Cultivating mussels

Adult mussels (*Geukensia demissa*) between 30 and 45 mm are obtained from Duke University (North Carolina), Dr. Rittschof's research group. The mussels are raised in the lab in two different tanks running in parallel under the same conditions and parameters values. One of the tanks has a capacity of ten gallons and the other holds twenty gallons. Conditions for an appropriate environment are provided through adjustment of temperature, salinity and feeding source. The parameters in the tank are tested periodically.

Setting up the aquarium. Safety and previous considerations

The location of the aquarium has to be strong enough to resist the weight. It is also required to be on a flat surface with easy access for researchers to manipulate the conditions as needed. One must be sure that the standing researcher can reach all corners of the tank with his hands before start filling the tank.

Electrical cords and tubing that run in and out of the tank must be arranged in a U-shape or in a loop. This prevents any leakage from the tank from running down the cord and onto the loop. Outlets around the tank are necessary, but they must be protected from any leakage, splash from the tank or experiment handling. An appropriate lid must be chosen and its placement ensured onto the tank to prevent from splashing.

Do not begin adding components or filling with water until be sure the location is appropriate. All safety issues must be discussed with the research advisor before setting up the aquarium.

For the first-use of the tank, clean with a diluted (1/5) solution of bleach accompanied by a very intense water rinse. A lid must be placed onto the surface to avoid excessive evaporation and contamination. This also prevents from splashing. The tank should not be exposed to direct sunlight due to subsequent promotion of algae growth. For a first-time use tank, was also necessary to leave the whole system running (air pump and filter) for at least 5 days.

The water in the aquarium was DI water (conductivity=18.0 Ω) obtained with Barnstead EASYpure ® II (ThermoScientific) and Instant Ocean® Sea Salt until the water has a value of specific gravity (measured by hydrometer) between 1.023 and 1.025. For a better mix between the water in the tank and the salt, high-concentrated dissolutions of salt are previously made in a beaker and then added to the tank. The air must be pumping at all times. A second smaller tank, around 10 gallons, was located next to the big tank in which the tests were made. The conditions on this tank are equal to that of the larger tank. In order to get accurate salinity values, approximately 50 grams of Sea Salt per liter must be added to the tank, but the measures must not be taken until at least 48 hours later, during which aeration must be active all the time.

Water in the tanks was continuously and vigorously aerated by using a pump (Top Fin® Air Pump AIR 3000), with 4 bubbling air stones in the big tank and only 2 for the small tank. Clear line plastic tubing was used to connect the air system. A water filter with a biologically supported system was used, Marineland® Penguin® Bio-Wheel Aquarium Power Filters (mod. 100B for the small tank and mod.200B for the big one). The filter must be working 24/7, except for a period of 8 hours after each feed.

Conditions in the tank

Conditions reproduced in the tanks are those (averaged through the last 5 years) for Gulf Jackson (Levy County, FL) during spring, considering these values as representing the west coast of Florida. Data is provided by the University of Florida/Institute of Food and Agricultural Sciences (IFAS) Shellfish Aquaculture Extension Program (SAEP), through the website http://shellfish.ifas.ufl.edu/. Those conditions are 74ºF, salinity of 32ppt (around 1.024 specific gravity according to NOAA conversion tables) and 7-7.5 pH. Temperature was measured with a floating thermometer. The value was 74ºF (24ºC) with no chilling or heating system attach to it. Salinity was measured weekly with a hydrometer and it had to be in the range of 1.020-1.025 all the time. The water was tested also for pH, ammonia, nitrite and nitrate once a week, and calcium, carbonate and phosphate once every two weeks, using API (American Pharmaceuticals) test kits.

Mussel aquarium maintenance protocol

A new protocol to raise mussels in the laboratory setting was developed to reduce mortality following the directions Dr. Stafslien (University of North Dakota) provided. I have created a schedule to facilitate the maintenance of the tank conditions. It has been uploaded to the Brennan group research drive ("FranciscoCastro"→Protocols→Water tank maintenance protocol). Table 4-1. shows the monthly schedule and some specific directions are explained in details in the following paragraphs:

Water replacement: 10% of the tank volume was replaced by fresh artificial sea water, produced by mixing DI water and Instant Ocean ® Sea salt. It was highly recommended to measure the specific gravity of water before adding the fresh water, so

the salinity parameter could be adjusted daily by adding a more or less concentrated portion of artificial sea water (value of specific gravity must be around 1.025 at all times). Another consideration was that the water replacement must take place before feeding the mussels and testings water conditions. Keep in mind, at least one hour must pass after the addition of fresh sea water before conditions can be tested.

Mussel feeding: DT's Premium Reef Blend Phytoplankton was fed to the mussel twice a week (Monday and Thursday). A pipette was used to measure the volume added. Mussel feeding was probably the most critical step in keeping healthy water conditions, since it can rapidly increase the ammonia content in the water and poison the animals. The ratio of feeding volume was of 0.3 mL per mussel per feeding. The water filter must be disconnected at least for 8 hours when algae culture was added to the tank.

Water testing: The water parameters to be tested are: pH, salinity, temperature, ammonia, nitrite, nitrate, phosphate, hardness and calcium. The tests were done using API (American Pharmaceuticals) test kits. Salinity was tested with a hydrometer and the temperature with a floating thermometer.

Complete water replacement: To prevent the build-up of algae, a complete water replacement was done every 4 weeks in every tank. Since the mussels were going to be transferred from one tank to the other both tanks were operated continuously so the conditions were constant. Complete water change could not occur at the same time in both tanks. After the water change the tank could not be used for the next 4 days, until proper parameters were reached again (Table 4-1.).

PDMSe patterned samples preparation

All the samples were prepared to be tested using PDMSe (Silastic® T2) from Dow Corning as a basis material, and the procedure followed instructions from the protocols previously reported by Dr. Brennan's research group, *Protocol for Making Patterned Slides Directly from Wafer* and *Unpatterned PDMSe slide preparation*.

All the samples were cast onto precleaned microscope glass slides (Fisher Scientific 75 x 50 x 1 mm). Before use, each glass slide bonding surface was pyrolyzed (both sides), using blue flame from a bunsen burner to remove the pretreated layer they come with from the factory. The slides were cooled in the air on top of clean kimwipe. The glass slides were then moved to the hood and covered carefully with a solution of allyltrimethoxysilane (ATS). The ATS solution was prepared in a polypropylene cup by mixing 30mL of ethanol (190 proof) with 0.17mL of ATS. Before the addition of the ATS, the pH had to be adjusted to around 4.5, generally by adding two drops of glacial acetic acid. The reaction was left for at least 5 minutes before use. After the glass slides reacted with the ATS solution for 3 minutes, the glass slides were rinsed with ethanol and place onto a dry kimwipe. Finally, after 10 minutes in the oven at 120ºC, the glass slides are ready to be used.

The wafers used to cast the textures on the silicones samples were made by photolithography as described in Alavi, et al. 1992. The wafers were cleaned with ethanol before use, dried with compressed nitrogen gas and placed in a vacuum chamber for 3 minutes to assure all water and contaminants were removed from the surface. The chamber was then disconnected from the pump, but the vacuum was not released, since it was used for vapor deposition of hexamethyldisiloxane. HMDS was coated onto the wafers by connecting a syringe line to the vacuum chamber and

allowing the transfer process to occur for 5 minutes. Two glass plates were used as a mold. The plates were covered with polyethylene terephthalate (PET) films with double-sided tape.

The unmodified silicone elastomer was prepared by mixing in a 10:1 ratio in weight (10 parts of resin to 1 part of curing agent) using approximately 25 grams per wafer. The mix was put in a tri-corner polypropylene (PP) beaker, where it was stirred for 5 minutes with a PP spatula, making sure to scrape the sides and bottom of the beaker to produce a better mixture. After this time, the beaker with the mixture was placed into a vacuum chamber for degassing over 15 minutes, to rid it of any trapped air bubbles.

The process of patterned PDMSe on top of a glass slide has two steps. First, a PDMSe film with the texture was cast. Glass slides are used as spacers (1,000 microns thick) by taping them to each corner. After this, wafers were also taped with double-sided tape to the PET film, and pre-cured PDMSe was poured on top of it. After pouring, bubbles, still trapped on top of the mixture, were released by using a syringe needle. Finally the other glass plate was placed on top of the PDMSe (with the PET facing down) and pressed until the top glass plate rests on top of all spacers (Figure 4-1). A 5 lb weight was placed on top of everything and allowed to cure for 24 hours. Once the 24 hours have passed, the PDMSe patterned sample needs to be carefully peeled from the wafers and the PET film, making sure the film was pulled when peeling in the same direction of the texture, to prevent from producing damage to the features. Then the PDMSe film was placed, with texture facing down, onto a glass plate (without the PET sheet). Spacers had to be put (1,600 microns) to ensure the thickness of the sample.

The other glass plate was covered with PET film and ATS-treated glass slides are taped using double-sided tape, with the treated side facing away from the glass. Again, mixture 10:1 of base to resin was poured on the back part of the textured PDMSe sample obtained the day before, and the two plates are pressed together, allowing the fresh, not cured, PDMSe acting as an adhesive. It must be pressed until the top plate rested on top of the spacers. The weight was placed on top of everything and the system was allowed to cure for 24 hours undisturbed. Finally, the glass slide was peeled and the excess PDMSe was cut along the edges (Figure 4-1).

The surfaces of the samples were pretreated before starting the test. This pretreatment consists of wetting the surface completely with water (from the aquarium). Since the samples present a rough topography, air pockets trapped between the spacing or air bubbles on the surface need to be prevented. To ensure that the surface was completely wet, the samples were submerged in the aquarium 24 hours previous to the mussel plaque production test.

PDMSe patterned samples characterization

Every sample was characterized in order to ensure the features were replicated from the wafer. In addition, the features were inspected for any deformation, missing ridges and heterogeneity of pattern. Also the size of the features was measured. Every sample produced was taken to the optical microscope, and observed at x10 magnification in different spots onto the surface. If the sample does not present any problems, it can then be used for testing. The direction of the channels must be examined as well, in order to place the mussel, always in the same direction, during the tests.

To verify that the size of the channels, height of the ridges and width of the spacing was correct, a sample silicone from each different texture was observed with Scanning Electron Microscope (FEI XL-40 FEG). Flat metallic stages were used for sample preparation to measure the width of the ridges and the spacing, and vertical stages for the depth of the features. All of the samples were gold-coated by plasma sputtering (Denton Vacuum, LLC, Desk II cold sputter/ECTH Unit and Carbon evaporation accessory). The process was carried out at a pressure of 50 mtorr and an intensity of 45 miliamps for 40 seconds. The voltage used in the SEM was 4 kV, which was bright enough to obtain good quality and to also prevent damage to the sample. The results were obtained by comparison with the automatic measure bar displayed in the pictures taken (Figure 4-2.).

Mussel plaque production

When a mussel was in contact with a surface, plaque production occurs naturally on top of any substrate, as a mechanism of survival. Nevertheless, the mussel foot detects the suitability of different sites around the animal and it may produce the migration of the mussel out of the sample, onto a more favored substrate. To prevent this from happening, a rubber band (length=7/8'' x width=1/16'' x gauge=1/32'', Universal®) was placed around the mussel and the sample so the plaque production was forced to happen onto the topography. The band must be strong enough to prevent the animals from moving but at the same time must permit the opening and closing of the shell, enough to let the foot extend out of the sample to produce the plaques.

Mussel selection was another important issue. Only healthy mussels were used. To ensure this good condition, byssus threads needed to have been deposited previously onto the substrate of the aquarium, and the animal had to prove motion

reaction when contact. No gaping, motionless organisms were used. It was also necessary that the mussels have been living at least for a week in the aquarium before they are used for experimentation. Selection based upon the size of the mussel was also mandatory. Since values of surface area of the plaques were highly dependent on the size of the mussels, they have to be selected within the narrow range of size (between 35-45 mm).

PDMSe topographies cast onto precleaned microscope glass slides (Fisher Scientific 75 x 50 x 1 mm) are be placed into the aquarium, and only ONE mussel for every sample (around 20 mm length) is attached with the rubber band to produce the interaction. Ten different mussels are tested for each sample. Topographies of a 1:1 ratio of 5, 20, 50, 100 and 200 microns, plus the smooth PDMSe used as a control are tested, adding up to a total of 60 mussels per experiment. The width of the ridges and the spacing was the same. The experiment run for 72 hours, the necessary amount of time according to literature (Burkett et al, 2009, Aldred et al, 2009) and previous observations done in the lab (data not shown) to produce adequate interaction and plaque adhesion. Mussels were observed daily during the experiment, ensuring proper placement throughout the trial.

The mussel was able to stick the foot out and move it around with a broad range of freedom, since the organ presents a high degree of flexibility and the capacity of getting to a long extension. Nevertheless, it has been proven previously in the laboratory (data not shown) that certain directions, in relation with the location of the mussel onto the sample, were preferred. To ensure reproducibility and homogeneity of the obtained data, the position of the mussel on the sample followed the same

orientation in all tests, so the animals were always on the same position with respect to the pattern (Figure 4-3.). This improved the statistical significance of the Nuclear Form Factor (NFF) values.

Extraction procedure

The method of extraction was very simple. First, the glass slide with the attached mussel was removed from the tank. The threads of each of mussel were cut carefully using small scissors or a razor. Detachment of the plaque at the plaque-surface interface was to be avoided by following appropriate procedure. Samples to be tested for strength were not cut from the surface.

Samples were cleaned using three different salt-water solutions followed by rinsing with three different ethanol-water solutions. Salt solutions with values of specific gravity of 1.015, 1.005 and DI water, were prepared. Sample is submerged in a Petri dish with the first solution (1.015), later with the second solution (1.005) and finally in the DI water, with a spacing of 6 minutes between each. The sample is then washed out with DI water, and cleaned with three ethanol-water solutions. The solutions have a composition of ethanol to water of 1:4, 2:4 and 3:4. There is also a gap of 6 minutes between them. Finally, the sample is put into a vacuum for 5 minutes to ensure a dry surface. This treatment prevented the plaque and the surface of the sample from cracking with drastic changes in salinity (Figure 4-4.), while also providing a clean surface.

Measuring number of plaques

Once the samples had been washed and dried, optical microscopy characterization was used to count the number of plaques produced on each sample. The whole patterned area of the sample was swept with the microscope (Axioplan 2,

Zeiss) at a magnification of x5, and a picture of each plaque encountered is taken. In some cases, more than one plaque appears on the screenshot. A second sweep at higher magnification (x10) was made for each sample. Pictures of individual plaques on the surface are also taken at this magnification (Figure 4-5.). Since this method proved itself to be unreliable, the number of plaques the mussel produced was measured directly by counting the number of steps (individual plaque detachment) from the data collected with the texture analyzer (See Tensile test: texture analyzer).

Pictures must be taken from the same orientation with respect to the topography pattern in order to certify that the measurements of the Nuclear Factor Form are all equal, as to obtain a common conclusion.

Measuring surface area and Nuclear Form Factor (NFF)

Since one of the aims of this study was to evaluate the effect of the topography on the mussel plaque adhesion and the spreading of the mussel adhesive onto a surface, measuring the surface area of the plaques onto different topographies was a critical issue of this study. Images from the optical microscope with a magnification of x10 were processed using ImageJ®. Eight of the pictures, taken for every topography, were selected randomly . Images where the edges of the plaque were diffused, where two or more plaques overlapped or the collagen threads or any other artifact decreased the quality of the image were automatically discarded.

A threshold was established, by ImageJ, for each image , to enhance the shape of the plaque relative to the pattern (Figure 4-6). Once the image was enhanced and the edges easily identified, the shape was traced manually, since the accuracy is higher than if automatically traced by the software. The length and the width, values necessary to define the Nuclear Form Factor (NFF), were also obtained manually. NFF is well

defined in Figure 4-7. . NFF was used previously by Carman et al. in 2006 for research on alignment of porcine cardiovascular endothelial cells, and was previously defined by Dunn and Heath in 1976, in their research on heart fibroblast cells contact guidance study.

Even though cells were not tested, the morphology of the adhesive (plaque) onto different samples was registered as a way of evaluating the capacity of the adhesive to adapt to different shapes according to the surface roughness and design, as to minimize the energy barriers that the spreading-front of the adhesive needs to undergo.

Degree of penetration (Scanning Electron Microscope)

The procedure and equipment used in this part were the same as those described previously in “PDMSe patterned samples characterization” section of this thesis. Other techniques and tools were tried unsuccessfully such as microtome and liquid nitrogen freezing split, but the size of the plaque and the properties (viscoelastic behavior) of the silicone made these processes not viable.

Tensile test (texture analyzer)

Tensile force of the mussel was measured in this project using a texture analyzer (XT plus Texture analyzer from Texture Technologies Corp.) (Figure 4-8.).

The mussel plaque production test was performed as described in the part “Mussel plaque production” of this thesis. The only difference is that the byssus production was ended after 48 hours instead of 72. Every mussel taped to the sample was extracted carefully from the water and the rubber band cut. In the case the plaque production was not satisfactory (less than 5 attachments by simple visual observation) the experiment was repeated on top of the same sample with a different mussel. The glass slide was mounted on the stage of the texture analyzer by taping just the side,

and the mussel was gripped with a clamp, properly mounted on the movable arm of the device (Figure 4-9.).

The test ran under steady elongation, which means that the mussel was pulled off at a continuous speed (0.5 mm/sec) while the force was measured at every instant. Settings for the test are 4 points per second, tension mode, 5 gr. trigger force and 70 mm maximum elongation. During the test the individual threads coming from the mussel and connected to the sample can be seen stretched and one by one they undergo failure (rupture). The experiment is finished when no threads can be observed connected to the sample. No more than 5 minutes passed from the mussel extraction to the end of the test, because Mfps change structure as they dry. According to literature plaques as well as threads removed from sea water experience changes in mechanical properties within 10 minutes (Burkett et al. 2009) (Data not published). The number of points varies according to the duration of the test. Number of plaques, strength of the adhesion and length of the byssus structure affect the data acquisition time of the experiment. When the mussel is being pulled off, the byssus stretches and creates a force that opposes the movement. This force was registered by the texture analyzer. First the force increased until a maximum load was reached and then it began decreasing zero load (some noise was always registered). The bell-shaped evolution of the force versus elongation (Figure 4-10) was explained by the detachment of the individual thread-plaque structure from the surface. In fact, different secondary “peaks” can be observed along the graph, corresponding each one with a different detachment event. By data processing with Excel ®, the peaks were identified and the difference

between a consecutive maximum and minimum attributed to the individual force component of each plaque.

Data was collected for 5 different samples (channels 5x5, 20x20, 50x50, 100x100 and 200x200) plus the control (smooth PDMSe), and each tensile test was run eight times in each different pattern. The data has been processed and the results are shown in the “Results” part of this thesis.

Table 4-1. Water tank maintenance monthly schedule

	MONDAY	TUESDAY	WEDNESDAY
1st week	Water replacement (1) Mussel feeding (2)	Water replacement	Water replacement WATER TEST (3)
2nd week	Water replacement Mussel feeding	Water replacement	Water replacement WATER TEST
3rd week	Water replacement Mussel feeding	Water replacement	Water replacement WATER TEST
4th week	Water replacement Mussel feeding	Water replacement	Water replacement WATER TEST

	THURSDAY	FRIDAY
1st week	Water replacement Mussel feeding	Water replacement
2nd week	Water replacement Mussel feeding	Water replacement
3rd week	Water replacement Mussel feeding	Water replacement
4th week	Water replacement Mussel feeding	Complete water replacement (4)

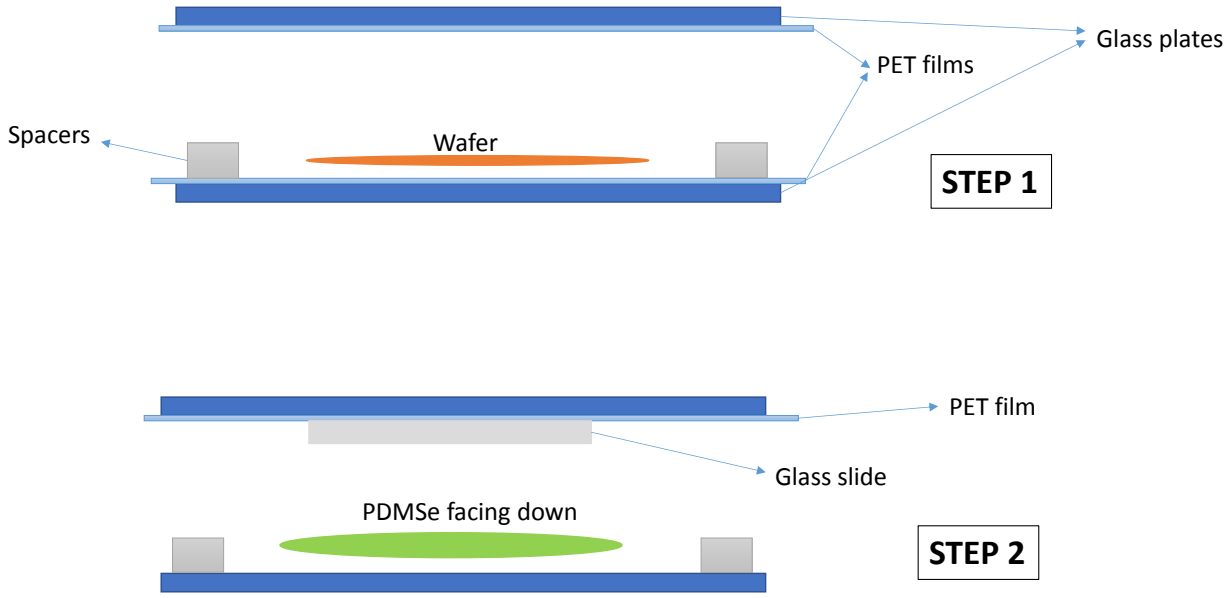

Figure 4-1. Mold setup for preparation of patterned PDMSe on glass slides (sectional view)

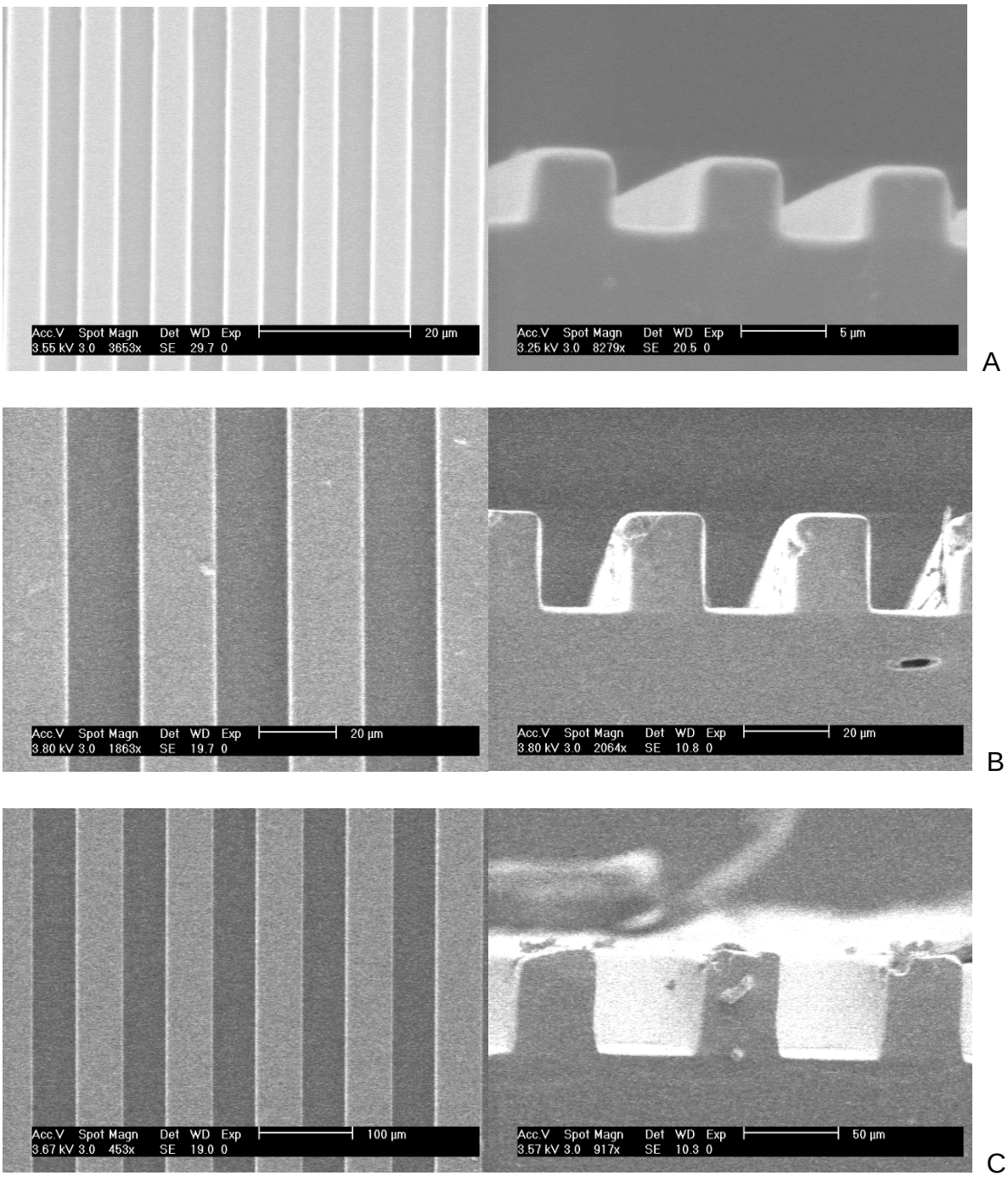

Figure 4-2. SEM captures the different topographies used in this study (3.67 kV), (A) 5 CH5x5, (B) 20 CH20x20, (C) 50 CH50x50, (D) 100 CH100x100, (E) 200 CH200x200 (Photo taken by author).

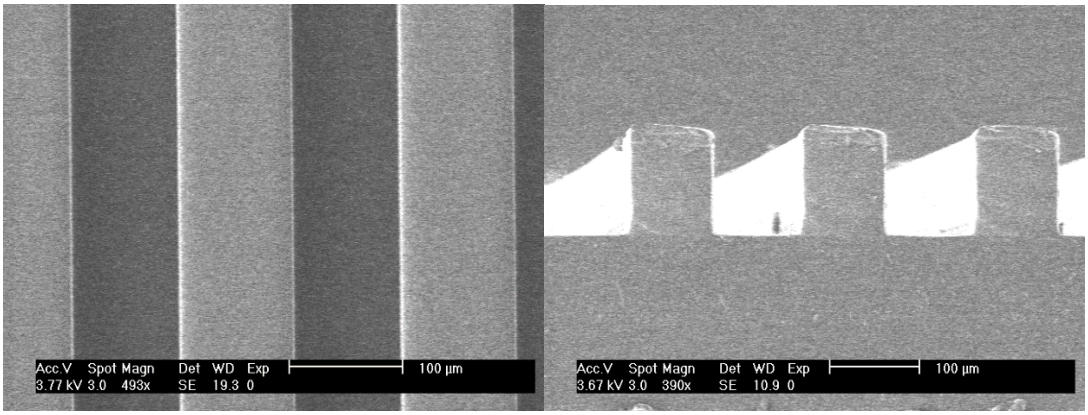

D

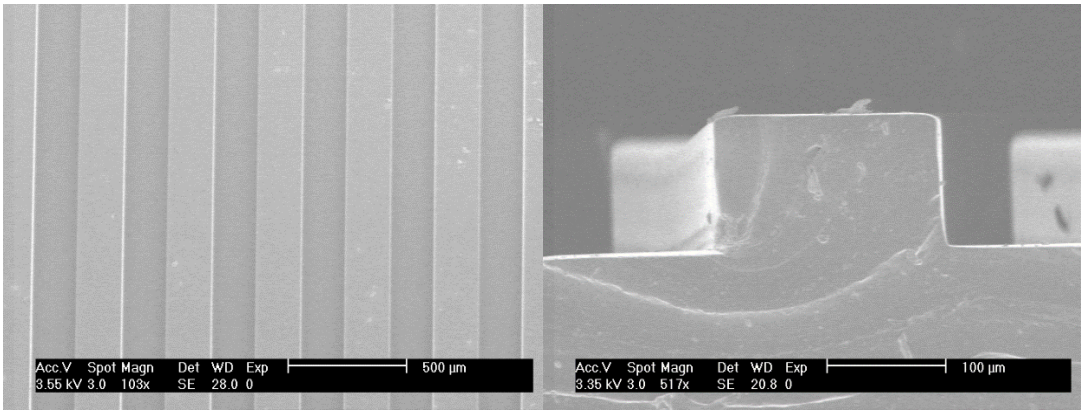

E

Figure 4-2. Continued

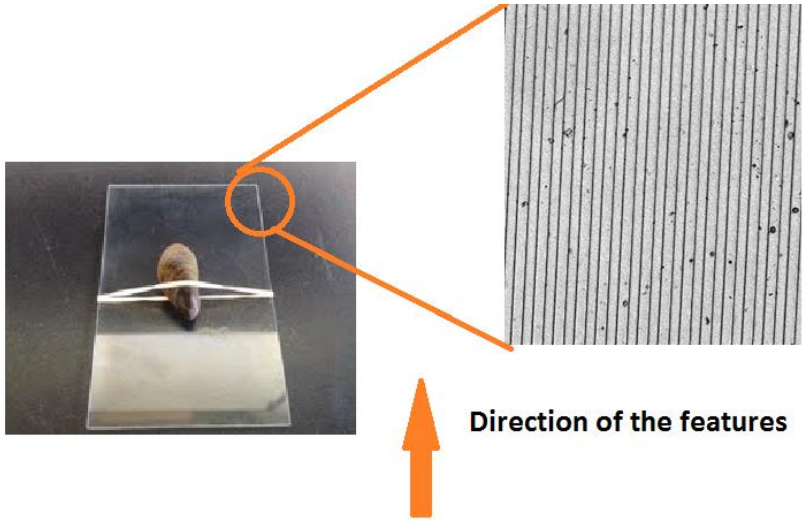

Figure 4-3. General plaque production experiment set and the direction corresponding to the position of the mussel

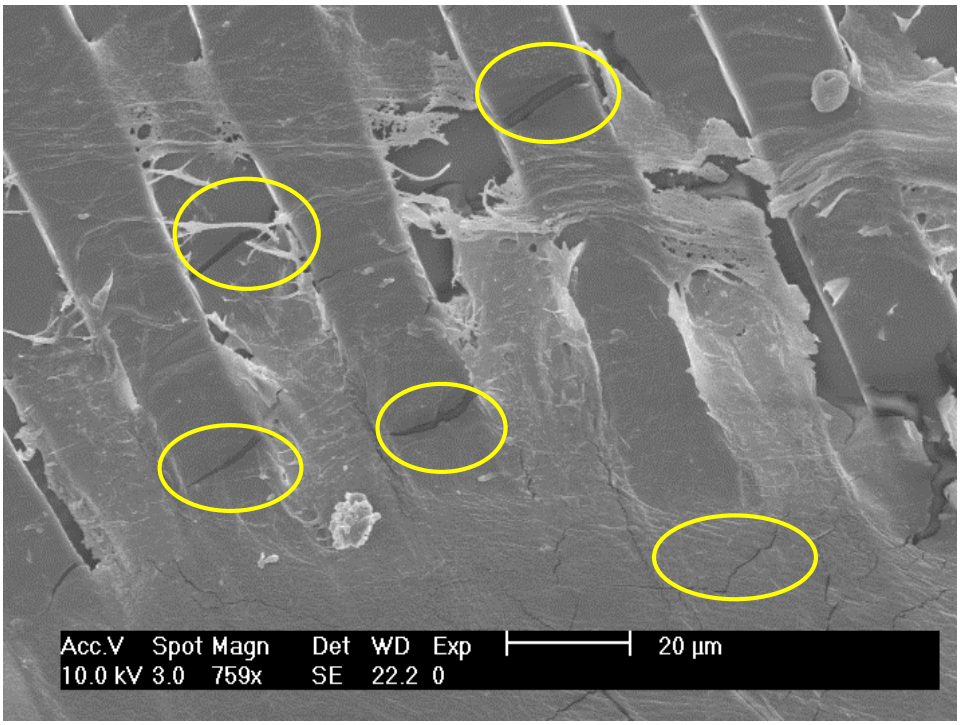

A

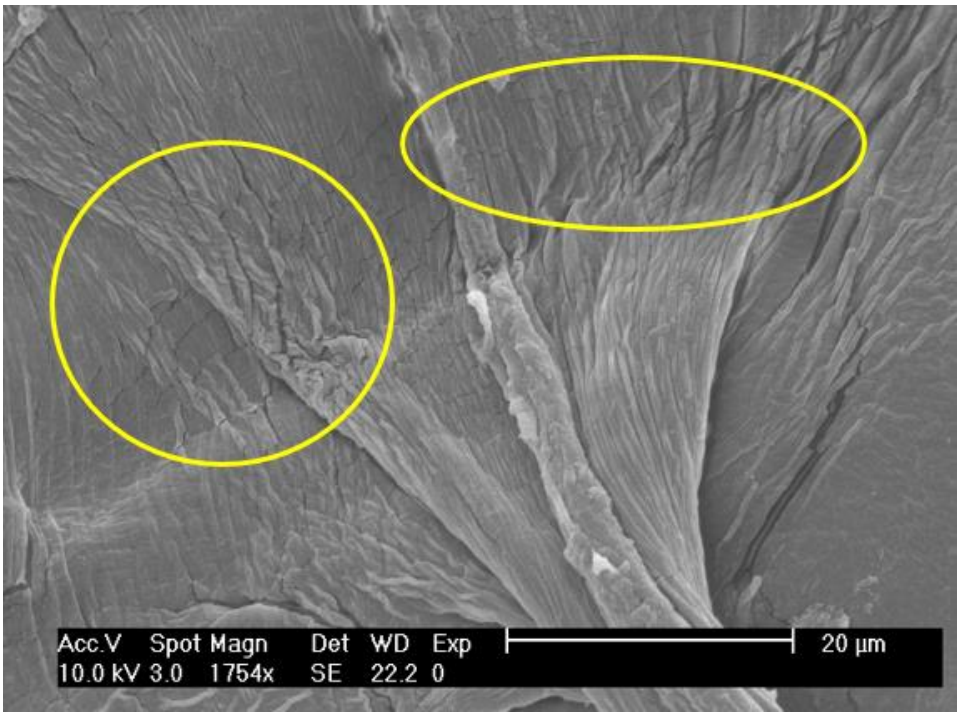

B

Figure 4-4. SEM micrograph of the edge of a plaque onto 10 CH 20x20. The plaque adhesive filling the spacing between the ridges can be observed. Cracks in both the PDMSe sample and the plaque are marked with yellow circles (Photo taken by author).

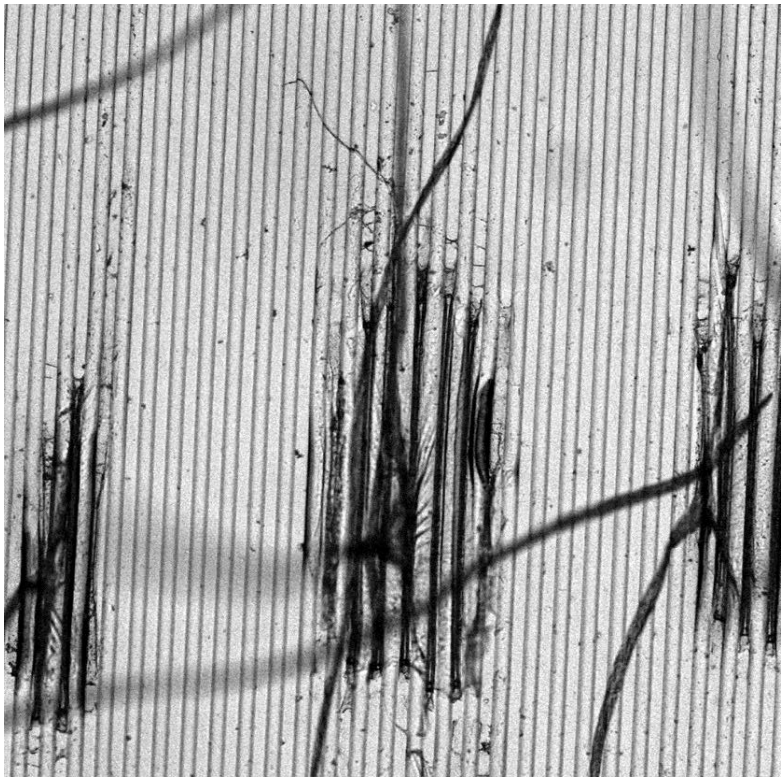

Figure 4-5. Optical microscope picture of mussel plaques onto 20 CH20x20 at x10 magnification (Photo taken by author).

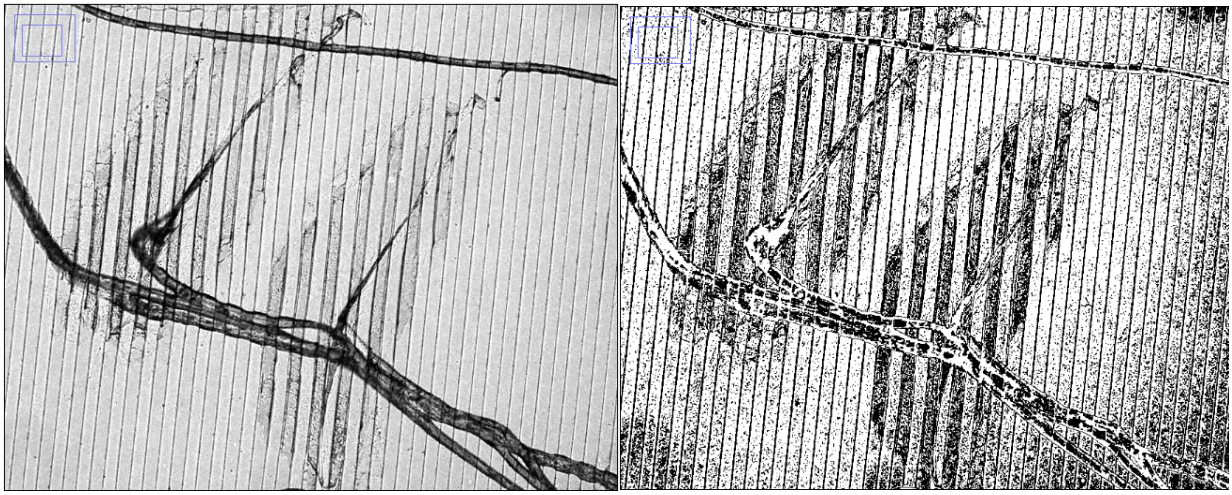

Figure 4-6. Optical microscope image of two mussel plaques onto 10 CH 20x20. On the left without image processing. On the right after threshold-enhanced processing with ImageJ® (Photo taken by author).

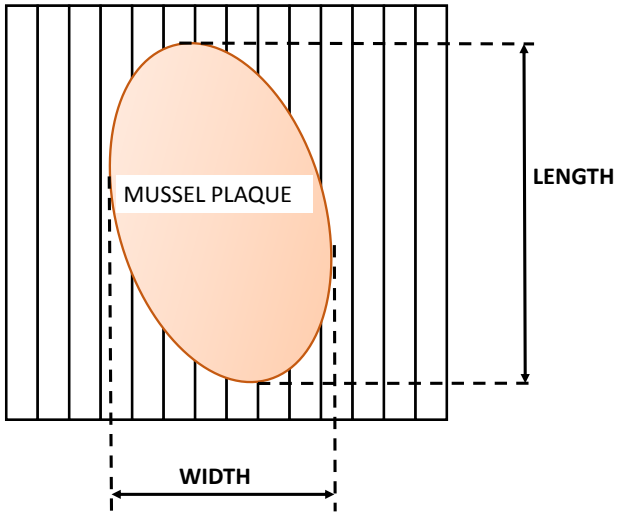

Figure 4-7. Schematic of the measurements taken by ImageJ® to calculate NFF where L is the length of the plaque parallel to the ridges and W is the width of the plaque orthogonal to the ridges.

Figure 4-8. Tensile analyzer (XT plus Texture analyzer from Texture Technologies Corp.) used in tensile force measurements (Photo taken by author).

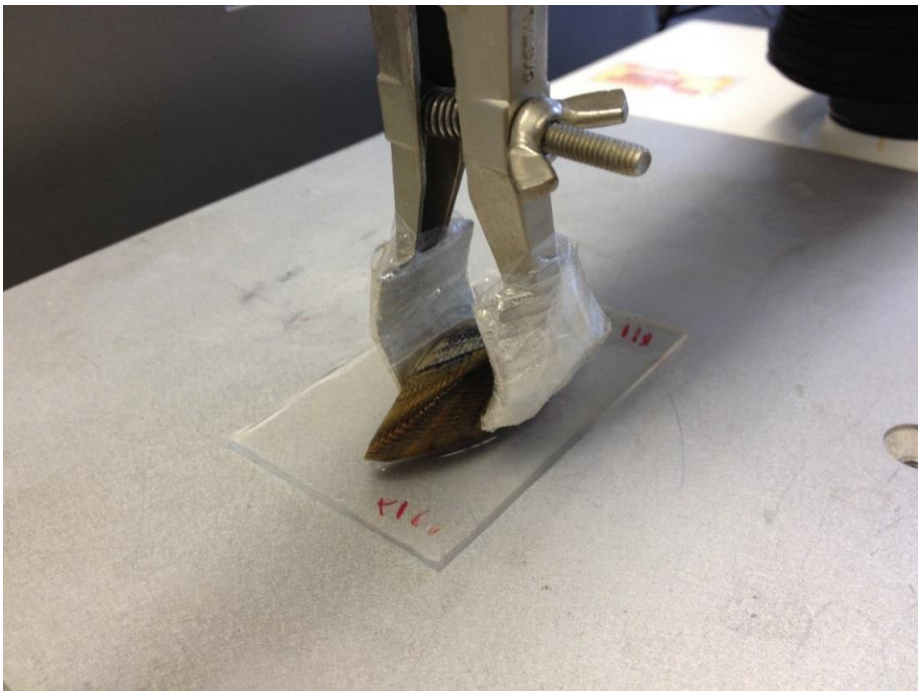

Figure 4-9. Texture analyzer set-up. Mussel is attached to the sample by different byssus structures (Photo taken by author).

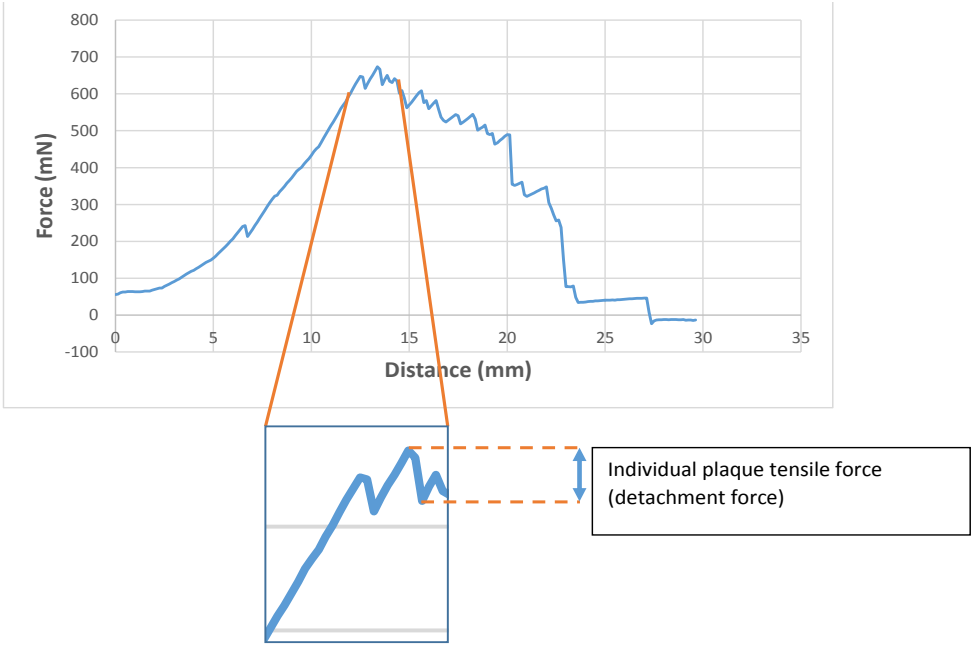

Figure 4-10. Example of force versus distance plot produced from data collected by texture analyzer for an individual mussel in a plaque strength test.

CHAPTER 5
RESULTS AND DISCUSSION

This study consisted of the measurement of geometrical factors of mussel plaques after plaque production experimentation, as well as tensile force experiments using 5 different patterns described in Table 5-1. . PDMSe smooth surfaces were also tested and used for comparison as a control.

Number of plaques

The number of plaques has proven to be a challenging factor to measure in our laboratory because of the size of the samples. For technical reasons, the size of the samples cannot be bigger than 50 by 50 mm and the size of the mussel permits the animal to reach out of the patterned area more often than desired with its extendable foot, causing experiments to be repeated. Actually it has been observed that most of the mussels tend to attach in those non-patterned areas, in other words, in the border of the sample (Data not shown). It seems like they purposefully avoided the patterned area (See Figure 5-1).

According to the experiments performed in this study, mussels produced an average of 16 and 23 plaques, which is in agreement with literature: between 10 and 40 (Burkett et al. 2009) within a very similar period of time (48 hours versus 72 hours in this case). It is important to mention that the specie of mussel used in this project is different than those in other papers. Table 5-2. shows that the lowest number of attachments occurred in those samples with dimensions of 50x50 microns feature size($\bar{x}$=16.38, SE=1.903, n=8) and the highest to 20x20 microns size ($\bar{x}$=22.75, SE=2.206, n=8).

In Figure 5-2a graph representing the same set of data can be observed. If the values are compared with the control value ($\bar{x}$=17.00, SE=1.62, n=8), the average

number of plaques for 50x50, 100x100 and 200x200 do not show statistical difference between themselves and the control. On the other hand, average values for 5x5 and 20x20 are very similar with respect to each other, but present a significant increase relevant to the smooth PDMSe. An explanation for this may be that features corresponding to 5x5 and 20x20 slightly promote the plaque production, while the other features follow the control fashion. It could also be that the individual plaque adhesion strength is weaker in the 5x5 and 20x20 so the mussel produces more byssus structures in order to provide itself with a stronger final adhesion value.

It is important to mention that the values of the standard deviation for all samples are considerably high, signifying the average values cannot be considered as highly accurate but still represent a valid approximation. For this reason the number of plaques was not considered for further discussion.

Plaque surface area

The plaque surface area average values were calculated with 8 different values obtained by 8 different tests. The area of 64 different plaques was measured by testing 8 different mussels for each different topography. The highest value was that for 5x5 ($\bar{x}$=0.541575 mm^2, SE=0.019021, n=8) and the lowest value was on 200x200 samples ($\bar{x}$=0.349550 mm^2, SE=0.049025, n=8) (Table 5-3.). Plaque surface area values for 5x5, 20x20 and control (smooth) did not show any significant difference (Table 5-3.). The value for 50x50 pattern goes slightly below the value range ($\bar{x}$=0.510939 mm^2, SE=0.031342, n=8). In the plaque surface area value for the 100x100 microns topography, a step appeared ($\bar{x}$=0.368991 mm^2, SE=0.051340, n=8), showing a significant difference with respect to the preceding size scale. In the following size (200x200 microns), the value for the plaque surface area did not present an important

change with the previous size, even though it decreased. Variance test ANOVA was applied to the different values of plaque surface area on each topography (Table 5-4.). The homogeneity of these parameters could not be rejected at 90% confidence level for each sample or between samples of a same group. Additional Tukey statistical analysis (Table 5-5.) proved that 50x50 topography did not exhibit a statistically significant difference with any other sample except for the 200x200 topography, and at the same time, the 200x200 tensile force value presented a significant difference with all topographies except that of the100x100.

It is noteworthy that the size of the plaque showed a steady decreasing while increasing the size of the features. An important step exists in the graph (Figure 5-3.), showing a transition in the range of the size (reducing the plaque surface area value to approximately 37%) that was exclusively related to the size of the feature. It could be that as the height of the ridges increases, the size becomes too large for the mussel adhesive to overcome. Thus, spreading is restricted such that the plaque size is reduced. The impossibility of a higher degree of spreading cannot be achieved, this may be considered as an energy barrier related to the surface tension of the adhesive. Remember that the surface tension of the mussel's adhesive must be low enough to spread onto the substrate but also, needs to have a high enough value to prevent from being dissipated in the water since all the process takes place under water.

To prove a mathematical correlation between the two parameters at hand (plaque surface area and size of the channels) a new graph was created (Figure 5-4.) and a linear correlation calculated. Even if the graph presents a good correlation (R^2=0.8424) it was clear that a pronounced step existed when increasing the size of the

features from 50x50 micron to 100x100 micron. This was indicative of the existence of a critical point in the features size between 50 and 100, marking an important transition of the spreading behavior of the adhesive. In this range of values, the channels topography had a significant effect on the plaque surface area. It was assumed that the amount of adhesive the mussel secreted every time it produced a byssus was the same no matter what substrate, so due to the larger features presenting larger wells between ridges, it seemed that a bigger portion of the adhesive filled the space between the ridges.

Nuclear Form Factor (NFF): Morphology of the plaques

Nuclear Form Factor (NFF) is a method based on the measurement of the length and the width of a two dimension feature, in this case the plaques. It indicated the degree to which the plaque adhesive adapted to various topographies by acquiring an elongated shape by following the direction of the channels. It was expected that during spreading, the adhesive front moved first into the spacing of the features since it is energetically favored due to two reasons. The first of these reasons is the space availability and pressure effect. Secondly is the difference in surface tension between the adhesive and the water being less than the difference between the adhesive and the substrate. This means that the expected shape of the plaque was to be roughly elongated in the direction of the channels. For more information, please refer to “Methods, Nuclear Form Factor” (Table 5-6.).

Data for the control are not shown because smooth samples did not present any topography. Statistical analysis was conducted by using ANOVA variance study (Table 5-7.). The means were statistically different from each other ($p=0.001$). A Tukey statistical analysis (Table 5-8.) showed that only the NFF value for 5x5 topography was

the only topography statistically different from the rest of NFF mean values. Also the 200x200 and 20x20 were shown to be statistically different.

The lowest NFF value was for 5x5 samples ($\bar{x}$=0.88, SE=0.076, n=8). The largest NFF value was for 200x200 feature-size samples ($\bar{x}$=1.91, SE=0.092, n=8). This means that the plaques presented a more elongated shape in the directions of the channel in the bigger size features. A continuous increase appeared in NFF with increasing size of the features, which can be observed (Figure 5-5.). NFF values were graphed versus size of the features (Figure 5-6.). The graph showed a good correlation (R^2=0.8471) even though it is important to point out that the change initially from 5x5 to 50x50 is larger than the change from 50x50 to 200x200, although the difference in size between the latter set of values is much larger. That can be explained considering that after a certain value, around 50 microns of the features, the degree of orientation of the plaque was affected more slowly. It was expected that larger features permit a better penetration of the adhesive between the ridges, since the adhesive could flow better.

Degree of penetration

The observation of the plaques onto the sample by Scanning Electron Microscope was very useful for characterization. It can be observed that the adhesive produced by the mussel filled the spacing between the ridges of the sample, as shown in the SEMs (Figure 5-7. to Figure 5-10.). Samples after the plaque production test, illustrate that the adhesive filled spaces changed with feature size. In the first two figures, the plaques were detached from the surface probably during the process of gold coating or by the effect of the electron beam in the SEM. It is easy to observe in these first two figures that the outline of the shape is not completely round and smooth. but is

disrupted by sharp steps of cured adhesive by following the fashion of the channel's spacing.

Some of the ridges have been bent and displaced out of the normal shape (Figure 5-10. D). It seems that the adhesive actively pulled the top of the ridges and caused them to shift together to the center point where the thread grew from. It could be that after spreading, the adhesive protein cures that produces the cross-linked structure. When curing, the structure shrinks around a central point in the middle of the plaque, causing the shape of the pattern to rearrange in order to adapt to the new stress. It could also be related to the dehydration process.

The degree of penetration of the adhesive between the ridges could have some implications in the attachment strength of the mussel to the substrate. If the adhesive has the ability of creating an effective adhesion to the wall of the ridges, this would mean that topography could contribute critically to the overall adhesion strength of the animal. In other words, those sizes in which the penetration into the topography is reduced the overall attachment strength would be increased by the increased area of the plaque. This subject is addressed later in this thesis when measurements of the actual adhesion are presented.

Texture analyzer

Eight different mussels for each of the 6 samples were used (48 different mussels in total). Each mussel was attached to the texture analyzer and then a tension force was applied to the animal in the vertical direction causing the plaques to detach from the substrate. Force was measured as well as distance and time. A series of data of force versus distance were displayed. It can be observed one of the moments during

the texture analyzer test when the byssus is being stretched, as an effect of the applied load (Figure 5-11.).

The graphs are approximately bell-shaped. In general the force that the mussel opposes stretching rises first, gets to a maximum peak and then goes back to zero or a value close to zero. A number of steps are observed along the graph. Counting the steps can be correlated to counting the number of plaques on top of the surface. This means that the number of steps equals the number of plaques onto the sample. There are a number of parameters mentioned in the analysis of the graphs that need to be addressed before going further into the study. These are described in the following lines:

- **Number of plaques and tensile load:** Each of the members on the list of numbers under the name of “Tensile strength (mN)” correspond to the difference in force values between the upper limit and the lower limit of each step, each of them corresponding to an individual plaque.
- **Maximum load:** Is the maximum value reached along the test. This is a measure of the tensile strength as a combination of a group of plaques work together.
- **Average tensile strength:** This tensile strength is the average of all the values for individual plaques for each test. It is an approximation of the adhesion strength value for the specific sample.
- **Cohesive failure:** Two different failures are contemplated in this project. Adhesive failure is that taking place at the plaque-material interface. Cohesive are those produced at some point along the collagen thread. It is important to be aware of the number of cohesive failures since those values do not give information of interaction between plaque-interface. This can be done by simple observation under the optical microscope once the test is finished.
- **Average tensile stress:** This tensile stress is obtained by dividing the different values of tensile strength by the value of the plaque surface area (fixed in every feature size, see results in plaque surface area).

Tensile force versus elongation was graphed for every different sample (Figure 5-12. to Figure 5-17.). In these graphs, the eight different tests per sample can be

observed in the same plot for each topography and the blank i.e. (smooth PDMSe). A large variety of results can be detected within the same sample such as largely different values of maximum tensile force and the shapes of the curves. This is because every mussel produces a different number of plaques and the distribution of the plaques were not the same each time. Many plaques can be produced around a very small spot, generating a high load by working collectively against the force applied. On the other hand the plaques were spread out all over the sample, so the resulting force does not count as a whole but the tension created by individual plaques in different stages of the test.

When the plaques were produced in a small region of the sample, none or very few steps are observed along the graph before the peak. The peak shape tends to be sharp as for the example in Test 1 (Figure 5-12.). When the sample exhibited two different regions of plaque attachment then the graph displays a primary maximum peak and a secondary peak as in Test 5 (Figure 5-14.). The other extreme is that the mussel produced the byssus on the substrate so the graph spreads out and does not include a differentiated maximum peak as in the case of Test 2 (Figure 5-12.).

Those steps that can be observed before the maximum are related to those threads that were weaker or located further from the shell. The farther they are from the shell, the faster they reach their maximum elongation and fail. One may notice that the graph always starts at 50 mN, because it was set as the trigger force in the texture analyzer system. It is important to mention that in some of the graphs, the end of the test shows neither a final value that is neither close to zero nor the starting value. This happened for two different reasons. First of all the noise present during the testing

process, which was assumed to be around 100 mN above and below the starting value. A second contribution to this deviation was the weight of the mussel that some tests seem to not correctly take into account.

These deviations did not negatively affect to the results. They cause the values to go off the range of the graph in a certain degree but the individual drop in tensile stress that configure the steps along the graph can be correlated with individual plaque attachments without concern. For this study, it was assumed that the tensile strength values were produced only through the breaking process of the plaques when detachment happens by the application of the external tensile load with the texture analyzer.

The fact that a correlation between the tensile force values and the individual plaque detachment process exists is supported when taking a look at the histograms. Histograms for all the registered tensile force values acquired with the tensile analyzer test are shown for each feature size (Figure 5-18. to Figure 5-23.). In all cases, a regular distribution is observed with a narrow range of values. The blank, or the control, presents the highest frequency in the range 10-15 mN, being the lowest tensile average force. 5x5 and 100x100 features present the highest frequency in the 15-20 mN range. 50x50 and 200x200 micron feature samples present the highest frequency in the 20-25 mN range. 20x20 features show the highest frequency, in the 25-30 mN range, being the highest tensile average force. These distributions of values are significant because they back up the theory that the steps in the tensile force versus elongation represent single detachments.

It is important to mention that two different types of failures were considered in this study. Adhesive failure is that produced at the interface between the adhesive and the substrate while cohesive is failure produced any point along the collagen thread or on top of the plaque. The differences were easily detected because the plaques are large enough to report the two different failures by optical microscopy. Those areas where adhesive failure happened were not chemically characterized to prove if any adhesive remained, so it was assumed the failure was complete and no adhesive stayed on the area. Values from 19% cohesive failure in 5x5 microns channels (minimum) to 35% cohesive failure in 20x20 microns features (maximum) were reported as averages. This involved that the rest of the data analysis in this project include an error since all failures are considered adhesive, nevertheless since cohesive failure percentage range is similar the effect in the study is minimized. Examples of adhesive failures in the different topographies are listed in

Tensile force

Table 5-9. lists the average values for tensile force obtained as an average of all individual plaque values gathered for each sample. The highest value in tensile force corresponds to 20x20 microns feature ($\bar{x}$=45.161 mN, SE=2.067, n=182), followed closely by that value on 5x5 ($\bar{x}$=42.368 mN, SE=2.331, n=177). The rest of the average values for tensile force in 50x50 ($\bar{x}$=36.425 mN, SE=2.301, n=131), 100x100 ($\bar{x}$=31.862 mN, SE=1.597, n=142) and 200x200 ($\bar{x}$=31.732 mN, SE=1.677, n=137) are along the same line of the value corresponding to the blank ($\bar{x}$=32.706 mN, SE=2.107, n=136), which does not represent a significant difference (p=1E-7). ANOVA statistical analysis show the differences in the tensile force values that were statistically different (Table 5-10.).

Additionally a Tukey statistical analysis (Table 5-11.) showed no statistical differences between 50x50, 100x100 and 200x200 tensile force mean values with respect to control. However 5x5 and 20x20 tensile force mean values were significant different from the blank. Also the 20x20 mean value was statistically different from the values of all topographies except that of the 5x5. In Figure 5-25. the graph shows all values for each sample analyzed. Looking at the graph, it is easier to see how values for the first two features in size, display an important difference with respect to the smooth surface. Decreasing the feature size of the topography improved the adhesion of the mussel adhesive on the substrate. Samples with 50x50 microns feature show a significant decrease.100x100 and 200x200 features have values similar to the blank. This indicates, that according to tensile force measurements, a larger size does not have a significant effect on the adhesion strength of the mussel adhesive. In general terms, the tensile force scales are inversely with respect to the feature size.

Tensile force versus plaque surface area

Considering that the adhesive secreted for the mussel has always the same composition, and that volume and chemistry of the substrate is the same in every test, it should be expected that a higher tensile force corresponds with a larger plaque surface area. This is because a larger adhesive surface area would create a larger number of molecular interactions with the substrate. Observing, the tensile force is reduced with the decreasing size of the mussel plaque (Figure 5-26.). In order to use plaque surface average values obtained from 72 plaque production experiments and relate them through tensile force values obtained from 48 hours experiments it was necessary to establish that no statistically difference is detected. For that purpose 10 different micrographs from the 48 hours experiment were evaluated in terms of plaque surface

area and compared to those values previously reported in the “Plaque surface area” section. ANOVA statistical analysis shows that no statistical difference exists (all “p” values over 0.05) between plaque surface area values from both 48 h and 72 h experiments (Table 5-12.).

When comparing values with the blank a number of important points should be addressed. First of all, in 5 CH5x5 the value for the tensile force was around 1/3 larger if compared with the blank, but the size of the plaque was not significantly different. This means that the 5x5 topography must promote adhesion. The same effect is observed when looking at the values for 20 CH20x20. This enhancement of adhesion was attributed to the topography and the fact that it provides more surface area for the mussel adhesive to attach. For 50x50, 100x100 and 200x200 features, the values of tensile force are in the same range as that of the smooth samples. Nevertheless the plaque surface area values decrease with respect to the value for the blank. This suggests that even if the area was smaller in the topographies, a certain degree of penetration was achieved on these sizes too.

Tensile stress

Table 5-9. also shows the average values for tensile stress (mN/mm2), obtained from the values of tensile force and the plaque surface area values calculated previously in this project. The maximum value corresponds to 200x200 samples ($\bar{x}$=90.779 mN/mm^2, SE=4.796, n=137) and the lowest value to 50x50 samples ($\bar{x}$=71.291 mN/mm^2, SE=4.504, n=131). Nevertheless all the values for the different features are significantly higher than the value for tensile stress in the blank ($\bar{x}$=60.977 mN/mm^2, SE=3.928, n=136), which proves the topography has an effect on the attachment stress. The values obtained in this study for tensile stress were

compared to those obtained for smooth PDMSe in literature (93.25 mN/mm^2 in Burcket et al. 2009). Recall that the specie used in the cited literature (Mytilus Edulis) is different than the one used in this study (Geukensia demissa). Mytilus Edulis is bigger in size, however the content of DOPA and the number of proteins in the byssus are essentially the same between different species and therefore allows this comparison. The bar chart of tensile stress values for the different topographies tested as well as the blank clearly illustrates the values increase with the size of the feature (Figure 5-27.). In this figure tensile stress values are calculated by applying roughness index (1 for the blank, 2 for 5x5, 20x20, 50x50 and 100x100, and 1.5 for 200x200). The tensile stress of the 50x50 was an exception which is interesting.

A comparison of the tensile stress (roughness index applied) and tensile force as a function of the feature dimension, provides some insight into the effect of the 50 micron features (Figure 5-28.). Both stress and force increase in response to the features until the +50SK50x50, at which point both decrease rapidly until the +100CH100x100 features are evaluated. The stress and force diverge at the +100CH200x200 topography. The overall tensile stress increases to the maximum value, while the tensile force decreased to the same value of the smooth PDMSe.

We have made the assumption that the composition of the adhesive is constant as well as the adhesion mechanism. This is reasonable since the animals were also a constant as well as the experimental conditions.

So, in order to explain this, it must be mentioned that plaque surface area was measured as a planar projection of the plaque onto the substrate. At the same time some degree of penetration into the spacing has also been previously observed (see

Results, Degree of penetration). This data shows that mussels achieve some degree of effective adhesion to the side of the ridges that is a function of the specific size of the features. This shows the effective area is not that measured of planar projection but instead, some other larger value.

Table 5-1. Different sizes of the features in the different patterns

Sample number	Pattern Design	Dimensions Width x Spacing (μm x μm)	Height (μm)
1	Channels	5 x 5	5
2	Channels	20 x 20	20
3	Channels	50 x 50	50
4	Channels	100 x 100	100
5	Channels	200 x 200	100

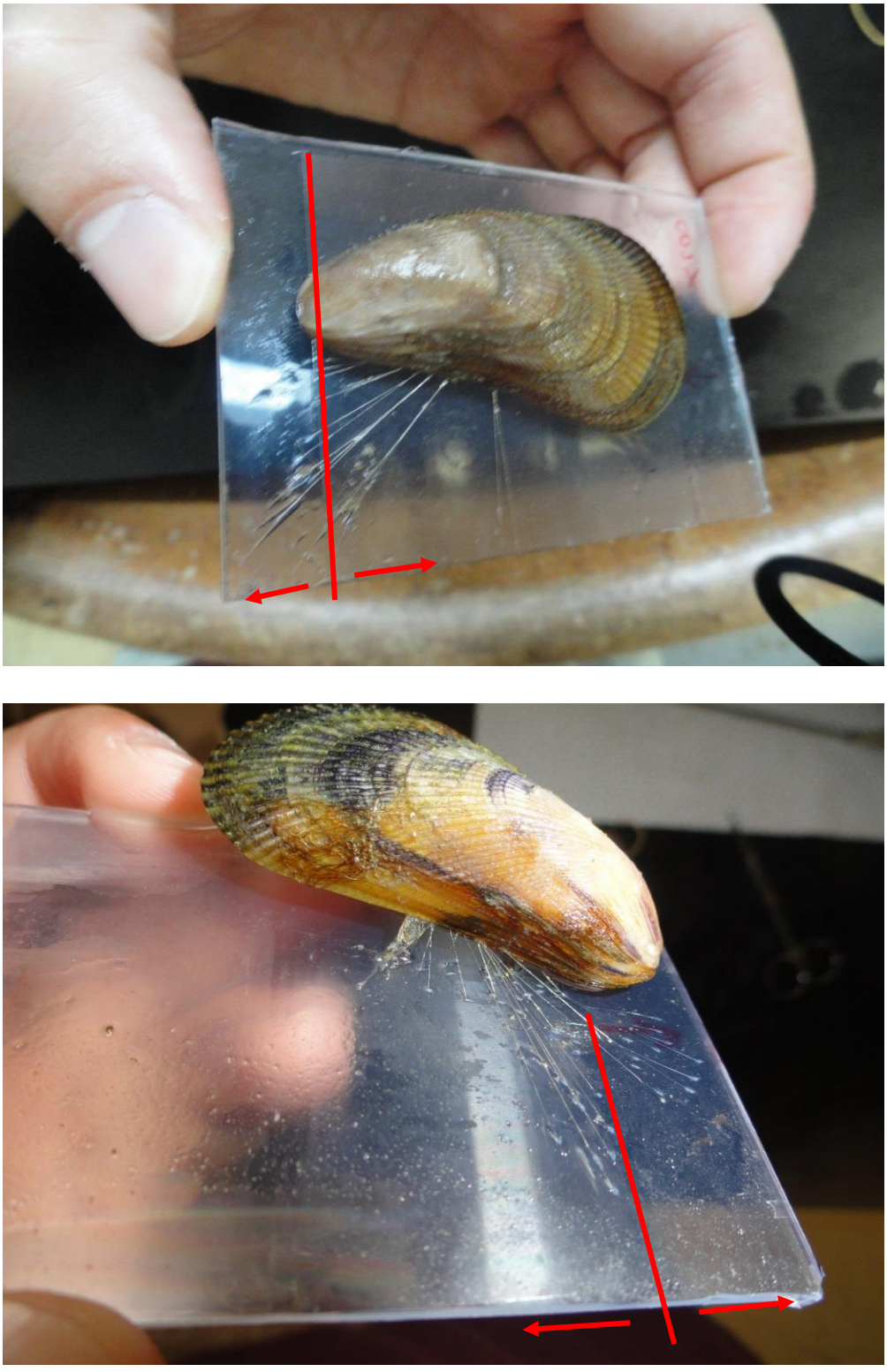

Figure 5-1. Pictures that illustrate the mussel plaque production extends beyond the patterned area. The border between the pattern and unpatterned area is marked with a red line (Photo taken by author).

Table 5-2. Table with the more significant statistical values of number of plaques for the different samples (data collected from the texture analyzer tests)

	Number of plaques	
	Average	17
	N	8
SMOOTH	st. dev.	4.58
	90%CI	2.66
	SE	1.62
	Average	22
	n	8
5X5	st. dev.	9.97
	90%CI	5.80
	SE	3.52
	Average	23
	n	8
20X20	st. dev.	6.24
	90%CI	3.63
	SE	2.21
	Average	16
	n	8
50X50	st. dev.	5.38
	90%CI	3.13
	SE	1.90
	Average	18
	n	8
100X100	st. dev.	8.09
	90%CI	4.70
	SE	2.86
	Average	17
	n	8
200X200	st. dev.	4.40
	90%CI	2.56
	SE	1.56

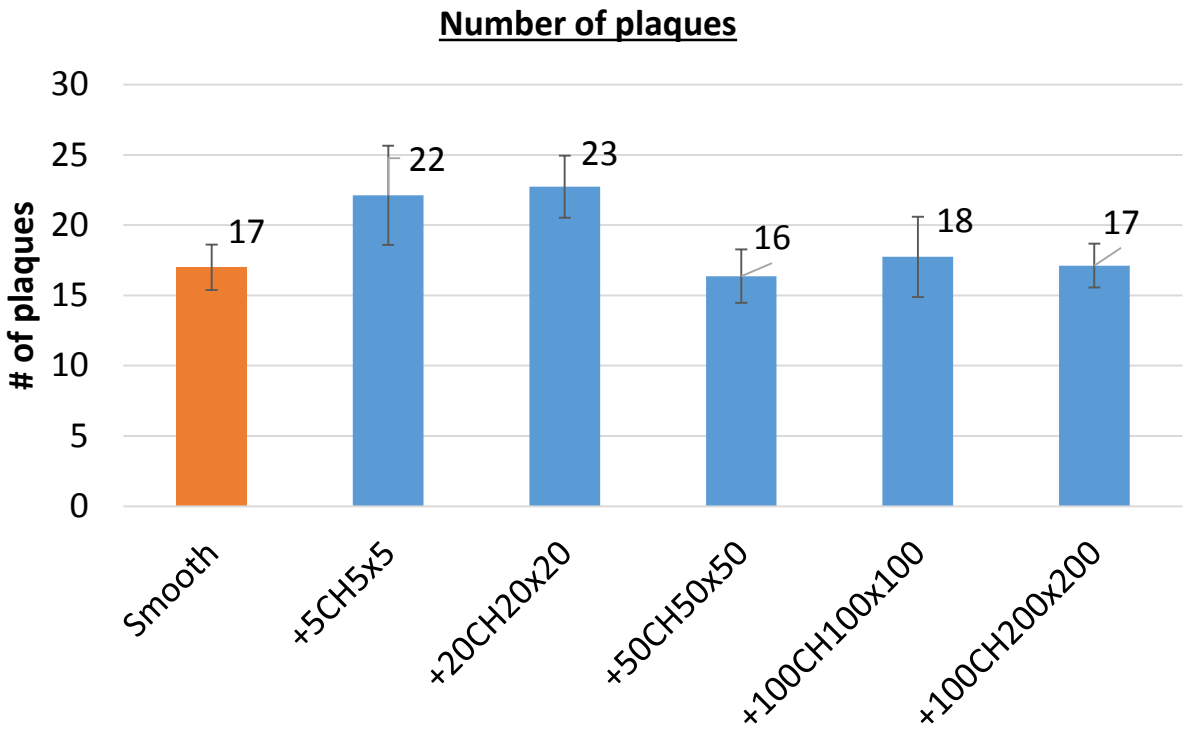

Figure 5-2. Number of plaques in different patterns (texture analyzer test) compared with control sample (smooth PDMSe). Values are averages and the error bars correspond to standard error (SE).

Table 5-3. Plaque surface area statistically most important parameters

		Plaque surface area (mm^2)
SMOOTH	Average	5.36E-01
	N	8
	st. dev.	5.38E-02
	90%CI	3.13E-02
	SE	1.90E-02
5X5	Average	5.42E-01
	n	8
	st. dev.	8.84E-02
	90%CI	5.14E-02
	SE	3.12E-02
20X20	Average	5.40E-01
	n	8
	st. dev.	1.06E-01
	90%CI	6.19E-02
	SE	3.76E-02
50X50	Average	5.11E-01
	n	8
	st. dev.	8.86E-02
	90%CI	5.16E-02
	SE	3.13E-02
100X100	Average	3.69E-01
	n	8
	st. dev.	1.45E-01
	90%CI	8.44E-02
	SE	5.13E-02
200X200	Average	3.50E-01
	n	8
	st. dev.	1.39E-01
	90%CI	8.06E-02
	SE	4.90E-02

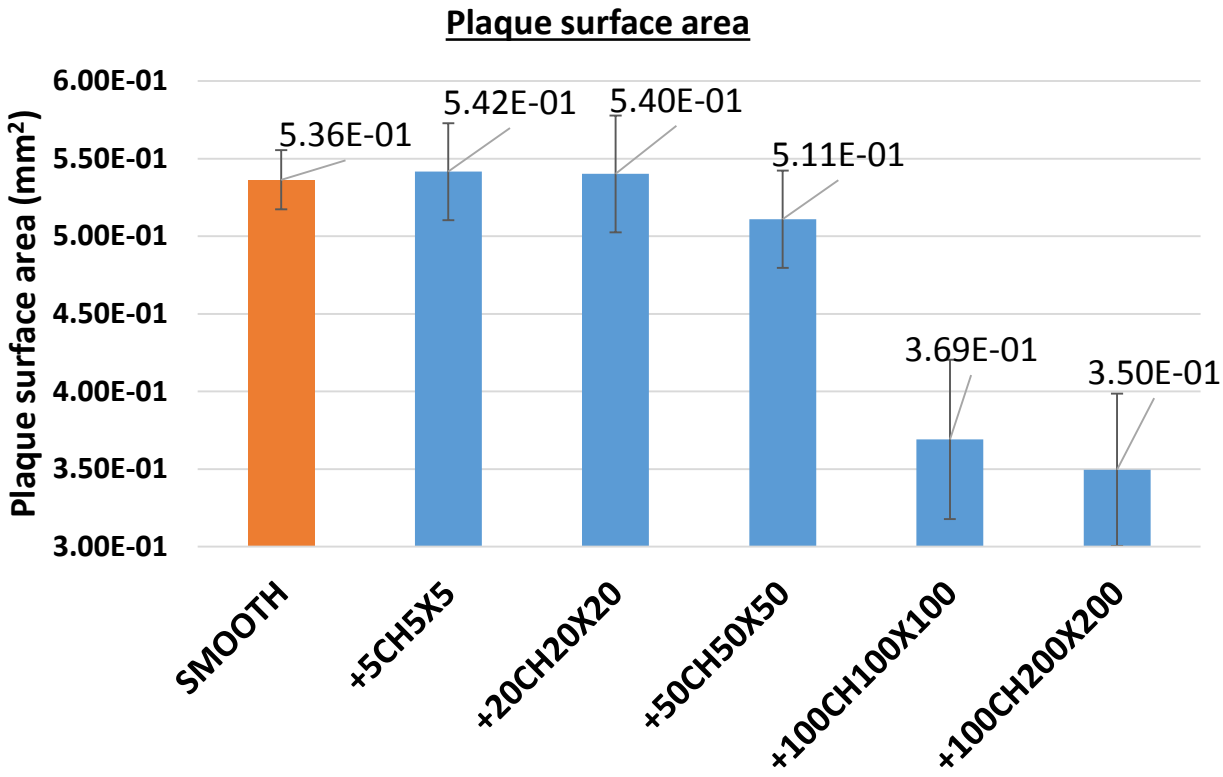

Figure 5-3. Plaque surface area values (mm2) of the different patterns tested (5x5, 20x20, 50x50, 100x100, 200x200 microns, width x spacing) compare to control (smooth PDMSe) Values are averages and the error bars correspond to standard error (SE).

Table 5-4. ANOVA variance study for the plaque surface area values on the different topographies

ANOVA

Source of Variation	SS	df	*MS*	*F*	*P-value*	*F crit*
Between Groups	0.3257	5	0.0651	4.8707	0.0013	2.43769264
Within Groups	0.5617	42	0.0134			
Total	0.8874	47				

Table 5-5. Tukey post-hoc analysis of plaque surface area values (being 1=smooth, 2=5x5, 3=20x20, 4=50x50, 5=100x100, 6=200x200)

```
Tukey 90% Simultaneous Confidence Intervals
All Pairwise Comparisons among Levels of Samples

Individual confidence level = 98.97%


Samples = 1 subtracted from:

Samples    Lower   Center    Upper  -------+---------+---------+---------+--
2        -0.1502   0.0052   0.1606           (-------*-------)
3        -0.1516   0.0038   0.1592           (-------*-------)
4        -0.1808  -0.0254   0.1299         (-------*------)
5        -0.3227  -0.1674  -0.0120   (-------*------)
6        -0.3422  -0.1868  -0.0314  (-------*------)
                                    -------+---------+---------+---------+--
                                        -0.20      0.00      0.20      0.40


Samples = 2 subtracted from:

Samples    Lower   Center    Upper  -------+---------+---------+---------+--
3        -0.1568  -0.0014   0.1540           (-------*-------)
4        -0.1860  -0.0306   0.1247         (------*-------)
5        -0.3280  -0.1726  -0.0172   (------*-------)
6        -0.3474  -0.1920  -0.0367  (------*-------)
                                    -------+---------+---------+---------+--
                                        -0.20      0.00      0.20      0.40


Samples = 3 subtracted from:

Samples    Lower   Center    Upper  -------+---------+---------+---------+--
4        -0.1846  -0.0292   0.1261         (-------*------)
5        -0.3266  -0.1712  -0.0158   (------*-------)
6        -0.3460  -0.1906  -0.0353  (------*-------)
                                    -------+---------+---------+---------+--
                                        -0.20      0.00      0.20      0.40


Samples = 4 subtracted from:

Samples    Lower   Center    Upper  -------+---------+---------+---------+--
5        -0.2973  -0.1419   0.0134    (-------*-------)
6        -0.3168  -0.1614  -0.0060   (-------*-------)
                                    -------+---------+---------+---------+--
                                        -0.20      0.00      0.20      0.40


Samples = 5 subtracted from:

Samples    Lower   Center   Upper  -------+---------+---------+---------+--
6        -0.1748  -0.0194  0.1359         (-------*-------)
                                    -------+---------+---------+---------+--
                                        -0.20      0.00      0.20      0.40
```

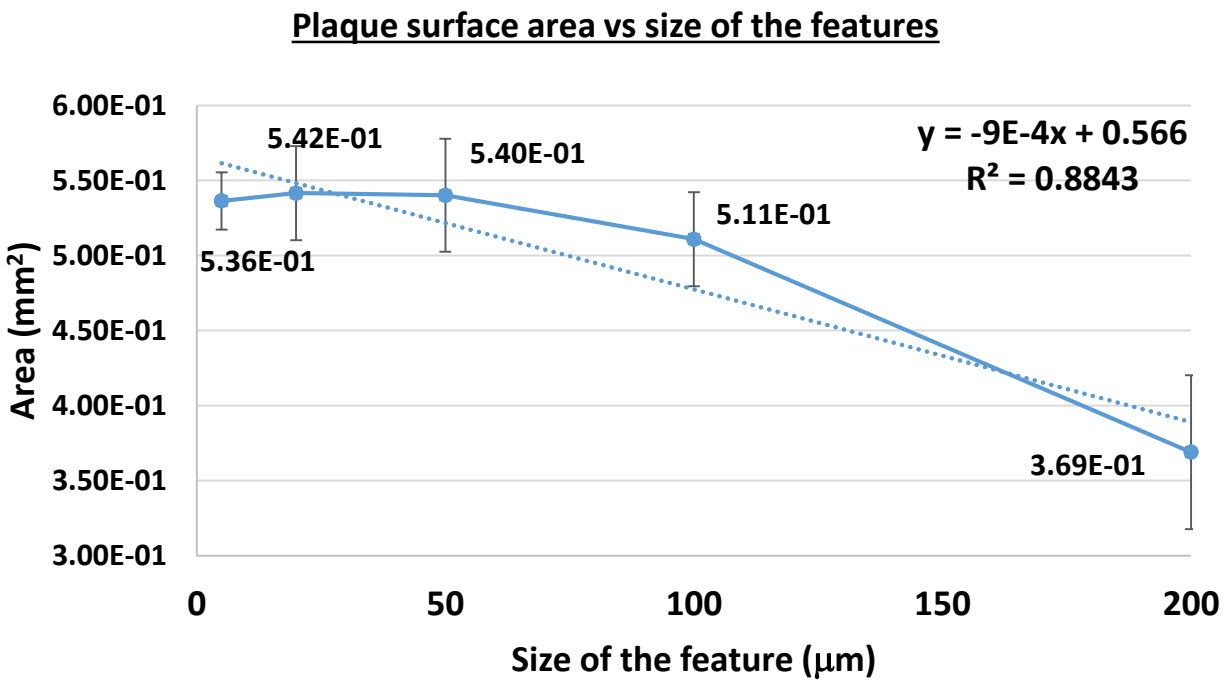

Figure 5-4. Plaque surface area values (mm^2) vs. size of the features (μm^2) (width/spacing, ratio 1:1) to show linear correlation between the two parameters. Values are average and the error bars correspond to standard error (SE).

Table 5-6. Nuclear Form Factor statistically most important parameters

		NFF
SMOOTH	Average	1.66E+00
	N	8
	st. dev.	1.77E-01
	90%CI	1.03E-01
	SE	6.27E-02
5X5	Average	8.85E-01
	n	8
	st. dev.	2.15E-01
	90%CI	1.25E-01
	SE	7.59E-02
20X20	Average	1.26E+00
	n	8
	st. dev.	4.47E-01
	90%CI	2.60E-01
	SE	1.58E-01
50X50	Average	1.46E+00
	n	8
	st. dev.	6.84E-01
	90%CI	3.98E-01
	SE	2.42E-01
100X100	Average	1.49E+00
	n	8
	st. dev.	3.70E-01
	90%CI	2.15E-01
	SE	1.31E-01
200X200	Average	1.91E+00
	n	8
	st. dev.	2.60E-01
	90%CI	1.51E-01
	SE	9.20E-02

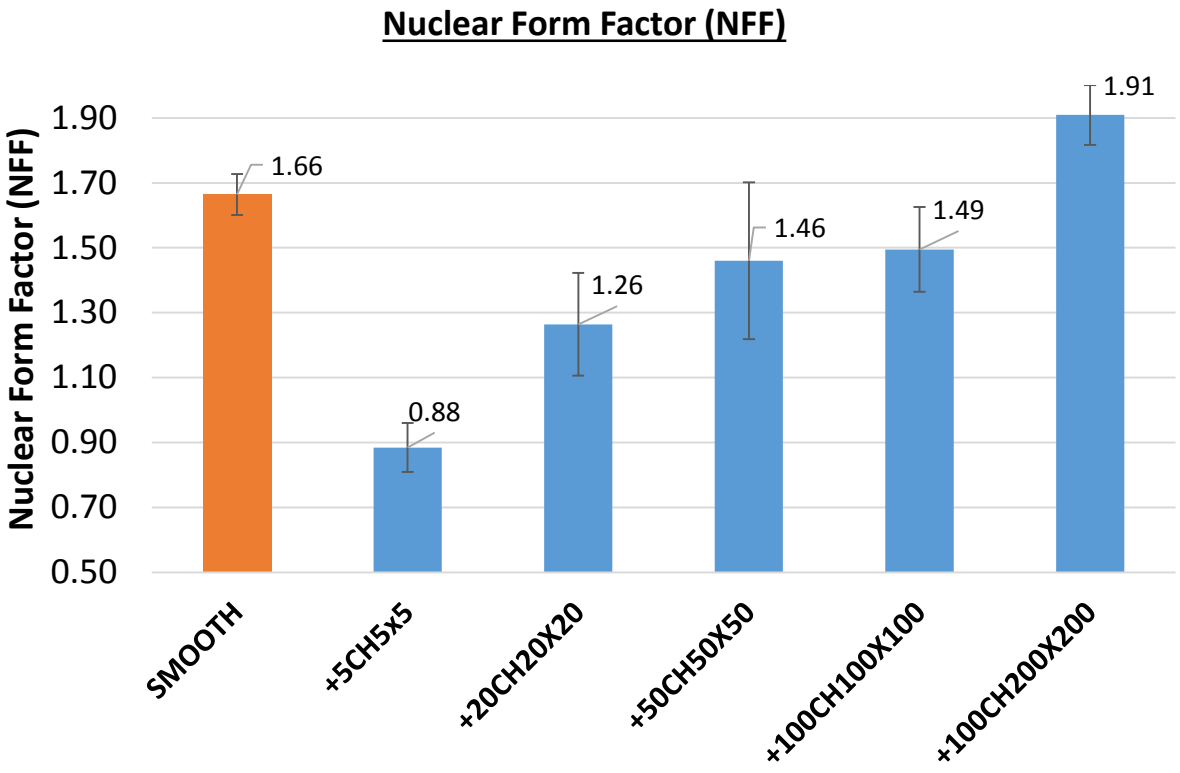

Figure 5-5. NFF values of the different patterns tested (5x5, 20x20, 50x50, 100x100, 200x200 microns, width x spacing) including Smooth (control). Values are averages and the error bars correspond to standard error (SE).

Table 5-7. ANOVA variance study for the Nuclear Form Factor (NFF) values on each topography

ANOVA

Source of Variation	SS	df	MS	F	P-value	F crit
Between Groups	4.904494	5	0.981	5.4189	0.0006	2.43769264
Within Groups	7.602537	42	0.181			
Total	12.50703	47				

Table 5-8. Tukey post-hoc analysis of nuclear form factor values (being 1=smooth, 2=5x5, 3=20x20, 4=50x50, 5=100x100, 6=200x200)

```
Tukey 90% Simultaneous Confidence Intervals
All Pairwise Comparisons among Levels of Samples

Individual confidence level = 98.97%


Samples = 1 subtracted from:

Samples    Lower   Center    Upper     +---------+---------+---------+---------
2        -1.3510  -0.7794  -0.2078        (------*------)
3        -0.9716  -0.4000   0.1716             (------*------)
4        -0.7754  -0.2038   0.3678               (------*-------)
5        -0.7407  -0.1691   0.4025               (------*------)
6        -0.3263   0.2453   0.8169                     (------*------)
                                   +---------+---------+---------+---------
                                -1.60     -0.80      0.00      0.80


Samples = 2 subtracted from:

Samples    Lower  Center   Upper     +---------+---------+---------+---------
3        -0.1922  0.3794  0.9510                     (------*------)
4         0.0040  0.5756  1.1472                       (------*------)
5         0.0387  0.6103  1.1819                       (-------*------)
6         0.4531  1.0247  1.5963                             (------*------)
                                   +---------+---------+---------+---------
                                -1.60     -0.80      0.00      0.80


Samples = 3 subtracted from:

Samples    Lower  Center   Upper     +---------+---------+---------+---------
4        -0.3754  0.1962  0.7678                   (------*-------)
5        -0.3407  0.2309  0.8025                    (------*------)
6         0.0737  0.6453  1.2169                         (------*------)
                                   +---------+---------+---------+---------
                                -1.60     -0.80      0.00      0.80


Samples = 4 subtracted from:

Samples    Lower  Center   Upper     +---------+---------+---------+---------
5        -0.5369  0.0347  0.6063                 (------*-------)
6        -0.1225  0.4491  1.0207                      (-------*------)
                                   +---------+---------+---------+---------
                                -1.60     -0.80      0.00      0.80


Samples = 5 subtracted from:

Samples    Lower  Center   Upper     +---------+---------+---------+---------
6        -0.1572  0.4144  0.9860                     (------*------)
                                   +---------+---------+---------+---------
                                -1.60     -0.80      0.00      0.80
```

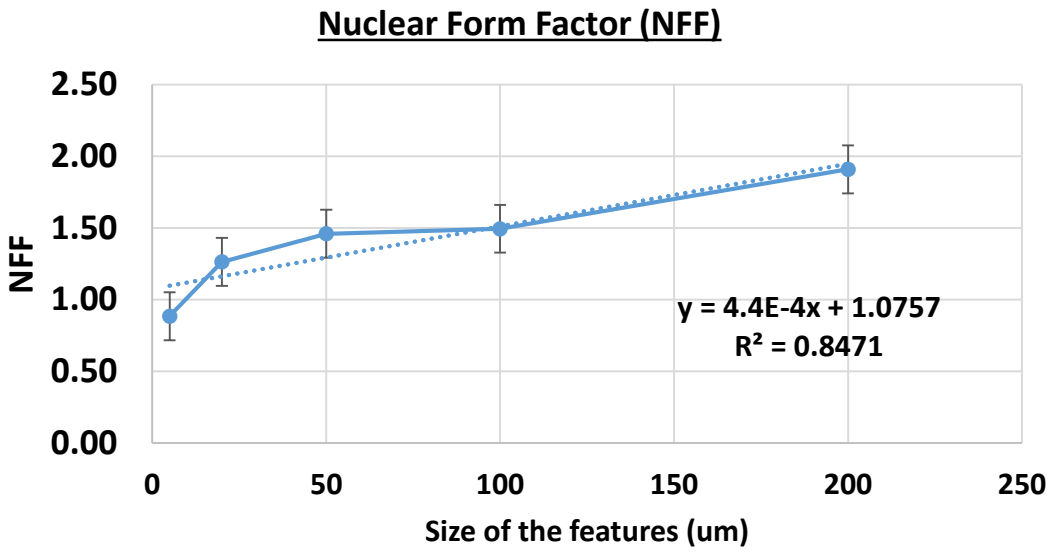

Figure 5-6. NFF values vs. size of the features (μm^2) (width/spacing, ratio 1:1) to show linear correlation between the two parameters considered. Values are average and the error bars correspond to standard error (SE).

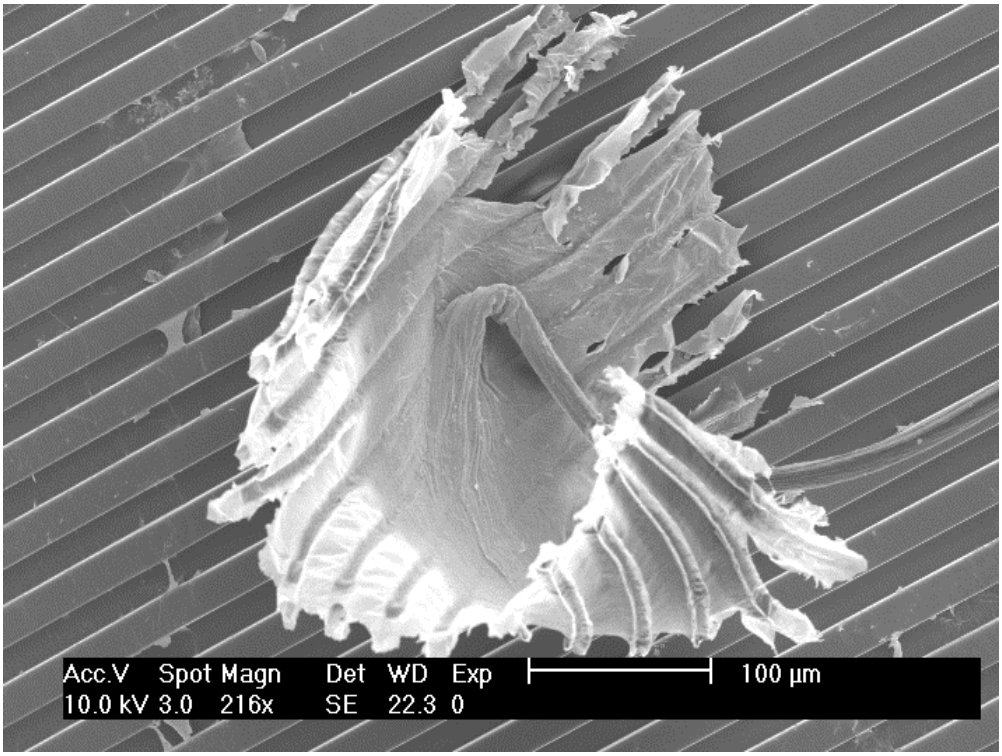

A

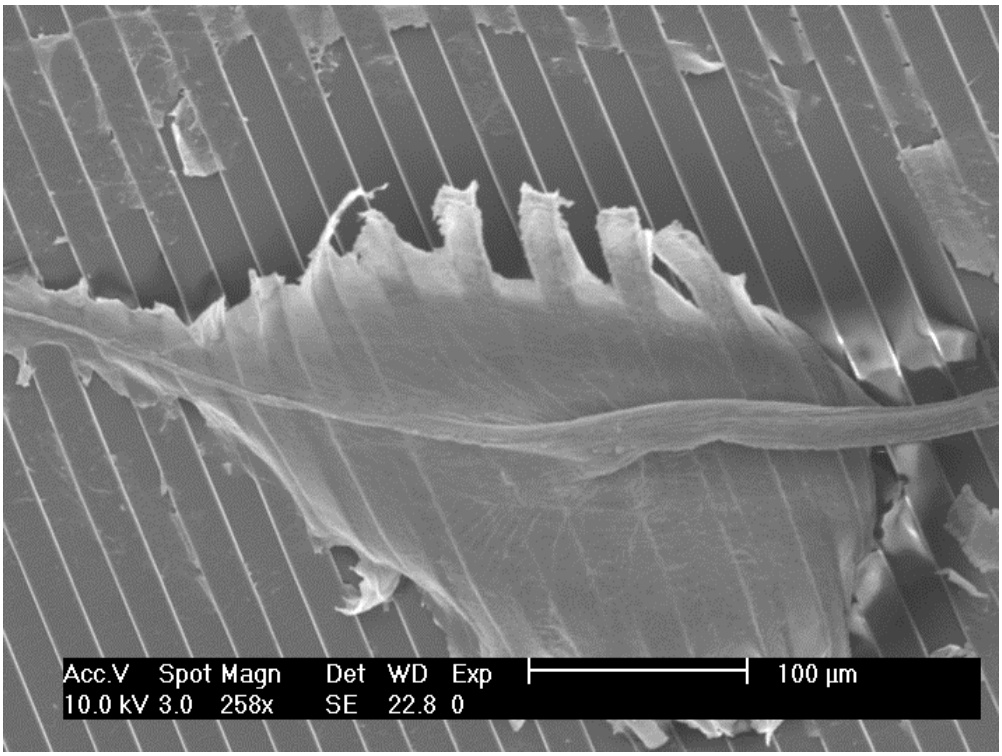

B

Figure 5-7. SEM pictures of detached mussel plaques on 20x20 microns channels feature (Photo taken by author).

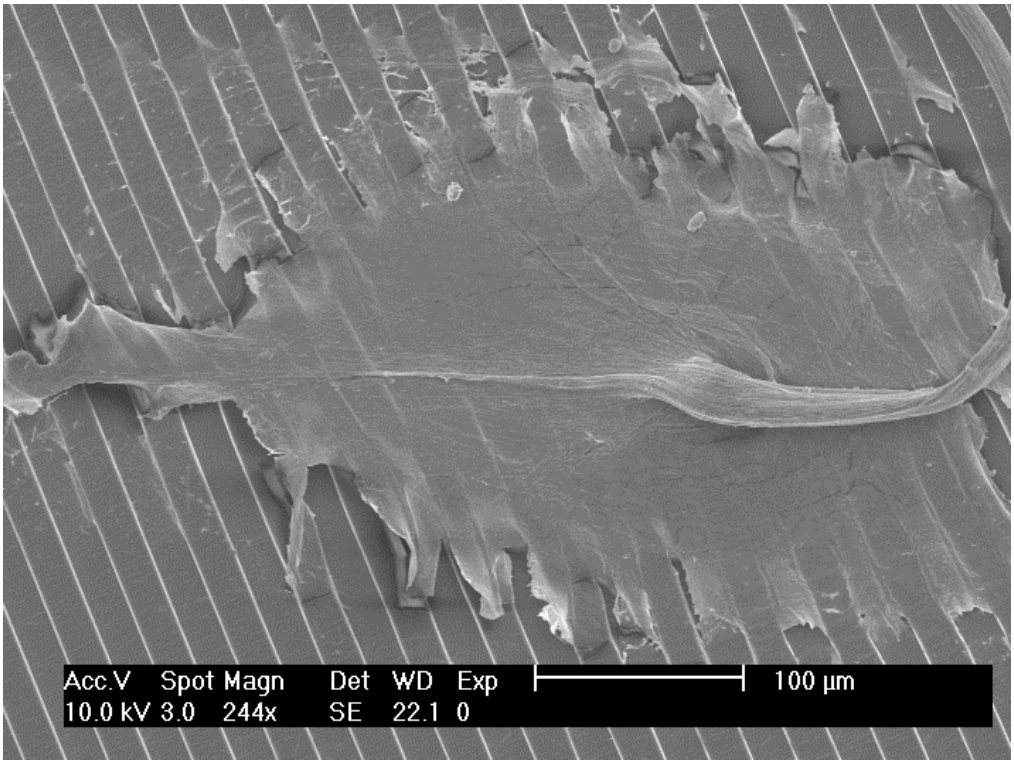

A

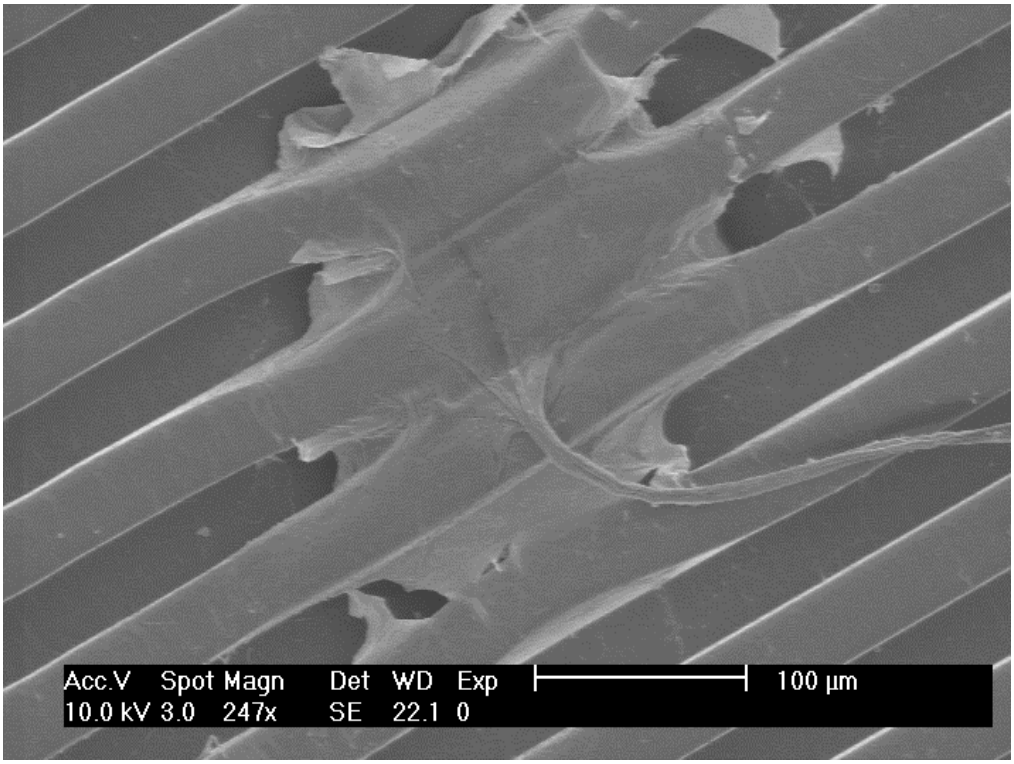

B

Figure 5-8. SEM pictures of attached mussel plaques on 20x20 microns channels feature (A) and 50x50 microns feature (B) (Photo taken by author).

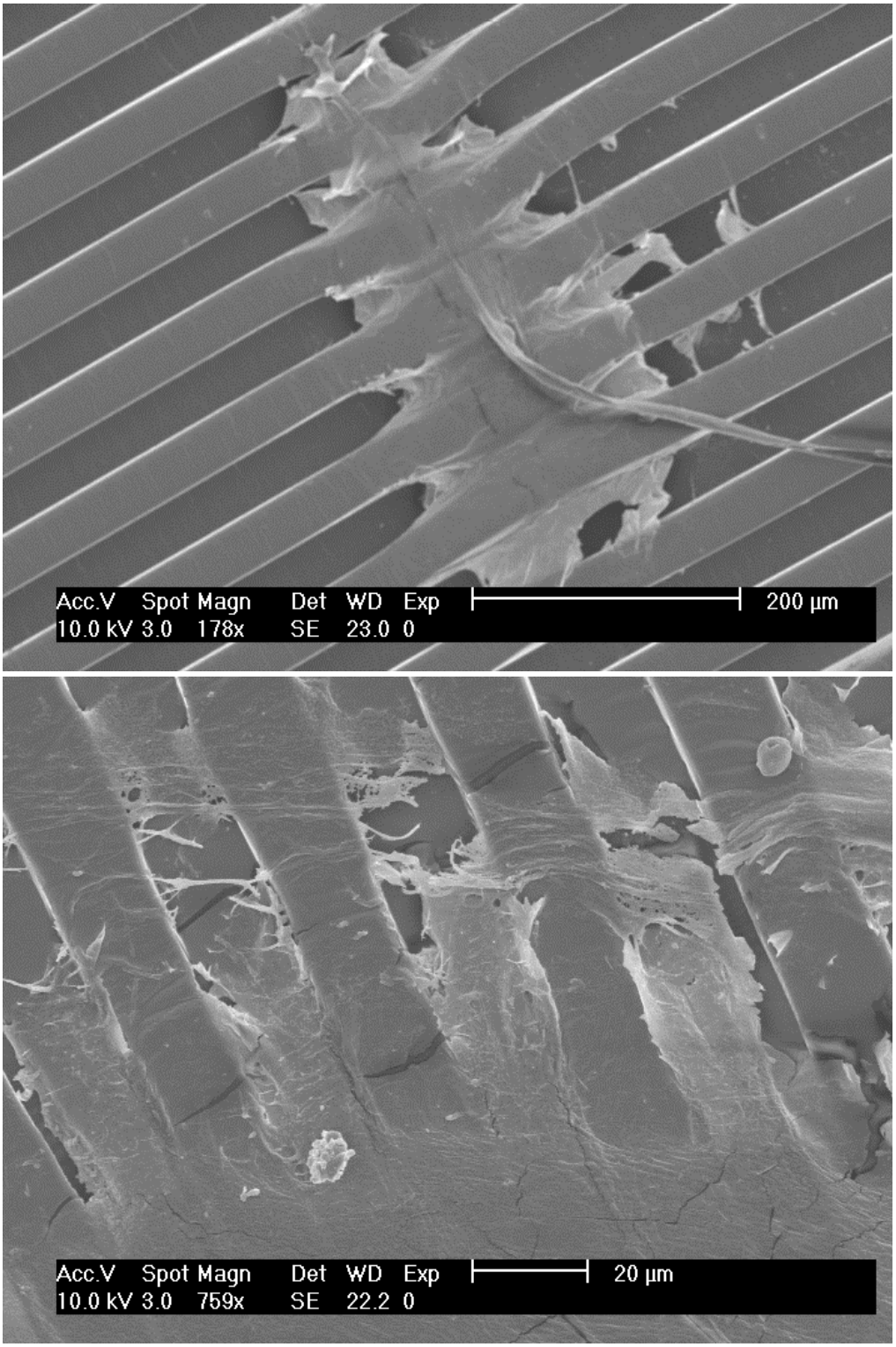

Figure 5-9. SEM pictures of attached mussel plaques on 50x50 microns channels feature (A) and 20x20 microns feature (B) (Photo taken by author).

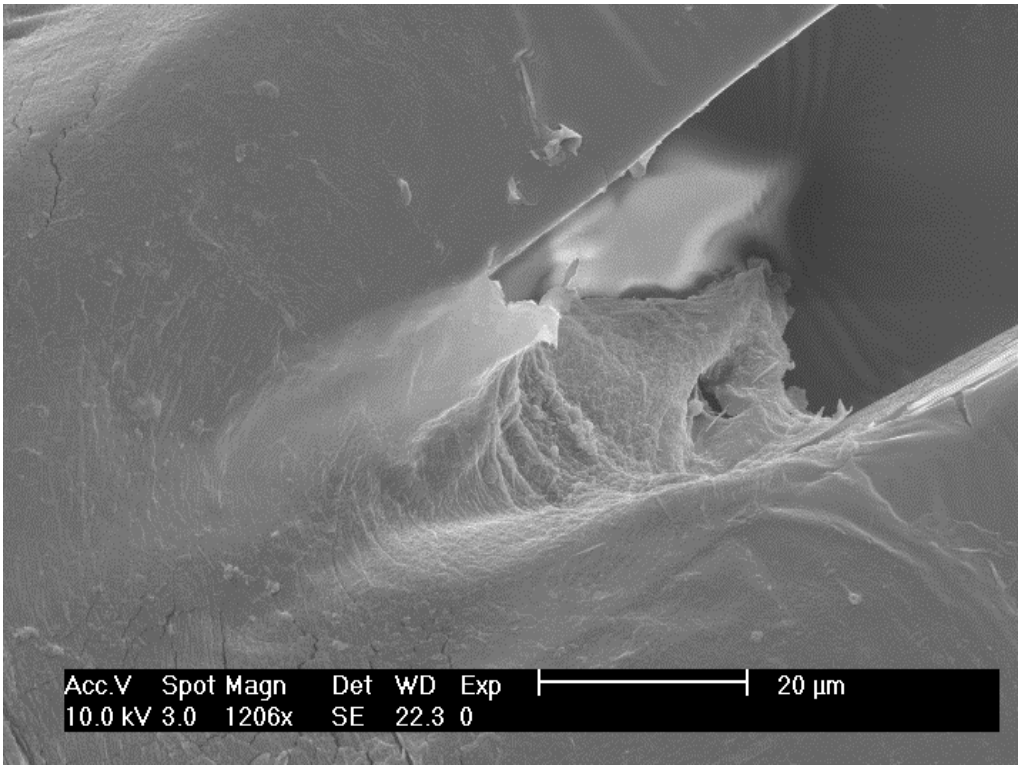

A

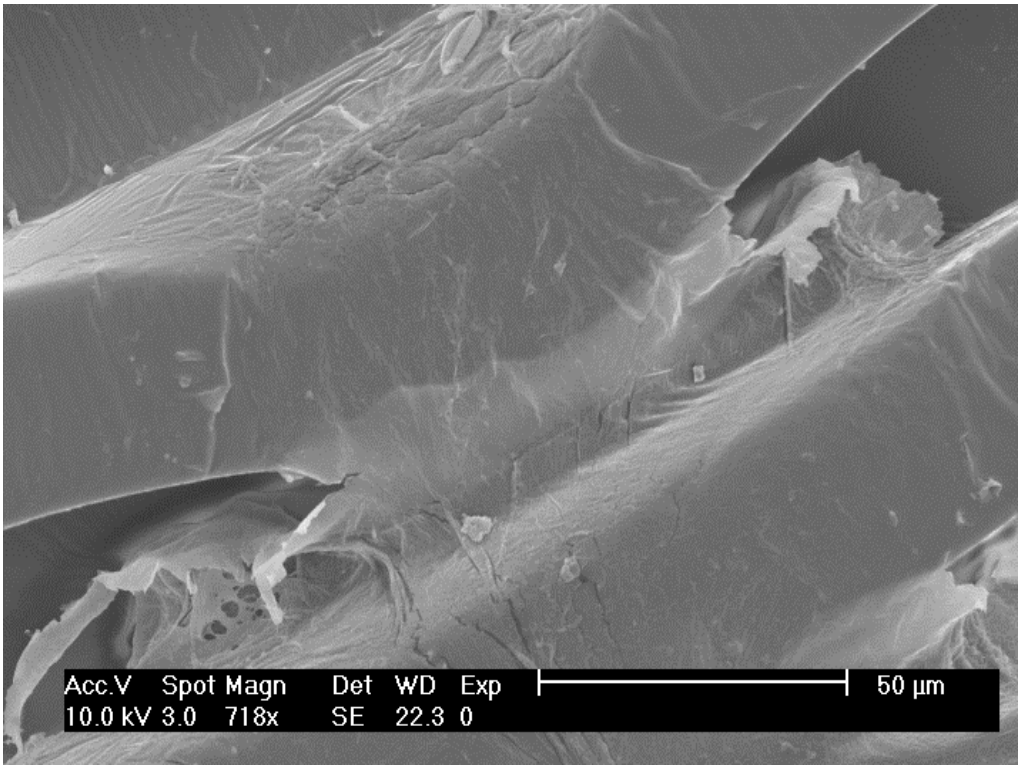

B

Figure 5-10. SEM pictures of attached mussel plaques on 50x50 microns feature (Photo taken by author).

Figure 5-11. Tensile test performed in texture analyzer. A number of threads can be observed going from the shell of the mussel to the substrate. The grip appears in the figure producing the load to the byssus system (Photo taken by author).

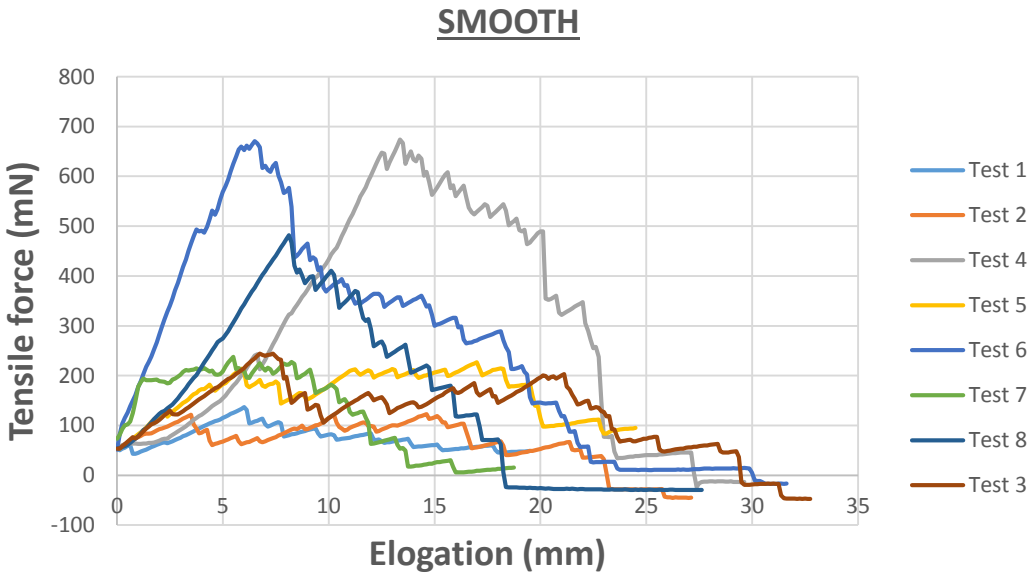

Figure 5-12. Results for the texture analyzer tensile test on smooth PDMSe. The graph shows tensile force (mN) versus elongation (mm) for 8 different tests.

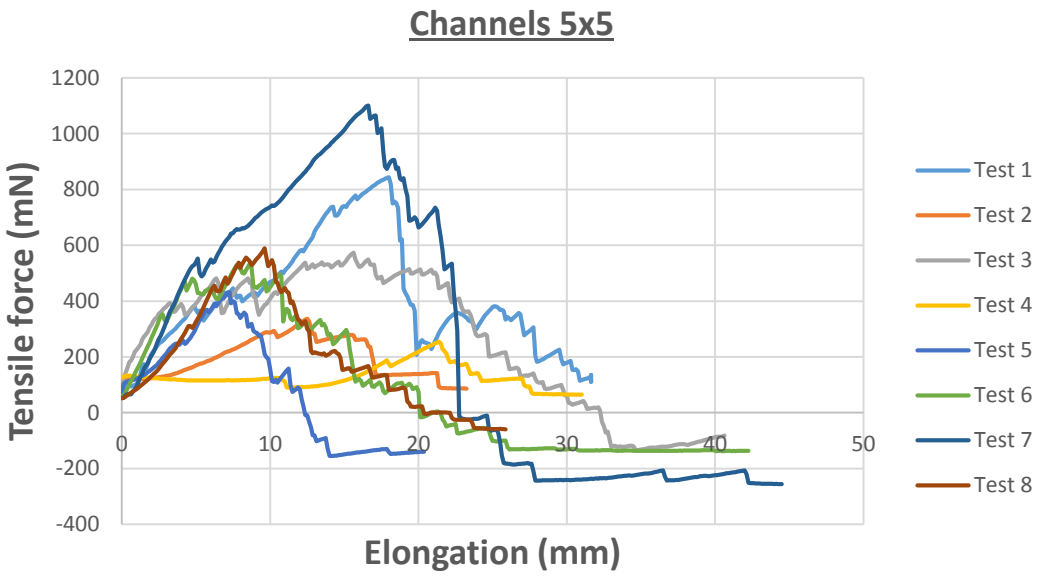

Figure 5-13. Results for the texture analyzer tensile test on channels 5x5 microns features. The graph shows tensile force (mN) versus elongation (mm) for 8 different tests.

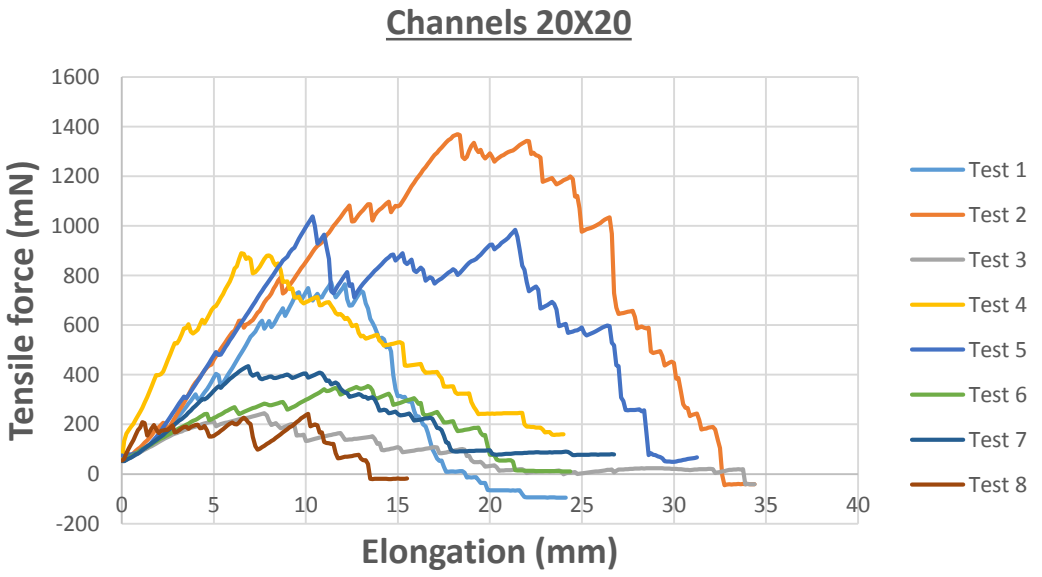

Figure 5-14. Results for the texture analyzer tensile test on channels 20x20 microns features. The graph shows tensile force (mN) versus elongation (mm) for 8 different tests.

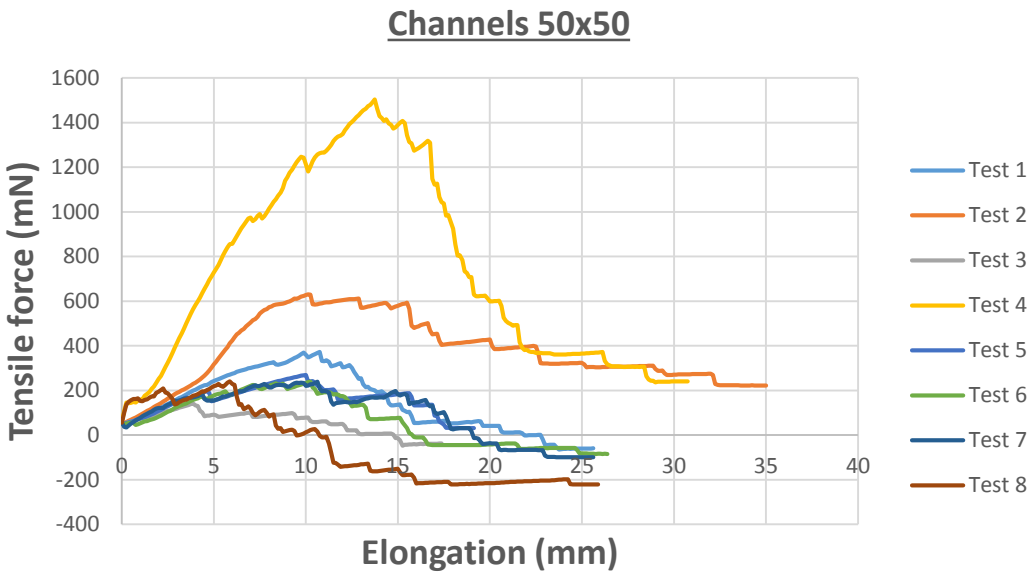

Figure 5-15. Results for the texture analyzer tensile test on channels 20x20 microns features. The graph shows tensile force (mN) versus elongation (mm) for 8 different tests.

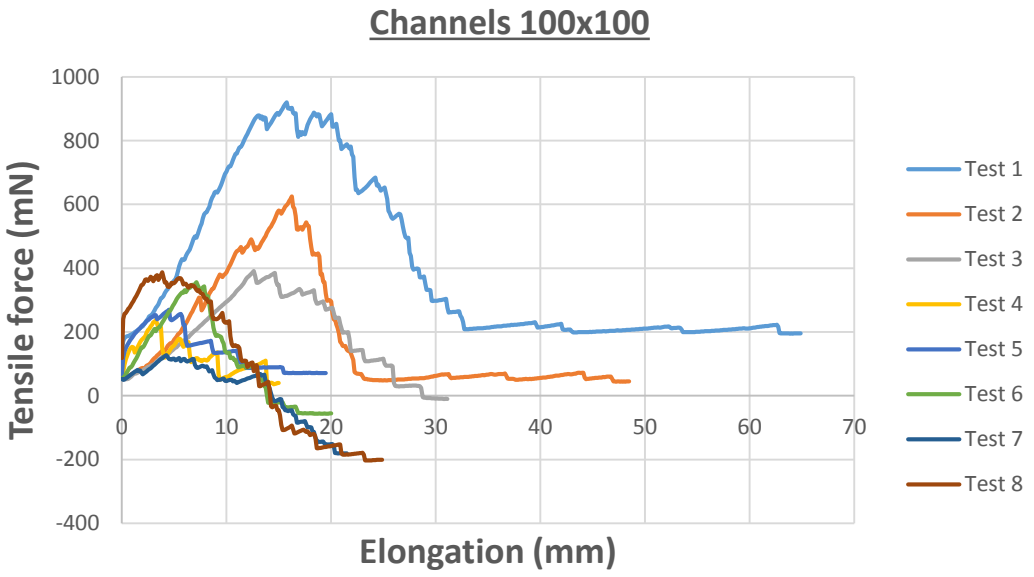

Figure 5-16. Results for the texture analyzer tensile test on channels 100x100 microns features. The graph shows tensile force (mN) versus elongation (mm) for 8 different tests.

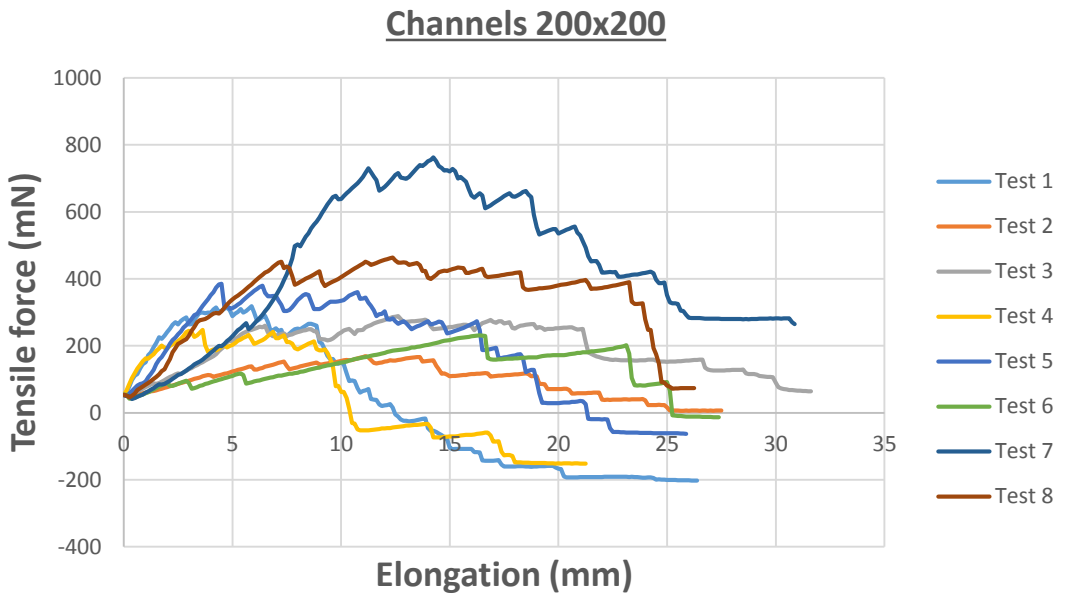

Figure 5-17. Results for the texture analyzer tensile test on channels 200x200 microns features. The graph shows tensile force (mN) versus elongation (mm) for 8 different tests.

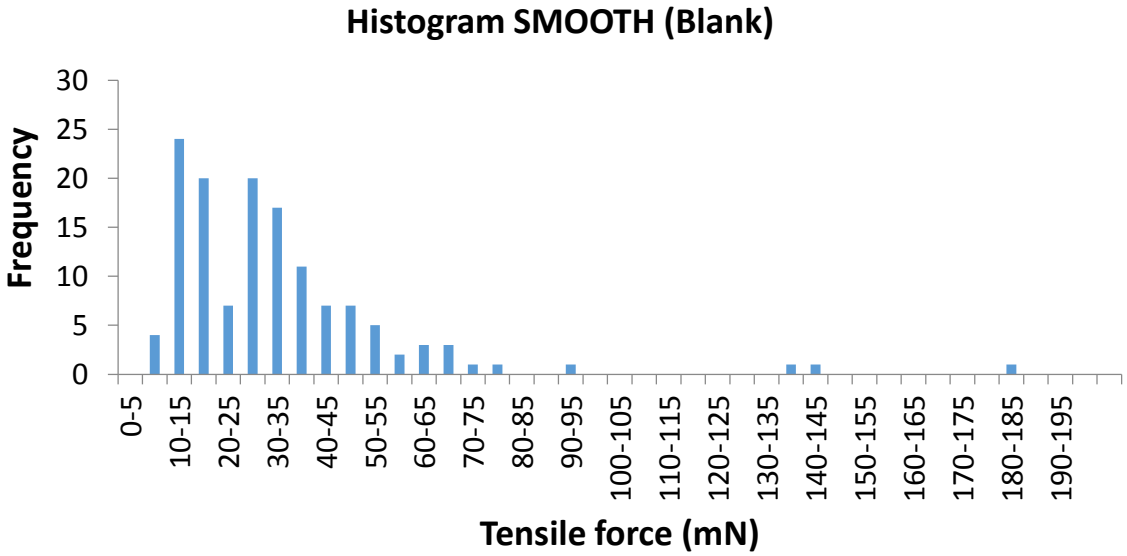

Figure 5-18. Histogram for the tensile force (mN) values of the different plaques for those tests on smooth PDMSe

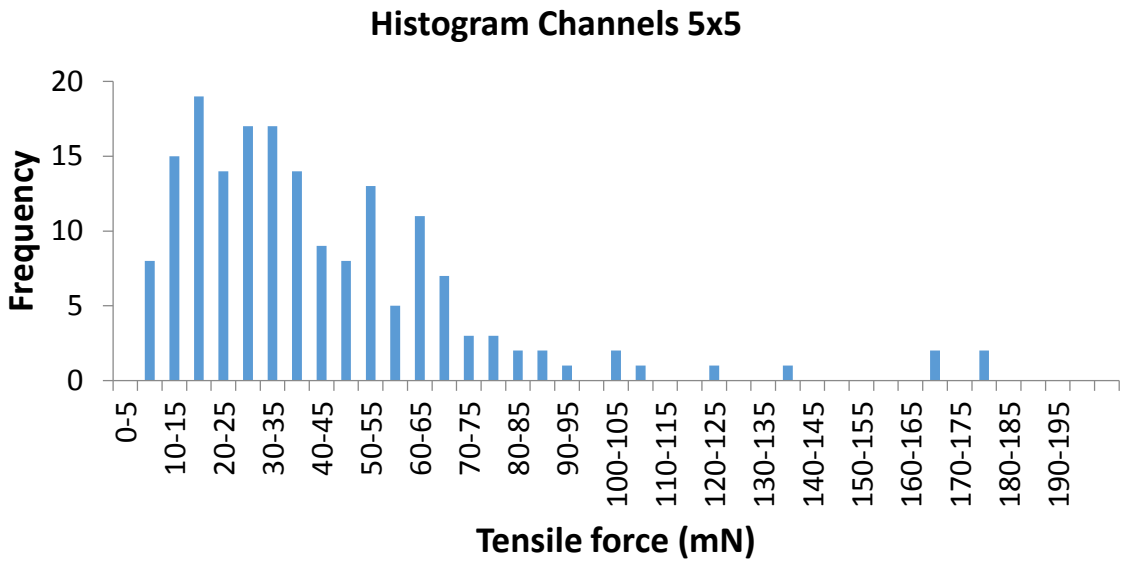

Figure 5-19. Histogram for the tensile force (mN) values of the different plaques for those tests on 5x5 microns channels samples

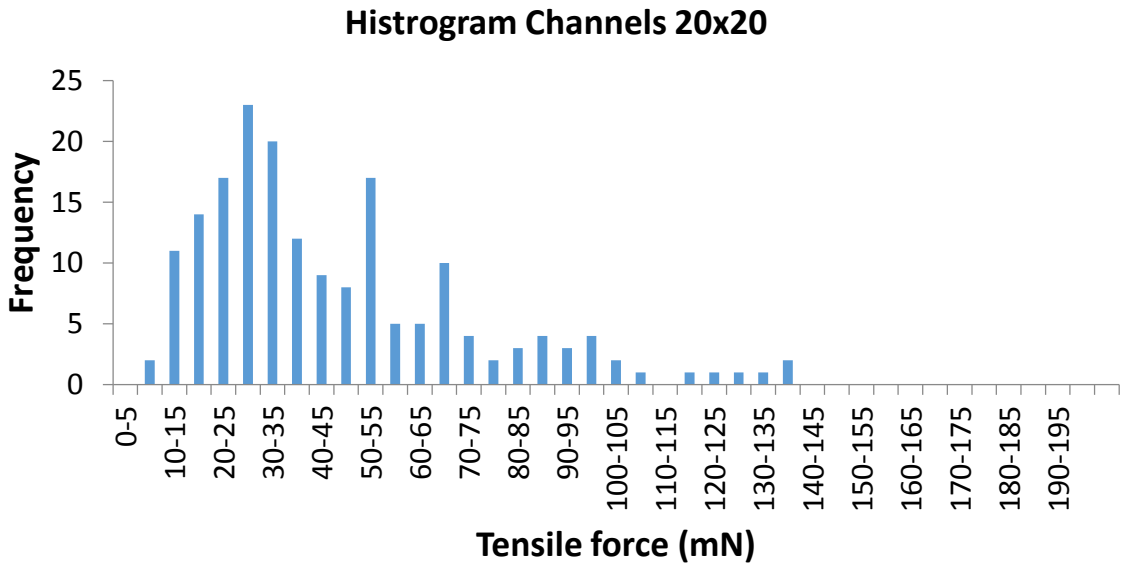

Figure 5-20. Histogram for the tensile force (mN) values of the different plaques for those tests on 20x20 microns channels samples

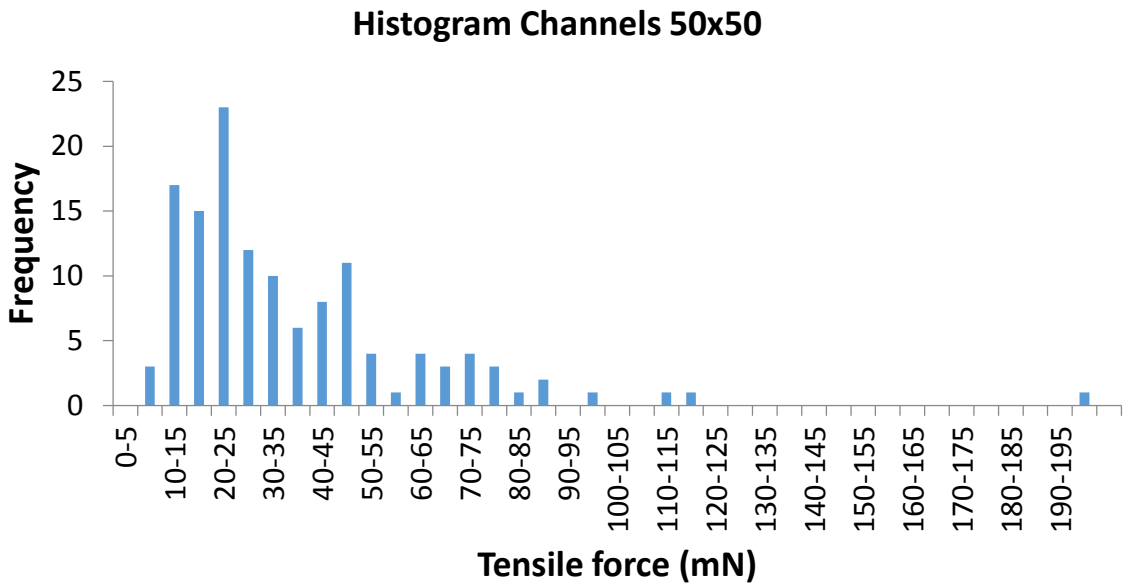

Figure 5-21. Histogram for the tensile force (mN) values of the different plaques for those tests on 50x50 microns channels samples

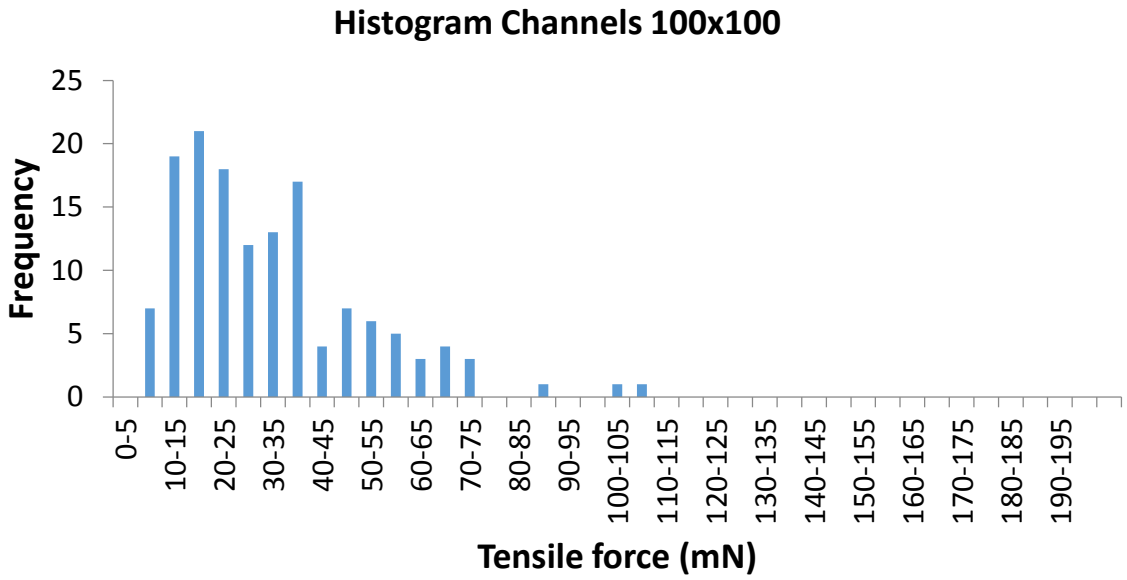

Figure 5-22. Histogram for the tensile force (mN) values of the different plaques for those tests on 100x100 microns channels samples

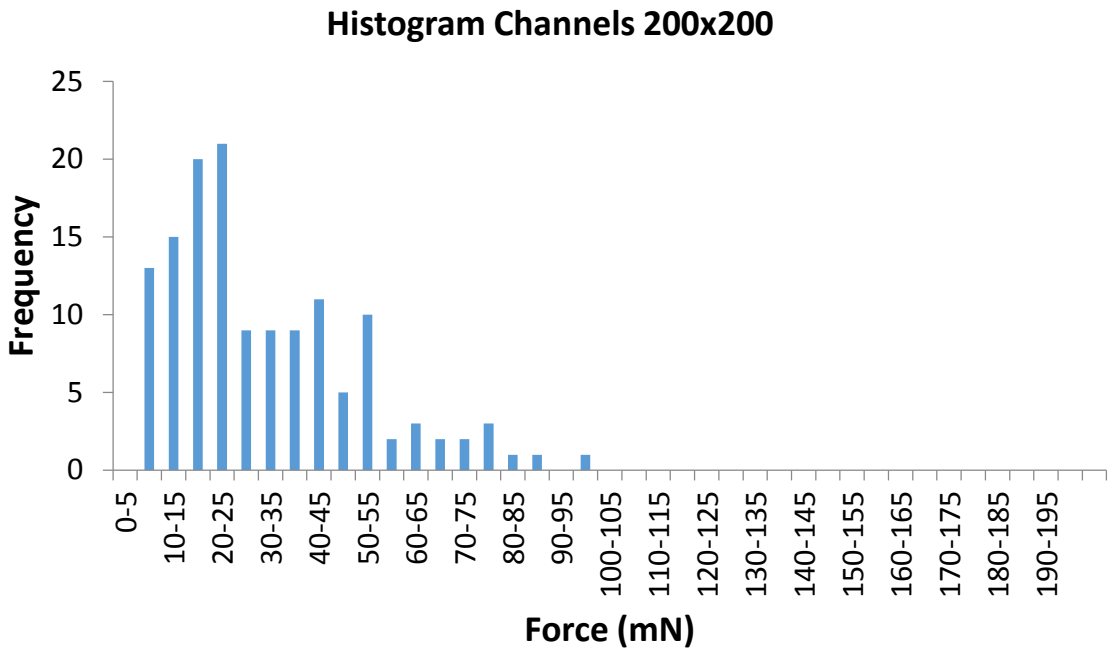

Figure 5-23. Histogram for the tensile force (mN) values of the different plaques for those tests on 200x200 microns channels samples

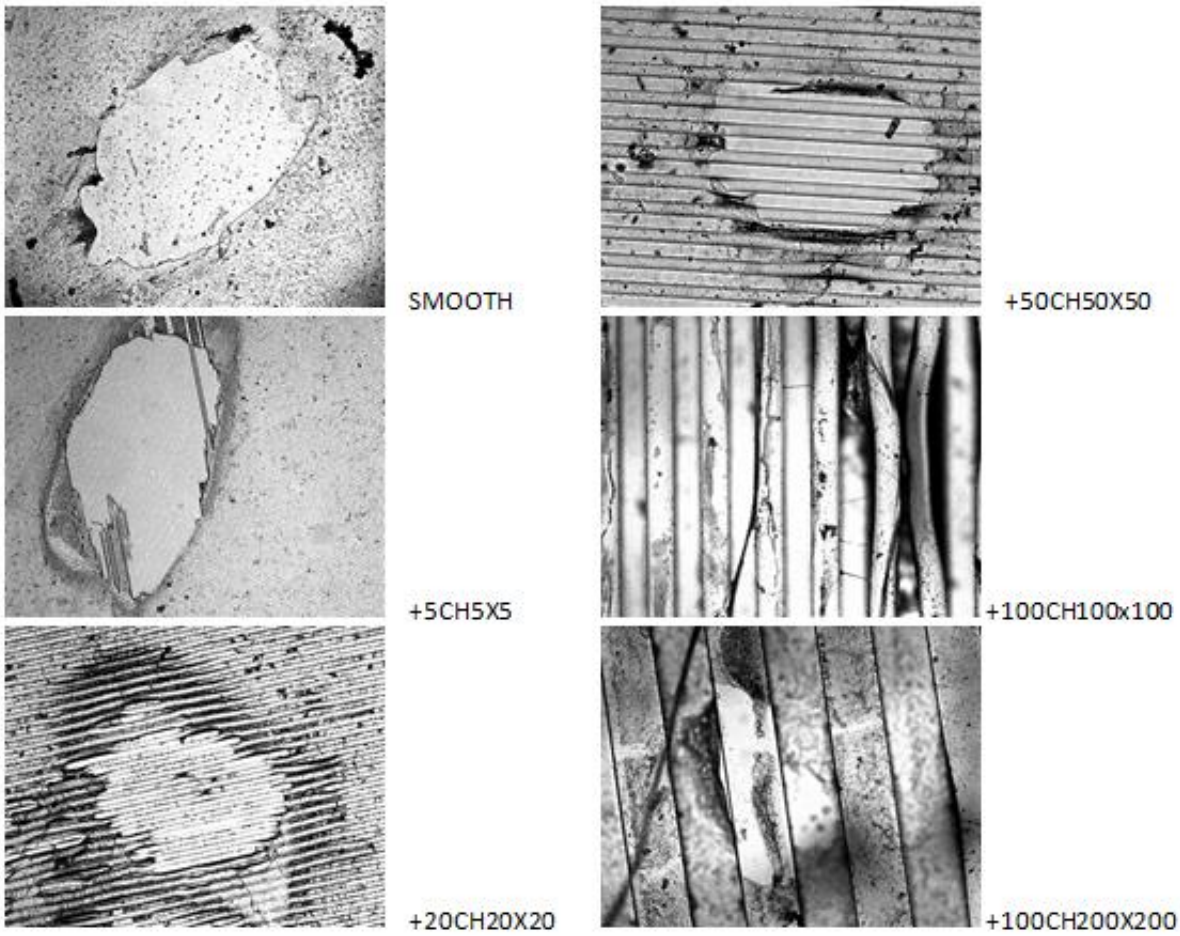

Figure 5-24. Adhesive failures of mussel plaques in the different topographies. Those failures on 100 CH100x100 and 100 CH200x200 are more difficult to observe in the picture due to the scale of the topography (Photo taken by author)

Table 5-9. Values of tensile force (mN) and Tensile stress (Pa) including basic statistical analysis for every sample tested in the texture analyzer

		Tensile force (mN)	Tensile stress$x10^{-3}$ (Pa)
	Average	32.706	60.977
	N	136	136
SMOOTH	st. dev.	24.567	45.803
	90%CI	3.465	6.460
	SE	2.107	3.928
	Average	42.368	78.231
	n	177	177
5X5	st. dev.	31.014	57.266
	90%CI	3.834	7.080
	SE	2.331	4.304
	Average	45.161	83.604
	n	182	182
20X20	st. dev.	27.892	51.634
	90%CI	3.401	6.295
	SE	2.067	3.827
	Average	36.425	71.291
	n	131	131
50X50	st. dev.	26.339	51.551
	90%CI	3.785	7.408
	SE	2.301	4.504
	Average	31.862	86.350
	n	142	142
100X100	st. dev.	19.031	51.576
	90%CI	2.627	7.119
	SE	1.597	4.328
	Average	31.732	90.779
	n	137	137
200X200	st. dev.	19.623	56.138
	90%CI	2.758	7.889
	SE	1.677	4.796

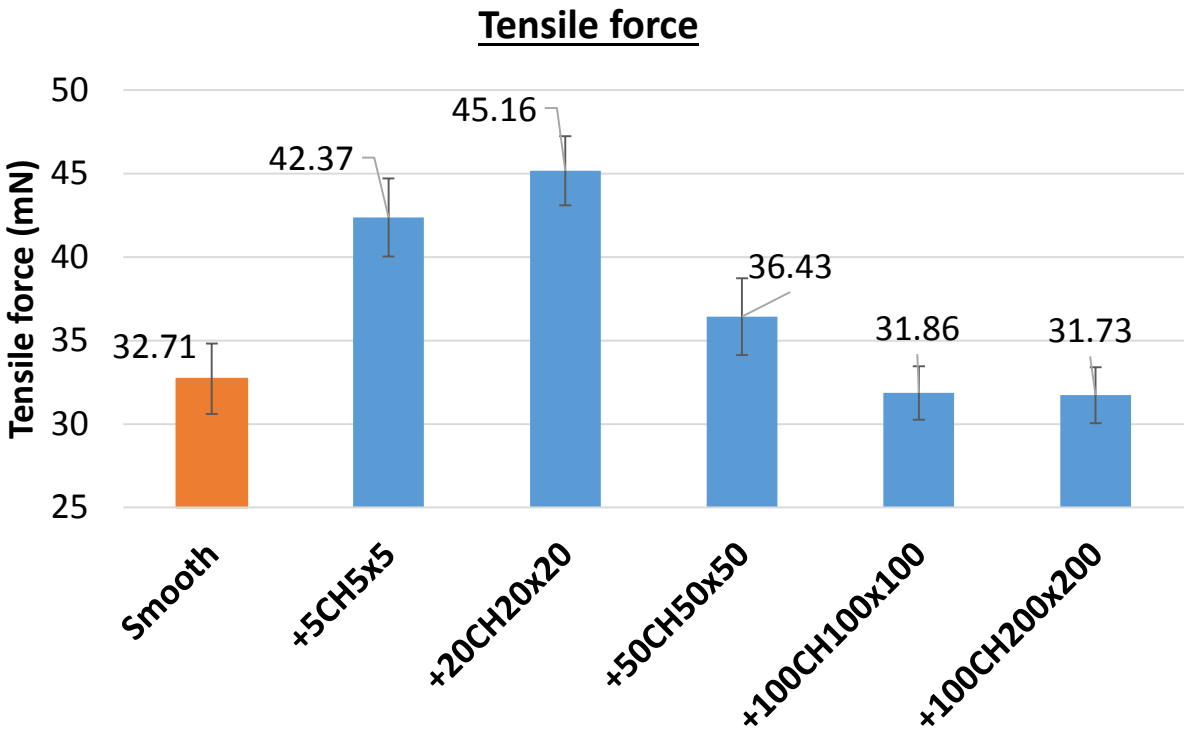

Figure 5-25. Tensile force (mN) for every sample (5x5, 20x20, 50x50, 100x100, 200x200, width x spacing in microns) and blank. Values are averages and the error bars correspond to standard error (SE).

Table 5-10. ANOVA variance study for tensile force values for each topography

ANOVA

Source of Variation	SS	df	MS	F	P-value	F crit
Between Groups	27207	5	5441.379652	8.305585654	1E-07	2.2241
Within Groups	588977	899	655.1470153			
Total	616184	904				

Table 5-11. Tukey post-hoc analysis of tensile force values (being 1=smooth, 2=5x5, 3=20x20, 4=50x50, 5=100x100, 6=200x200)

```
Tukey 90% Simultaneous Confidence Intervals
All Pairwise Comparisons among Levels of Samples

Individual confidence level = 99.02%

Samples = 1 subtracted from:

Samples  Lower  Center  Upper  -------+---------+---------+---------+--
2         2.11    9.66  17.22                    (-----*-----)
3         4.95   12.45  19.96                      (-----*------)
4        -4.39    3.72  11.83             (------*------)
5        -8.79   -0.84   7.10          (-----*------)
6        -8.99   -0.97   7.04          (-----*------)
                               -------+---------+---------+---------+--
                                    -12         0        12        24

Samples = 2 subtracted from:

Samples   Lower  Center  Upper  -------+---------+---------+---------+--
3         -4.20    2.79   9.79              (-----*-----)
4        -13.58   -5.94   1.69        (-----*-----)
5        -17.97  -10.51  -3.04    (-----*-----)
6        -18.17  -10.64  -3.10    (-----*-----)
                               -------+---------+---------+---------+--
                                    -12         0        12        24

Samples = 3 subtracted from:

Samples   Lower  Center  Upper  -------+---------+---------+---------+--
4        -16.33   -8.74  -1.15     (------*-----)
5        -20.72  -13.30  -5.88  (-----*-----)
6        -20.92  -13.43  -5.94  (-----*-----)
                               -------+---------+---------+---------+--
                                    -12         0        12        24

Samples = 4 subtracted from:

Samples   Lower  Center  Upper  -------+---------+---------+---------+--
5        -12.59   -4.56   3.46         (-----*------)
6        -12.79   -4.69   3.40        (------*------)
                               -------+---------+---------+---------+--
                                    -12         0        12        24

Samples = 5 subtracted from:

Samples  Lower  Center  Upper  -------+---------+---------+---------+--
6        -8.06   -0.13   7.80           (------*------)
                               -------+---------+---------+---------+--
                                    -12         0        12        24
```

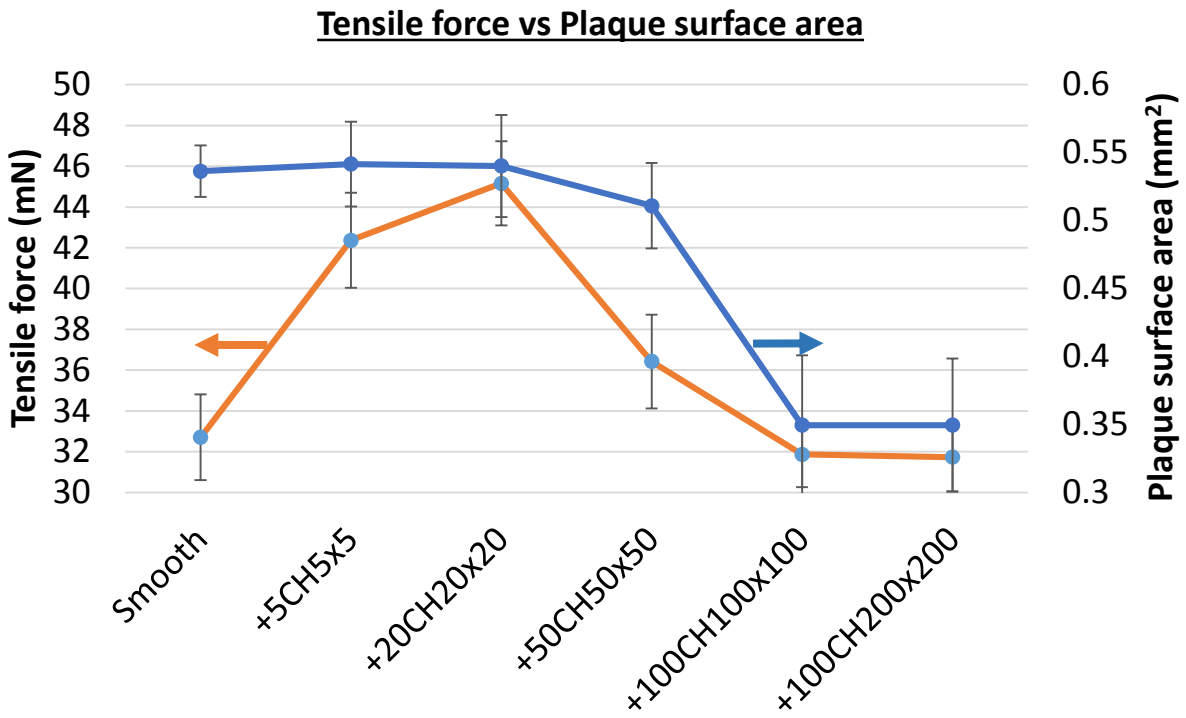

Figure 5-26. Comparison between data collected for tensile force (left axis) and plaque surface area (right axis). Values are averages and the error bars correspond to standard error (SE).

Table 5-12. Comparison with ANOVA statistical analysis (Minitab) between plaque surface area values of the 48 h and 72 h experiments

One-way ANOVA: 5CH5X5 (48 h), 5 CH5X5 (72 h)

Source	DF	SS	MS	F	P
Factor	1	0.00166	0.00166	0.39	0.539
Error	16	0.06741	0.00421		
Total	17	0.06907			

S = 0.06491 R-Sq = 2.41% R-Sq(adj) = 0.00%

One-way ANOVA: 20CH20X20 (48 h), 20CH20X20 (72 h)

Source	DF	SS	MS	F	P
Factor	1	0.00295	0.00295	0.31	0.586
Error	16	0.15266	0.00954		
Total	17	0.15561			

S = 0.09768 R-Sq = 1.89% R-Sq(adj) = 0.00%

One-way ANOVA: 50CH50X50 (48 h), 50CH50X50 (72 h)

Source	DF	SS	MS	F	P
Factor	1	0.00001	0.00001	0.00	0.969
Error	16	0.07976	0.00498		
Total	17	0.07977			

S = 0.07060 R-Sq = 0.01% R-Sq(adj) = 0.00%

One-way ANOVA: 100CH100X100 (48 h), 100CH100X100 (72 h)

Source	DF	SS	MS	F	P
Factor	1	0.0213	0.0213	1.56	0.230
Error	16	0.2192	0.0137		
Total	17	0.2405			

S = 0.1171 R-Sq = 8.86% R-Sq(adj) = 3.17%

One-way ANOVA: 100CH200X200 (48 h), 100CH200X200 (72 h)

Source	DF	SS	MS	F	P
Factor	1	0.0012	0.0012	0.10	0.756
Error	16	0.1924	0.0120		
Total	17	0.1936			

S = 0.1097 R-Sq = 0.62% R-Sq(adj) = 0.00%

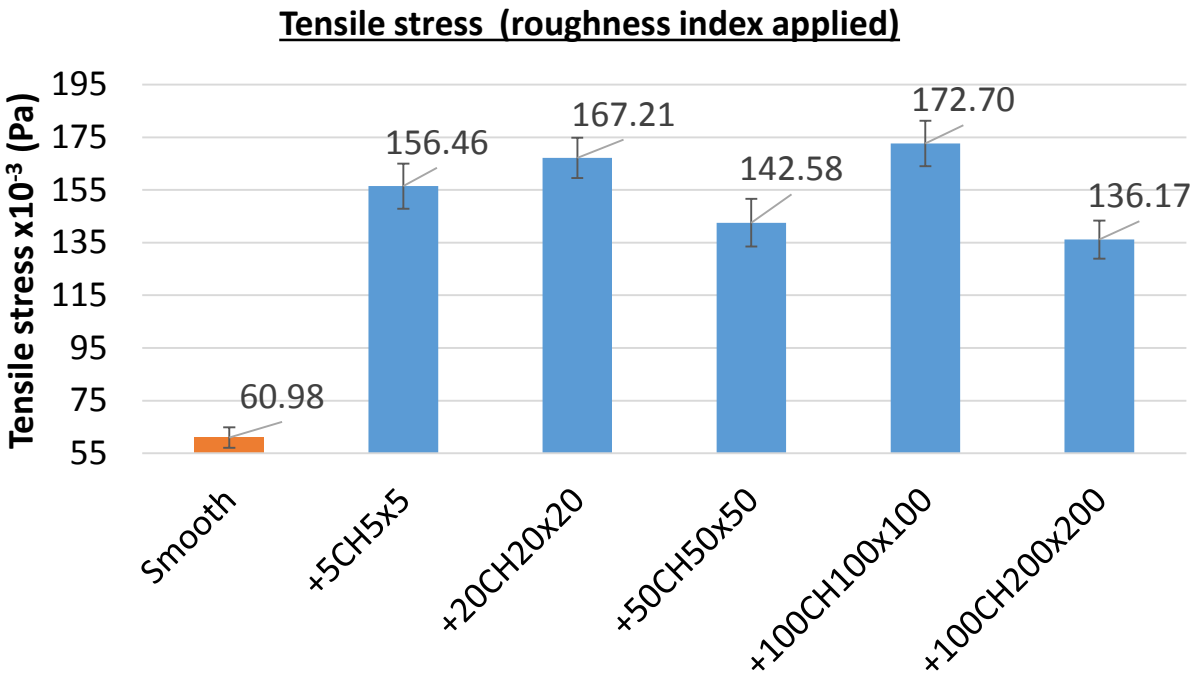

Figure 5-27. Tensile stress (x10-3 Pa) for every sample (5x5, 20x20, 50x50, 100x100, 200x200, width x spacing in microns) and blank applying roughness index. Values are averages and the error bars correspond to standard error (SE).

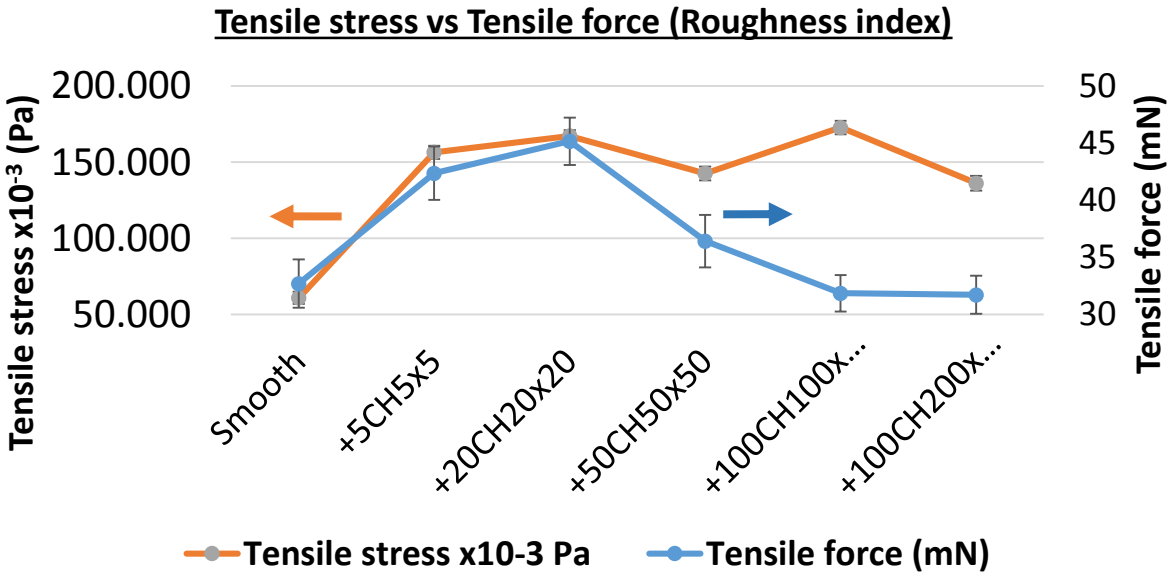

Figure 5-28. Comparison between data collected for tensile force (right axis) and tensile stress (left axis). Values are averages and the error bars correspond to standard error (SE).

CHAPTER 6
CONCLUSIONS AND FUTURE WORK

Conclusions

As was previously mentioned in this thesis, the number of plaques does not represent a confident measurement for technical reasons. However it was worth mentioning that the values, although rough, are considered valid estimations that can be compared with previous studies.

Plaque surface area has been shown in this study to decrease with increasing size of the channels on the topography, since the adhesive spreads faster when the "spreading front" encounters smaller size features. Another effect of the topography on the adhesive was the shape of the plaques. The degree of alignment of the plaques with the topography is proportional to the size of the features. The wider the spacing, the easier it was for the adhesive to advance between ridges producing an elongation in the direction of the channels.

Tensile force scaled inversely proportional to the feature size. Since the only interaction measured was the interaction between the adhesive and the PDMSe, the only effect that possibly produces those changes, is the size of the topography. In this way, the topography proves to have a significant effect on mussel attachment, reducing the force of every individual plaque attachment by increasing the size of the features. Nonetheless the difference between the biggest topography and the smooth PDMSe is not significant.

The tensile stress measured in this project scaled directly proportional to the feature size. If we consider all the assumptions made, the value of the tensile stress for

each topography should be constant. To explain the observed unexpected effect, some considerations need to be made.

The plaque surface value measured in this experiment was that obtained by the planar projection of every plaque on the topography. This means that the only effective area considered to calculate stress was the planar projection, when in reality, an extra effective adhesion area must exist that was not considered, but plays an important role in adhesion. In other words, topography creates a larger effective area (side of the ridges) where attachment happens. So the degree of penetration of the adhesive is big enough to produce an important effect. A good method to estimate the effect of the topography is the Engineering Roughness Index (ERI), but in this case the parameters of the equation are the same for most of the samples used in this study.

Two concepts play an equally important role in this study: plaque surface area and degree of penetration, both of them affected by the size of the different topographies. First of all, the bigger the size of the topography, the smaller the plaque surface area because the features act as obstacles in the mussel adhesive spreading and therefore decrease adhesion strength. The degree of penetration promotes adhesion strength by filling the space between the features. It could be that the adhesive undergoes a different degree of effective adhesion depending on the different topographies. The adhesive may create an effective adhesion to most of the small features by adapting to them but not achieve an extensive adhesion in those larger features (Figure 6-1.). Nevertheless, no degree of penetration measurements have been done in this study and this is only a hypothesis. Further study in this subject could help explain the observed behavior.

In general this study provided enough information to state that channel topographies (ratio 1:1) within the range of 5x5 microns and 50x50 microns enhance the adhesion, providing extra surface to the adhesive where attachment happens, and that bigger topographies present values very similar to those found on smooth PDMSe. For this reason, based on this study it is recommended the use of patterns around 100-200 microns, in order to reduce attachment strength of the mussel to a surface.

Future work

There are many options to obtain a deeper understanding of mussel adhesion and mussel adhesive spreading behavior in engineered topographies. Most of which will lead to further experimentation.

Comparison with commercial adhesives

If the same technique and method described in this study is repeated using different commercially available adhesives, this could help to understand what makes the mussel attachment procedure so unique. This could be done easily by depositing a known volume of adhesive on top of different topographies and allowing the spreading to occur naturally underwater. Another modification of this test could be to force the spreading of the adhesive by applying a specific load also in underwater conditions. Values of plaque surface area, NFF, and tensile force could be compared with those obtained in this study.

Test other engineered topographies

Further experimentation with different topography design would be beneficial to understand the response of the mussel with respect to the surface in the early stage. It could help us to prove if the mussel foot is sensitive to changes and if the mussel has

the ability to spot and discriminate different sites on the topography. This study helps to understand which size enhances or prevents the adhesion of the mussel.

Measure the penetration degree

In this study, the penetration degree of the mussel adhesive has been reported qualitatively but no measurement technique has been applied. Microtomy was tried unsuccessfully in the early stage of the study. Due to the nature of the PDMSe and the proteins in the plaque, this method was abandoned. Not a single sectional slice was obtained by this method because the process completely ruins the plaque attachment due to shear forces on the polymer. One of the techniques recommended is cryogenic microtomy. Temperatures below the Tg will ensure the polymer has a sufficient modulus to achieve clean section can be obtained. Another possible way to observe and to measure the degree of penetration between the ridges is direct observation with a high resolution camera. It may be possible to obtain an image clear enough to quantify distance.

Measure the exact volume of adhesive secreted by the mussel

In order to measure the volume of the plaque all dimensions need to be taken into account and not only the planar projection. To get this information some techniques such as confocal microscopy or even atomic force microscopy (AFM) could be helpful. This would provide information about the height of the plaque. But there is still some of the adhesive that also fills the space between the channel walls that has to be measured.

Analyze the surface where adhesive failure happens.

This study assumed that all the mussel adhesive was removed when the plaque undergoes adhesive failure, In order to make this assumption more confidently, a

chemical analysis of the specific spot on the topography should take place to ensure the assumption is correct. The plaque detachment leaves an easily detected spot, even visually, so it is big enough to reduce the characterization surface to that specific area. Some of the techniques could be infrared analysis (FTIR) or X-Ray Photoelectron Spectrometry (XPS).

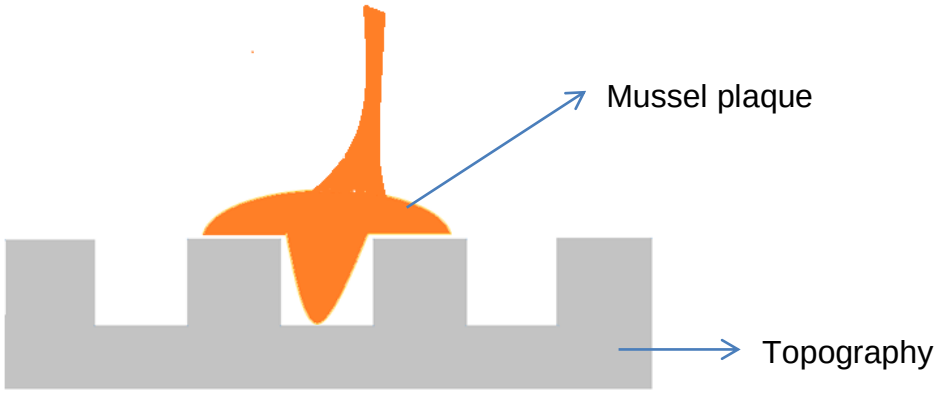

Larger size topography
Degree of effective attachment to the features is reduced because the adhesive capacity to fill the spacing is reduced

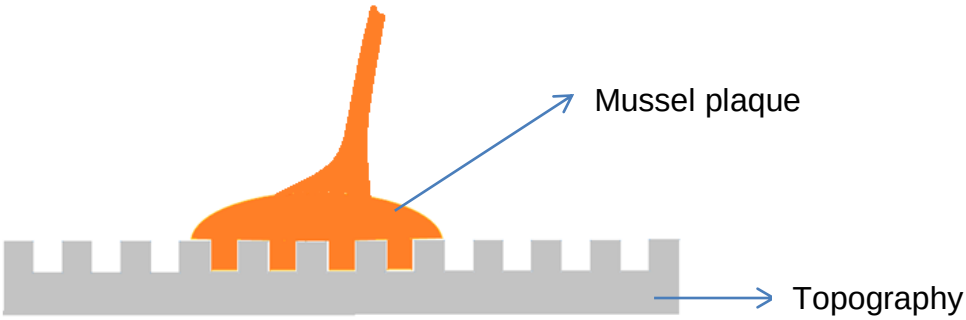

Smaller size topography
Degree of effective attachment to the features is higher since the adhesive achieves to fill the spacing

Figure 6-1. Scheme of the effect of the topography size on mussel plaque adhesion (adhesive attachment)

LIST OF REFERENCES

Ackerman, J. D., Cottrell, C. M., Ethier, C. R., Allen, D. G., & Spelt, J. K. (1996). Attachment strength of zebra mussels on natural, polymeric, and metallic materials. *Journal of Environmental Engineering, 122*(2), 141-148.

Ackerman, J. D., Ethier, C. R., Allen, D. G., & Spelt, J. K. (1992). Investigation of zebra mussel adhesion strength using rotating disks. *Journal of Environmental Engineering, 118*(5), 708-724.

Ackerman, J. D., Ethier, C. R., Spelt, J. K., Allen, D. G., & Cottrell, C. M. (1995). A wall jet to measure the attachment strength of zebra mussels. *Canadian Journal of Fisheries and Aquatic Sciences, 52*(1), 126-135.

Ackerman, J. D., Sim, B., Nichols, S. J., & Claudi, R. (1994). A review of the early life history of zebra mussels (Dreissena polymorpha): comparisons with marine bivalves. *Canadian Journal of Zoology, 72*(7), 1169-1179.

Alavi, M., Büttgenbach, S., Schumacher, A., & Wagner, H.-J. (1992). Fabrication of microchannels by laser machining and anisotropic etching of silicon. *Sensors and Actuators A: Physical, 32*(1), 299-302.

Aldred, N., Ista, L., Callow, M., Callow, J., Lopez, G., & Clare, A. (2006). Mussel (Mytilus edulis) byssus deposition in response to variations in surface wettability. *Journal of The Royal Society Interface, 3*(6), 37-43.

Aldred, N., Scardino, A., Cavaco, A., de Nys, R., & Clare, A. S. (2010). Attachment strength is a key factor in the selection of surfaces by barnacle cyprids (Balanus amphitrite) during settlement. *Biofouling, 26*(3), 287-299.

Baum, C., Meyer, W., Roessner, D., Siebers, D., & Fleischer, L.-G. (2001). A zymogel enhances the self-cleaning abilities of the skin of the pilot whale (Globicephala melas). *Comparative Biochemistry and Physiology Part A: Molecular \& Integrative Physiology, 130*(4), 835-847.

Bayne, B. (1964). Primary and secondary settlement in Mytilus edulis L.(Mollusca). *The Journal of Animal Ecology*, 513-523.

Brennan, A. B., Baney, R. H., Carman, M. L., Estes, T. G., Feinberg, A. W., Wilson, L. H., et al. (2010, January). Surface topographies for non-toxic bioadhesion control. *Surface topographies for non-toxic bioadhesion control*. Google Patents.

Burkett, J. R., Wojtas, J. L., Cloud, J. L., & Wilker, J. J. (2009). A method for measuring the adhesion strength of marine mussels. *The Journal of Adhesion, 85*(9), 601-615.

Callow, J. A., & Callow, M. E. (2006). The Ulva spore adhesive system. In *Biological adhesives* (pp. 63-78). Springer.

Carl, C., Poole, A. J., Williams, M. R., & de Nys, R. (2012). Where to Settle—Settlement Preferences of Mytilus galloprovincialis and Choice of Habitat at a Micro Spatial Scale. *PloS one, 7*(12), e52358.

Carl, C., Poole, A., Sexton, B., Glenn, F., Vucko, M., Williams, M., et al. (n.d.). Enhancing the settlement and attachment strength of pediveligers of Mytilus galloporovincialis by changing surface wettability and microtopography. *Journal Title, 2012*, 1-27.

Carl, C., Poole, A., Vucko, M., Williams, M., Whalan, S., & de Nys, R. (2012). Enhancing the efficacy of fouling-release coatings against fouling by Mytilus galloprovincialis using nanofillers. *Biofouling, 28*(10), 1077-1091.

Carman, M. L., Estes, T. G., Feinberg, A. W., Schumacher, J. F., Wilkerson, W., Wilson, L. H., et al. (2006). Engineered antifouling microtopographies--correlating wettability with cell attachment. *Biofouling, 22*(1), 11-21.

Chiovitti, A., Dugdale, T. M., & Wetherbee, R. (2006). Diatom adhesives: molecular and mechanical properties. In *Biological adhesives* (pp. 79-103). Springer.

Dunn, G., & Heath, J. (1976). A new hypothesis of contact guidance in tissue cells. *Experimental cell research, 101*(1), 1-14.

Efimenko, K., Finlay, J., Callow, M. E., Callow, J. A., & Genzer, J. (2009). Development and testing of hierarchically wrinkled coatings for marine antifouling. *ACS applied materials \& interfaces, 1*(5), 1031-1040.

Farsad, N., & Sone, E. D. (2012). Zebra mussel adhesion: Structure of the byssal adhesive apparatus in the freshwater mussel, Dreissena polymorpha. *Journal of Structural Biology, 177*(3), 613-620.

Gantayet, A., Ohana, L., & Sone, E. D. (2013). Byssal proteins of the freshwater zebra mussel, Dreissena polymorpha. *Biofouling, 29*(1), 77-85.

Gibson, A. L. (2002). *Chemical modificaton of silicone elastomer for controlled biological interactions on microtextured surfaces.* Ph.D. dissertation, University of Florida.

Gilbert, T. W., & Sone, E. D. (2010). The byssus of the zebra mussel (Dreissena polymorpha): spatial variations in protein composition. *Biofouling, 26*(7), 829-836.

Hillborg, H., & Gedde, U. (1998). Hydrophobicity recovery of polydimethylsiloxane after exposure to corona discharges. *Polymer, 39*(10), 1991-1998.

Hoipkemeier-Wilson, L., Schumacher, J. F., Carman, M. L., Gibson, A. L., Feinberg, A. W., Callow, M. E., et al. (2004). Antifouling potential of lubricious, micro-engineered, PDMS elastomers against zoospores of the green fouling alga Ulva (Enteromorpha). *Biofouling, 20*(1), 53-63.

Holm, E. R., Kavanagh, C. J., Meyer, A. E., Wiebe, D., Nedved, B. T., Wendt, D., et al. (2006). Interspecific variation in patterns of adhesion of marine fouling to silicone surfaces. *Biofouling, 22*(4), 233-243.

Homma, H., Kuroyagi, T., Izumi, K., Mirley, C., Ronzello, J., & Boggs, S. (2000). Evaluation of surface degradation of silicone rubber using gas chromatography/mass spectroscopy. *Power Delivery, IEEE Transactions on, 15*(2), 796-803.

Kamino, K. (2006). Barnacle underwater attachment. In *Biological adhesives* (pp. 145-166). Springer.

Lee, B. P., Messersmith, P. B., Israelachvili, J. N., & Waite, J. H. (2011). Mussel-inspired adhesives and coatings. *Annual review of materials research, 41*, 99.

Lee, H., Scherer, N. F., & Messersmith, P. B. (2006). Single-molecule mechanics of mussel adhesion. *Proceedings of the National Academy of Sciences, 103*(35), 12999-13003.

Lin, Q., Gourdon, D., Sun, C., Holten-Andersen, N., Anderson, T. H., Waite, J. H., et al. (2007). Adhesion mechanisms of the mussel foot proteins mfp-1 and mfp-3. *Proceedings of the National Academy of Sciences, 104*(10), 3782-3786.

Long, C. J., Schumacher, J. F., Robinson, P. A., Finlay, J. A., Callow, M. E., Callow, J. A., et al. (2010). A model that predicts the attachment behavior of Ulva linza zoospores on surface topography. *Biofouling, 26*(4), 411-419.

Lötters, J., Olthuis, W., Veltink, P., & Bergveld, P. (1997). The mechanical properties of the rubber elastic polymer polydimethylsiloxane for sensor applications. *Journal of Micromechanics and Microengineering, 7*(3), 145.

Lu, Q., Danner, E., Waite, J. H., Israelachvili, J. N., Zeng, H., & Hwang, D. S. (2013). Adhesion of mussel foot proteins to different substrate surfaces. *Journal of The Royal Society Interface, 10*(79).

Marmur, A. (2013). Superhydrophobic and superhygrophobic surfaces: From understanding non-wettability to design considerations. *Soft Matter*.

Matos-Pérez, C. R., White, J. D., & Wilker, J. J. (2012). Polymer Composition and Substrate Influences on the Adhesive Bonding of a Biomimetic, Cross-Linking Polymer. *Journal of the American Chemical Society, 134*(22), 9498-9505.

Morra, M., Occhiello, E., Marola, R., Garbassi, F., Humphrey, P., & Johnson, D. (1990). On the aging of oxygen plasma-treated polydimethylsiloxane surfaces. *Journal of Colloid and Interface Science, 137*(1), 11-24.

Nicklisch, S. C., & Waite, J. H. (2012). Mini-review: The role of redox in Dopa-mediated marine adhesion. *Biofouling, 28*(8), 865-877.

Scardino, A. J., & de Nys, R. (2011). Mini review: Biomimetic models and bioinspired surfaces for fouling control. *Biofouling, 27*(1), 73-86.

Scardino, A., Guenther, J., & De Nys, R. (2008). Attachment point theory revisited: the fouling response to a microtextured matrix. *Biofouling, 24*(1), 45-53.

Scardino, A., Hudleston, D., Peng, Z., Paul, N., & De Nys, R. (2009). Biomimetic characterisation of key surface parameters for the development of fouling resistant materials. *Biofouling, 25*(1), 83-93.

Schultz, M., Bendick, J., Holm, E., & Hertel, W. (2011). Economic impact of biofouling on a naval surface ship. *Biofouling, 27*(1), 87-98.

Schumacher, J. F., Aldred, N., Callow, M. E., Finlay, J. A., Callow, J. A., Clare, A. S., et al. (2007). Species-specific engineered antifouling topographies: correlations between the settlement of algal zoospores and barnacle cyprids. *Biofouling, 23*(5), 307-317.

Schumacher, J. F., Carman, M. L., Estes, T. G., Feinberg, A. W., Wilson, L. H., Callow, M. E., et al. (2007). Engineered antifouling microtopographies--effect of feature size, geometry, and roughness on settlement of zoospores of the green alga Ulva. *Biofouling, 23*(1), 55-62.

Silverman, H. G., & Roberto, F. F. (2007). Understanding marine mussel adhesion. *Marine Biotechnology, 9*(6), 661-681.

Smith, A. M., & Callow, J. A. (2006). *Biological adhesives.* Springer Berlin.

Smith, P. J., Owen, M. J., Holm, P., & Toskey, G. (1992). Surface studies of corona-treated silicone rubber high-voltage insulation. *Electrical Insulation and Dielectric Phenomena, 1992. Annual Report. Conference on*, (pp. 829-836).

Stevens, C. (1998). Environmental degradation pathways for the breakdown of polydimethylsiloxanes. *Journal of inorganic biochemistry, 69*(3), 203-207.

Tóth, A., Bertóti, I., Blazsó, M., Bánhegyi, G., Bognar, A., & Szaplonczay, P. (1994). Oxidative damage and recovery of silicone rubber surfaces. I. X-ray photoelectron spectroscopic study. *Journal of applied polymer science, 52*(9), 1293-1307.

Vrolijk, N., Targett, N., Baier, R., & Meyer, A. (1990). Surface characterisation of two gorgonian coral species: implications for a natural antifouling defence. *Biofouling, 2*(1), 39-54.

Waite, J. (1987). Nature's underwater adhesive specialist. *International Journal of Adhesion and Adhesives, 7*(1), 9-14.

Wake, W. C., & Kinloch, A. (1977). *Developments in adhesives. I.* Applied Science Publishers.

Wake, W., & Kinloch, A. (1981). *Developments in adhesives 2.* Applied Science.

Wells, S., & Sytsma, M. (2009). A Review of the Use of Coatings to Mitigate Biofouling in Freshwater. *Portland State University Center for Lakes and Reservoirs*.

Wiegemann, M. (2005). Adhesion in blue mussels (Mytilus edulis) and barnacles (genus Balanus): mechanisms and technical applications. *Aquatic Sciences-Research Across Boundaries, 67*(2), 166-176.

Wilker, J. J. (2010). Marine bioinorganic materials: mussels pumping iron. *Current opinion in chemical biology, 14*(2), 276-283.

Yu, J., Wei, W., Danner, E., Ashley, R. K., Israelachvili, J. N., & Waite, J. H. (2011). Mussel protein adhesion depends on interprotein thiol-mediated redox modulation. *Nature chemical biology, 7*(9), 588-590.

BIOGRAPHICAL SKETCH

Francisco Castro Cara was born in Zurich Switzerland in 1986 to Encarnacion Cara Lopez and Francisco Castro Castro. In order to be close to the rest of the family, Francisco moved to Churriana de la Vega, Spain at only two years old with his mother and father where he was raised. Soon after arriving to Spain, Francisco became a big brother to Esteban Castro Cara.

Francisco graduated from his hometown high school as valedictorian in 2004, where he made some of the best memories and closest friends. During his high school studies, Francisco chose to focus on science courses, sparking his interest in the field of engineering. Directly after high school, he was accepted to the University of Granada's Master in Chemical Engineering program. The next six years were spent learning, both in and out of the classroom. He worked part time as a science and math tutor in which he developed excellent organization and communication skills. The experience of sharing his knowledge and passion for science was also very rewarding. He explored his creative side by joining a theater group for a year and by submitting creative writing stories to various contests. His summers were spent working at his father's grocery store as well as the town florist shop.

The last year at the University of Granada was spent working on a design project entitled "Exploitation of Crude Glycerin as Byproduct in Biodiesel Production". A soon as he defended his project in front of the department's committee, he set his sights on continuing his education and acquiring international experience, which lead him to the University of Florida. Getting there was not an easy path. After a long application process, Francisco moved to the other side of the ocean on August 12th 2012, to begin the Materials Science and Engineering program at UF. Shortly after starting his first

semester, he joined Dr. Anthony Brennan's research group, where he was assigned a project based on biofouling. This work permitted him to write the present thesis. It also allowed him to meet and work alongside a great group of people who became not only colleagues but friends. Along with the help from Dr. Brennan, the group collaboration as a whole, was a vital part in the success of this project.

Francisco made an important decision last November, when he married his wife Andrea Castro Cara, who has played the most important part in helping him achieve his goals. He hopes that his knowledge in the chemical engineering and materials science field, combined with his research experience and determination will make him an excellent engineer at his future place of employment.